การปรับปรุงสมบัติทางไฟฟ้าของพีดอท พีเอสเอส ด้วยการเติมกราฟีนและวิธีการจุ่มในตัวทำละลาย

นางสาวชุติมา ดีท้วม

บทคัดย่อและแฟ้มข้อมูลฉบับเต็มของวิทยานิพนธ์ตั้งแต่ปีการศึกษา 2554 ที่ให้บริการในคลังปัญญาจุฬาฯ (CUIR)

เป็นแฟ้มข้อมูลของนิสิตเจ้าของวิทยานิพนธ์ ที่ส่งผ่านทางบัณฑิตวิทยาลัย

The abstract and full text of theses from the academic year 2011 in Chulalongkorn University Intellectual Repository (CUIR)

are the thesis authors' files submitted through the University Graduate School.

วิทยานิพนธ์นี้เป็นส่วนหนึ่งของการศึกษาตามหลักสูตรปริญญาวิศวกรรมศาสตรดุษฎีบัณฑิต
สาขาวิชาวิศวกรรมเคมี ภาควิชาวิศวกรรมเคมี
คณะวิศวกรรมศาสตร์ จุฬาลงกรณ์มหาวิทยาลัย
ปีการศึกษา 2557
ลิขสิทธิ์ของจุฬาลงกรณ์มหาวิทยาลัย

ELECTRICAL IMPROVEMENT OF PEDOT:PSS BY INCORPORATION OF GRAPHENE AND

SOLVENT DIPPING TREATMENT

Miss Chutimar Deetuam

A Dissertation Submitted in Partial Fulfillment of the Requirements

for the Degree of Doctor of Engineering Program in Chemical Engineering

Department of Chemical Engineering

Faculty of Engineering

Chulalongkorn University

Academic Year 2014

Thesis Title	ELECTRICAL IMPROVEMENT OF PEDOT:PSS BY INCORPORATION OF GRAPHENE AND SOLVENT DIPPING TREATMENT
By	Miss Chutimar Deetuam
Field of Study	Chemical Engineering
Thesis Advisor	Associate Professor Anongnat Somwangthanaroj, Ph.D.

Accepted by the Faculty of Engineering, Chulalongkorn University in Partial Fulfillment of the Requirements for the Doctoral Degree

....Dean of the Faculty of Engineering

(Professor Bundhit Eua-arporn, Ph.D.)

THESIS COMMITTEE

....Chairman

(Associate Professor Muenduen Phisalaphong, Ph.D.)

....Thesis Advisor

(Associate Professor Anongnat Somwangthanaroj, Ph.D.)

....Examiner

(Assistant Professor Apinan Soottitantawat, Ph.D.)

....Examiner

(Doctor Chutimon Satirapipathkul, D.Eng.)

....External Examiner

(Assistant Professor Suttinun Phongtamrug, Ph.D.)

ชุติมา ดีท้วม : การปรับปรุงสมบัติทางไฟฟ้าของพีดอท พีเอสเอส ด้วยการเติมกราฟีนและ วิธีการจุ่มในตัวทำละลาย (ELECTRICAL IMPROVEMENT OF PEDOT:PSS BY INCORPORATION OF GRAPHENE AND SOLVENT DIPPING TREATMENT) อ.ที่ปรึกษา วิทยานิพนธ์หลัก: รศ. ดร. อนงค์นาฏ สมหวังธนโรจน์, 119 หน้า.

ในงานวิจัยนี้ สภาพนำไฟฟ้าของหมึก พีดอท พีเอสเอส ถูกปรับปรุงโดยการเติมกราฟีนซึ่ง เป็นวัสดุที่มีสภาพนำไฟฟ้าได้ดีเยี่ยม ในที่นี้ปฏิกิริยาคลิกซึ่งเป็นการต่อหมู่ฟังก์ชันทางเคมีถูกนำมาใช้ เพื่อปรับปรุงการกระจายของกราฟีนใน พีดอท พีเอสเอส ปฏิกิริยาคลิกสามารถเกิดขึ้นได้ภายใต้ สภาวะการเกิดปฏิกิริยาแบบไม่รุนแรงและให้ผลผลิตสูง กราฟีนถูกสังเคราะห์ด้วยวิธีของฮัมเมอร์แบบ ปรับแต่งตามด้วยปฏิกิริยารีดักชันด้วยไฮดราซีน หมู่ฟังก์ชันปลายแอลไคน์บนกราฟีนถูกเตรียมได้จาก ปฏิกิริยาแอมิเดชันในขณะที่หมู่ฟังก์ชันปลายเอไซด์ บนพีดอท พีเอสเอส ได้ถูกสังเคราะห์ หมู่ฟังก์ชัน แอลไคน์และเอไซด์ถูกเชื่อมด้วยปฏิกิริยาคลิกโดยใช้ทองแดงเป็นตัวเร่งปฏิกิริยา ผลการทดลองแสดง ถึงกราฟีนที่ถูกปรับแต่งกระจายได้ดีใน พีดอท พีเอสเอส คอมพอสิต เมื่อเปรียบเทียบกับกราฟีนที่ไม่ ถูกปรับแต่ง เป็นผลอันเนื่องมาจากอันตรกิริยาที่ถูกปรับปรุงให้ดีขึ้น แต่มีแนวโน้มที่จะรวมตัวกันเมื่อ ปริมาณของกราฟีนเพิ่มขึ้น นอกจากนั้น สภาพนำไฟฟ้าของ พีดอท พีเอสเอส-กราฟีน คอมพอสิตที่ ถูกปรับแต่ง มีค่าสูงกว่าสารที่ไม่ถูกปรับแต่ง อย่างไรก็ตามสภาพนำไฟฟ้าที่ได้ยังไม่สูงเท่าที่คาดไว้ กระบวนการจุ่มฟิล์ม พีดอท พีเอสเอส จึงถูกนำมาศึกษา พบว่าสภาพนำไฟฟ้ามีค่าเพิ่มขึ้นอย่างมีนัย ยะเมื่อฟิล์ม พีดอท พีเอสเอสถูกจุ่มในสารละลายไดเมทิลซัลฟอกไซด์ความเข้มข้นต่ำในน้ำ นอกจากนั้นฟิล์มที่ถูกจุ่มยังแสดงความโปร่งใสสูงและความขรุขระของพื้นผิวต่ำโดยไม่พบรอยย่นและ แผ่นขาวบนพื้นผิวฟิล์มซึ่งรอยเหล่านี้อาจพบได้บนฟิล์มที่ถูกจุ่มในน้ำบริสุทธิ์และไดเมทิลซัลฟอกไซด์ บริสุทธิ์

ภาควิชา	วิศวกรรมเคมี	ลายมือชื่อนิสิต ....
สาขาวิชา	วิศวกรรมเคมี	ลายมือชื่อ อ.ที่ปรึกษาหลัก ....
ปีการศึกษา	2557	

5271805121 : MAJOR CHEMICAL ENGINEERING

KEYWORDS: PEDOT:PSS / GRAPHENE / CLICK REACTION / CONDUCTIVE POLYMER COMPOSITES / DIPPING

CHUTIMAR DEETUAM: ELECTRICAL IMPROVEMENT OF PEDOT:PSS BY INCORPORATION OF GRAPHENE AND SOLVENT DIPPING TREATMENT. ADVISOR: ASSOC. PROF. ANONGNAT SOMWANGTHANAROJ, Ph.D., 119 pp.

In this research, the electrical conductivity of poly(3,4-ethylenedioxythiophene): poly(styrene sulfonate) (PEDOT:PSS) ink was improved by adding graphene which is the excellent material in terms of electrical conductivity. Here, click reaction was conducted as a chemical functionalization for improving graphene dispersion in PEDOT:PSS. Click reaction was carried out under mild reaction condition with high yield. Graphene was synthesized via modified Hummer method following by reduction with hydrazine. A terminal alkyne modified graphene sheet was prepared by amidation, while the terminal azide modified PEDOT:PSS was synthesized. The alkyne and azide functional groups were coupled via click reaction using copper as catalyst. The results showed that the modified graphene was well dispersed in PEDOT:PSS composites in comparison with the unmodified graphene as a result of improved interaction but it tended to aggregate as loading increased. Furthermore, the electrical conductivities of modified PEDOT:PSS-graphene composites were higher than those of unmodified ones. However, the electrical conductivity was still not high as expected; the dipping method of dried PEDOT:PSS films was also studied. It was found that the electrical conductivity was significantly improved when the PEDOT:PSS film was dipped in low concentration of aqueous dimethyl sulfoxide solution. Moreover, the dipped film showed high transparency and low surface roughness without crinkles and white patches which might be found in case of the film dipped in pure water and pure dimethyl sulfoxide.

Department:	Chemical Engineering	Student's Signature	....
Field of Study:	Chemical Engineering	Advisor's Signature	....
Academic Year:	2014		

ACKNOWLEDGEMENTS

CONTENTS

LIST OF TABLES

LIST OF FIGURES

Figure   **Page**

Figure   **Page**

Figure **Page**

LIST OF ABBREAVIATIONS

AFM	Atomic force microscopy
BP	Boiling point
CNT	Carbon nanotube
CVD	Chemical vapor deposition
CY	Char yield
DMSO	Dimethyl sulfoxide
Eg	Band gap energy
EDOT	3,4-ethylenedioxythiophene
EDX	Energy dispersive X-ray
FTIR	Fourier transform infrared
GO	Graphene oxide
ITO	Indium tin oxide
NMR	Nuclear magnetic resonance
OLED	Organic light emitting diodes
OPV	Organic photovoltaic
PANI	Polyaniline
PEDOT	Poly(3,4-ethylenedioxytriophene)
PSS	Polystyrene sulfonate

PSSNa	Poly(sodium 4-styrenesulfonate)
PPY	Polypyrrole
RMS	Root mean square
Rq	RMS roughness
SEM	Scanning electron microscopy
Td	Degradation temperature
TGA	Thermogravimetric analysis
XPS	X-ray photoelectron spectroscopy

CHAPTER I

INTRODUCTION

1.1 Overview

Nowadays, the electronics manufacturing industries have been rapidly growing to respond human needs; meanwhile, the electronic wastes released to the surroundings cause serious illness and environmental pollution. Therefore, metals used in electronics, i.e., copper, silver, lead and cadmium, have to be managed with caution. Moreover, the waste treatments of these metals are complex, high cost and high energy consumption. Concerning the environmental effects, conductive polymer, which was first discovered in the mid-1970s, plays a key role in achieving high performance and environmentally-friendly electronic devices to replace the traditional metals like indium tin oxide (ITO). Further, it is easy to eliminate by combustion with less remaining traces. Moreover, the electronic patterns forming from conductive polymer require lower energy compared to metallic materials and they can be deposited on the flexible electronic packaging with smaller size and lighter weight.

The organic conductive polymer is a hydrocarbon compound containing the conjugated double bonds, aromatic ring or both resulting in high electron transfer along the polymer backbone. It possesses high electrical conductivity to apply in many electronics applications. One of the most widely used conductive polymers is

polyelectrolyte complex of poly(3,4-ethylenedioxytriophene) (PEDOT) and polystyrene sulfonic acid (PSS), also known as PEDOT:PSS. In comparison to other conductive polymers such as polypyrrole, polyaniline and polythiophene, PEDOT:PSS has higher electrical conductivity, transparency and stability in moist condition. Unfortunately, the electrical conductivity of pristine PEDOT:PSS is relatively low (∼0.3 S/cm) compared with metals, leading to a restriction of organic electronics development [1]. Thus, the enhancement of the electrical conductivity is greatly necessary for the usage in advanced applications such as Organic Photovoltaics (OPVs).

From this reason, this research has attempted to improve the electrical properties of PEDOT:PSS by two different methods. The first method is the straightforward addition of electrically conductive particles into the PEDOT:PSS. Herein, graphene was chosen because of its outstanding electrical conductivity compared with other fillers such as graphite and carbon nanotubes (CNTs) [2-5]. Graphene is a single layer of carbon atom rearranging in hexagonal lattice. It has been interested in enhancing polymer's properties. Although graphene can be prepared by various methods, the chemical method was selected in this work because it does not require complex instruments and can easily be scaled-up from laboratory process to industrial process. Nevertheless, graphene inherits hydrophobicity, resulting in poor dispersion in common organic solvents. Without surface modification, the agglomeration of these graphene particles also results in poor electrical conductivity. To improve the dispersibility of graphene in PEDOT:PSS, graphene was functionalized to increase the

chemical interaction with PEDOT:PSS solution via click reaction. This reaction was performed because it was a simple and fast reaction between azide groups (-N$_3$) and alkyne groups (-C≡C) with the presence of Cu(I) catalyst, which gives high selectivity and high yield of the final product. Graphene was modified to obtain terminal alkyne-modified graphene sheets (graphene-alkyne) and PEDOT:PSS was also functionalized to produce azide-modified PEDOT:PSS (PEDOT-N$_3$:PSS). After the click reaction, alkyne-modified graphene and azide-modified PEDOT:PSS were coupled together, forming triazoles linkages. To confirm the formation of click reaction, the chemical structure of synthesized product was characterized. The electrical properties of clicked PEDOT:PSS-graphene composites were measured and compared with that of synthesized PEDOT:PSS. Moreover, the dispersibility of graphene in PEDOT:PSS and surface morphology of the composite film were also explored. In this work, the highly electrically conductive ink (clicked PEDOT:PSS-graphene composite) was obtained.

In addition, another conductivity method is a post treatment of the PEDOT:PSS by dipping in the organic solvents. PEDOT:PSS thin films was fabricated on glass substrates by spin coating and subsequently dipping them into aqueous DMSO solution. The effect of the concentration of DMSO in an aqueous solution on the surface morphology, surface chemistry and electrical conductivity of the PEDOT:PSS thin films after the dipping process were investigated. The low concentration range of DMSO between 0-5 vol% was studied.

1.2 Objectives of the research

1. To improve the electrical conductivity of PEDOT:PSS by incorporation of graphene

2. To investigate the surface morphology, surface chemistry, dispersibility and electrical property and thermal stability of clicked and unclicked PEDOT:PSS-graphene composites.

3. To improve the electrical properties, surface topography and transparency of PEDOT:PSS films by dipping process in aqueous DMSO solution

1.3 Scope of the research

1. Graphene is synthesized from graphite via modified Hummers method following by reduction with hydrazine. The graphene content in PEDOT:PSS is varied between 0-5 wt%.

2. PEDOT-N_3:PSS is synthesized by a polymerization reaction of EDOT-N_3 in presence of PSS. Graphene-alkyne sheet is a functionalization of graphene oxide by amidation reaction, following by reduction with hydrazine. Moreover, azide group of PEDOT:PSS is reacted with alkyne group of graphene via click reaction.

3. The chemical chemistry, surface morphology, electrical conductivity and thermal stability of the clicked PEDOT:PSS-graphene composite are studied.

4. The effect of dipping treatment of spin coated PEDOT:PSS films in pure water, pure DMSO and aqueous DMSO solution at low concentrations of 0-5 vol% is examined.

CHAPTER II

THEORY AND LITERATURE REVIEWS

In this chapter, types of the conductive polymer and the mechanism of electrons transfer are introduced. The properties of PEDOT:PSS and its electrical enhancement are reviewed. Graphene synthesis and properties are also discussed. Since graphene cannot be well dispersed in PEDOT:PSS solution, functionalized graphene and PEDOT:PSS are coupled via click reaction in this study. Click reaction is also discussed in this part. Finally, the development of conductive polymer from the mixture of PEDOT:PSS and graphene to be used in electronic applications is reviewed.

2.1 Conductive polymer

Conductive polymer is sometimes called *conjugated conductive polymer* or *organic polymeric conductor*. It is the hydrocarbon material containing double bonds or aromatic cycles or both along their backbone that can transfer electron intrinsically. The first discovery of the conductive polymer in the mid-1970s opens the door to the organic electronics world; since then, it has been continuously developed to substitute metal-based materials like indium tin oxide. Polyacetylene is the first discovered conductive polymer; however, it still has some drawbacks such as poor electrical properties and instability in moist condition [6]. Thus, a large variety of the conductive polymers have been developed for improving the disadvantages of polyacetylene such

as polyaniline, polypyrrole, polythiophene and poly(3,4-ethylenedioxythiophene) as shown in Figure 2.1.

Polyacetylene

Polyaniline (PANI)

Polypyrrole (PPY)

Polythiophene

Poly(3,4-ethylenedioxythiophene) (PEDOT)
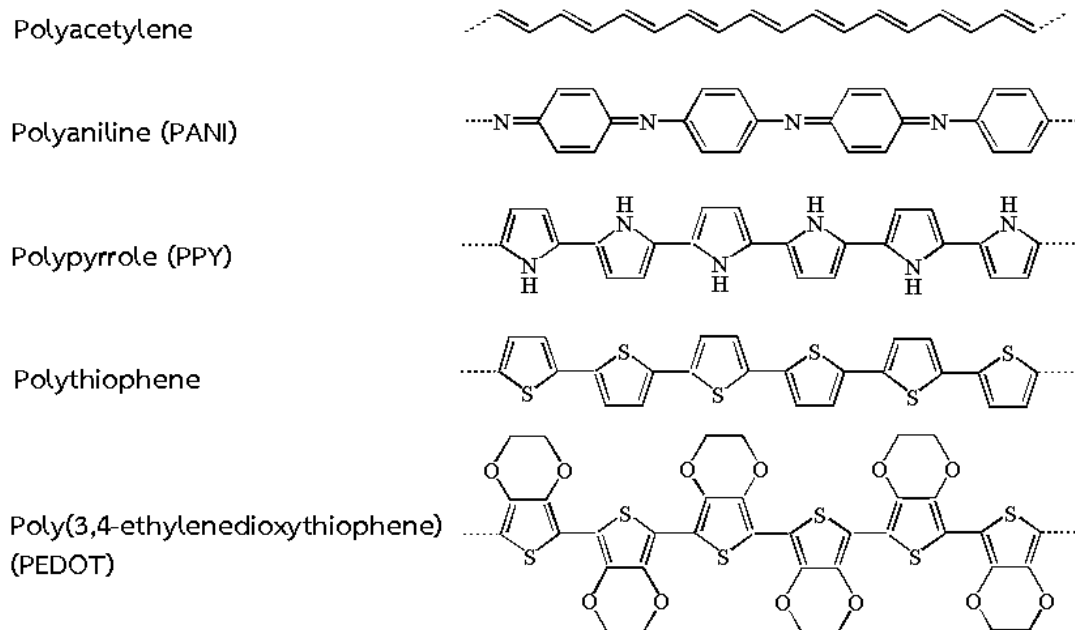
Figure 2.1 Common conductive polymers

Generally, the conductive polymer is in a form of stable dispersion in the solvents, which is easily deposited on the flexible substrates. The patterns made from the conductive polymer are more variety and adjustable than the metallic material. Furthermore, the organic electronic products are environmentally friendly concerning the waste management. From this reasons, the organic conductive polymers have been attracting great attention for a few decades for applying in a wide range of

electronics fields including biosensors [7, 8], solid electrolyte capacitors [9, 10], organic

light emitting diodes (OLEDs) [11, 12], and electrochromic displays [13, 14].

2.2 Mechanism of electrical transfer in conductive polymer

The chemical structures of common polymers like polyolefin are saturated; all

valence electrons are occupied in covalent sigma bonds (σ-bonds) causing very large

band gap between the valence band and conduction band, thus the electrons cannot

transfer along the polymer backbone. Nevertheless, the band gap of conductive

polymer is narrower than the saturated polymers which can be explained by band

model as shown in Figure 2.2.
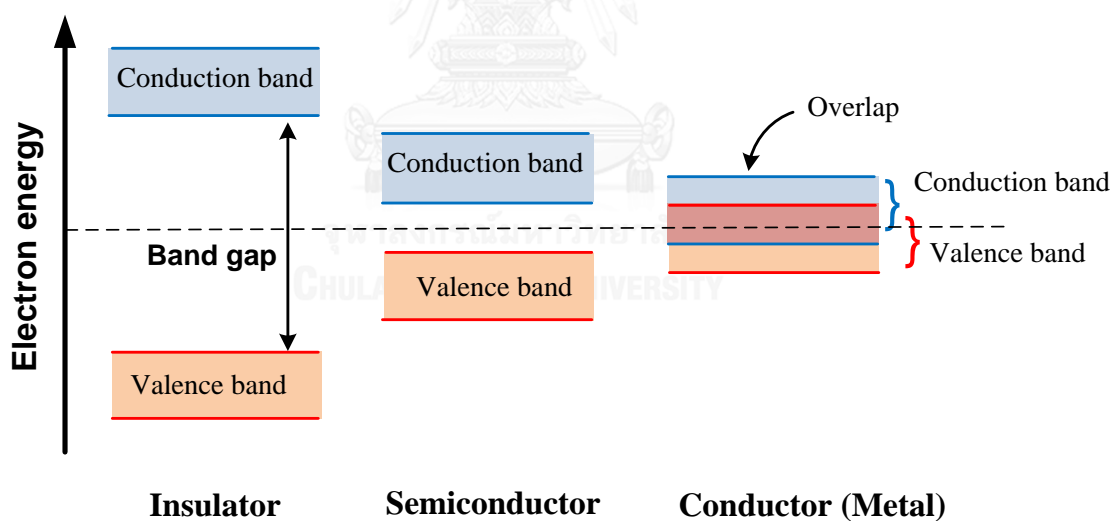
Figure 2.2 Three classes of materials (metal, semiconductor and insulator)

Generally, the materials can be classified into three main categories according

to their electrical conductivity at room temperature: insulators, semiconductors and

metals. The band gap energy (E_g) is the energy difference between the highest valence

band and the lowest conduction band.

Conductivity (S/cm)		Materials
Metallic conductors	10^6 10^4 10^2	Copper Iron Graphite Bismuth
Semi- conductors	10^0 10^{-2} 10^{-4} 10^{-6} 10^{-8}	Indium/Antimony Gallium/Arsenic Germanium Silicon
Insulators	10^{-10} 10^{-12} 10^{-14} 10^{-16} 10^{-18} 10^{-20}	Glass Diamond Sulfur Polyethylene Polystyrene Teflon Quartz
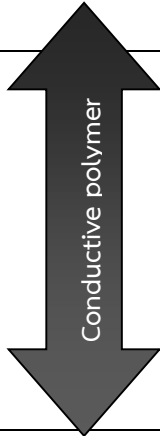
Figure 2.3 Range of electrical conductivity of the materials [15, 16]

The conduction occurs when electrons are excited from one band to another band.

For the saturated polymers, the band gap is very large, for example 10 eV, electrons

need high energy to excite to the conduction band, indicating that the material shows

insulating properties at room temperature. On the other hand, in case of metals such

as silver and copper, the valence band and the conduction band are overlapped;

therefore, the electrons can move across freely without necessarily receiving additional

energy from the valence band to the conduction band, leading to high electrical

conductivity as shown in Figure 2.3.

The conductive polymer has small band gaps, for example 1.0 eV, electrons

are able to excite to the conduction band suggesting that the conductive polymer is a

semiconductor. The π-system of the conjugated chains is formed along the polymer

backbone, three σ-bonds of carbon atoms are formed with neighboring atoms and the

remaining p orbitals engage in the π-system. For the conjugated polymer such as

polyacetylene, each carbon in the polymer backbone is π-bonded to two neighboring

carbon atoms and one hydrogen atom with one π electron per carbon remains. Hence,

the repeating unit can be written as –CH=CH–. The length of σ-bond of carbon is equal,

as for the remaining π electrons, which is found in one-half filled continuous band.

The result is an energy band gap between a completely occupied π-band and an

empty π^*-band, the energy saving due to the new band gap outweighs the energy cost

of rearranging the carbon atoms. This bond-alternating structure is typically found in

all conjugated polymers for using as semiconductors [17]. The electrical conductivities

of conductive polymer vary from 10^{-8}-10^{2} Siemens/cm (1 Siemens = 1 Ω^{-1}, S/cm

= Ω^{-1} cm^{-1}, which is the reciprocal of the electrical resistance (unit of Ω)).

2.3 Poly(3,4-ethylenedioxythiophene):poly(styrene sulfonate) (PEDOT:PSS)

Among commercial conductive polymers, PEDOT:PSS is an intriguing material that has been paid attention for many electronics devices, *i.e.*, organic photovoltaic devices (OPVs), organic light emitting diodes (OLEDs), and chemiresistive sensors, because it possesses the outstanding properties including high electrical conductivity and high transparency [18-22]. Normally, PEDOT is intrinsically insoluble in water; therefore, the incorporation of water-soluble insulating PSS leads to the enhancement of the dispersibility in an aqueous solution and some polar organic solvents due to the formation of the polyelectrolyte complex of PEDOT:PSS, resulting in better processibility on the flexible substrates such as PET and PI [23]. Film forming techniques, *i.e.*, drop casting and spin coating, have been performed to deposit the conductive polymers owing to an ease to create the small scale of patterns.

2.3.1 Development of PEDOT:PSS

PEDOT is polymerized from 3,4-ethylenedioxythiophene (EDOT). the chemical structure of EDOT is shown in Figure 2.4, which was first discovered by Bayer AG, Leverkusen [16].
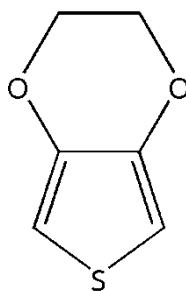
Figure 2.4 Chemical structure of EDOT

PEDOT has many advantages such as environmental stability in moist condition and at elevated temperature [24]. The processing of EDOT is simple and the polymerization of EDOT in the presence of oxidants does not require cooling to slow down. The reaction is fastened for an efficient application to electrolytic capacitors [16]. Furthermore, EDOT is not classified as a toxic chemical like pyrrole, thus its handling is much safer and it has been considered as an excellent commercial conductive polymer for many electronic applications.

However, PEDOT, which is classified as the polycation, shows poor solubility and the stability in common solvents. Only 0.21 g of PEDOT can be dissolved in 100 ml of water at 20°C. This drawback of PEDOT can be overcome by electrochemical polymerization in presence of suitable polyanion to form polyelectrolyte complex. The mixed solutions of polycations and polyanions or the polyelectrolyte complex can form water soluble complex. Many polyanions for PEDOT have been reported; Sonmez and coworkers successfully prepared the polyelectrolyte films by using poly(2-acrylamido-2methyl-1-propane sulfonate) as counterion. It showed the

conductivity of 80 S/cm with electrochromic and cation exchange properties [25]. In 1995, Yamato and coworkers reported the electrochemical polymerization of EDOT in presence of the high efficiency counterion substance, polystyrenesulfonic acid (PSS), to improve the stability of PEDOT in solvent; however, the conductivity of complex PEDOT:PSS decreased compared to pristine PEDOT (50-80 S/cm) [26, 27]. At present, PSS is an appropriate polyelectrolyte for PEDOT, which is commercially available in a wide range of molecular weights with different dispersibility. Besides, helping in dispersibility of PEDOT:PSS complex, PSS forms durable films and shows no absorption in the visible range of light. The PEDOT:PSS structure is shown in Figure 2.5.
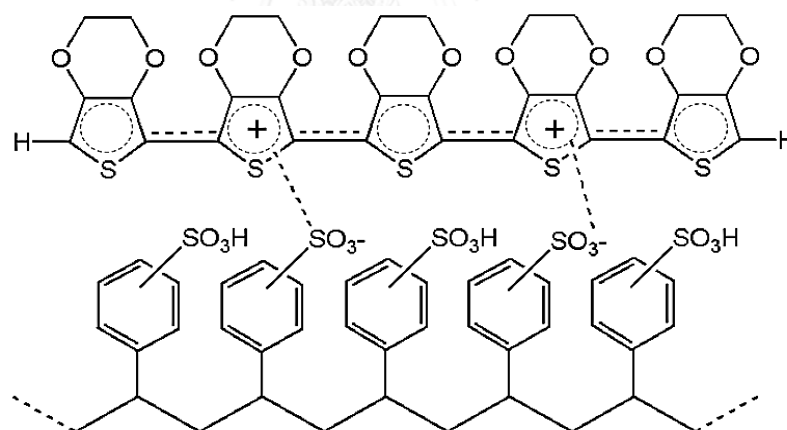
Figure 2.5 Chemical structure of PEDOT:PSS [28]

2.3.2 Properties of PEDOT:PSS

PEDOT:PSS dispersed in water or organic solvents can be uniformly deposited on the surface of various substrates (also called pattern) by drop casting, spin coating,

screen printing, inkjet printing, and spraying [16, 29-33]. To achieve the good film's quality, the viscosity, surface tension, and adhesion to the substrate of conductive ink have to be controlled. Many grades of PEDOT:PSS are commercially available in the conductive polymer markets. The solid content, ratio of PEDOT to PSS and gel particle distribution are varied from each supplier. Each deposition technique has distinct specific requirements; for example, the screen printing requires high viscous ink and the inkjet printing requires small particle size of conductive grain to protect the nozzle clogging. The properties of inks can be adjusted by the addition of water soluble or dispersible additives (i.e., surfactants, stabilizers, and cross-linking agents or inert polymers as binders).

The H.C. Stack Clevios GmbH under the trade name of Clevios^{TM} is the main manufacturer and distributer of the PEDOT:PSS in water. The specification of commercial grade PEDOT:PSS are summarized in the Table 2.1. Although PEDOT:PSS possesses outstanding properties in terms of thermal and mechanical properties, the electrical conductivity of unmodified PEDOT:PSS is still lower compared to the metallic materials, leading to poor performance and unreliability patterns of electronic packaging. Therefore, the improvement of electrical properties of PEDOT:PSS is very necessary.

Table 2.1 Specification of commercial PEDOT:PSS in water [16]

Trade name	Solid content (wt%)	PEDOT:PSS ratio (w/w)	Viscosity at 20°C (mPa.s)	Particle size (nm)	Conductivity (S/cm)
Clevios P	1.3	1:2.5	80	80	<10
Clevios PH	1.3	1:2.5	20	30	<10
Clevios P VP AI 4083	1.5	1:6	10	40	10^{-3}
Clevios P VP CH 8000	2.8	1:20	15	25	10^{-5}
Clevios PH 500	1.1	1:2.5	25	30	500[a]
Clevios PH 750	1.1	1:2.5	25	30	750[a]
Clevios PH 1000	1.1	1:2.5	30	30	1000[a]

[a] Conductivities are measured for dispersion containing 5% dimethyl sulfoxide.

2.3.3 Modification of PEDOT:PSS

Many articles relating to the electrical conductivity enhancement including acidic treatments, thermal annealing and chemical treatments have been published for a decade [34, 35]. Concerning the environmental impact, the acidic treatment was unsuitable because the used chemicals are hazardous and corrosive, and acid might damage the ITO electrodes. The thermal annealing treatment was easy to conduct;

however, the electrical conductivity was improved slightly about one order of magnitude [36]. High annealing temperature resulted in one-third resistivity compared with that annealed at low annealing temperature [29]. Direct addition of high boiling point organic solvents into PEDOT:PSS, also known as solvent doping method, increased the electrical conductivity of PEDOT:PSS more than 100 times when compared with unmodified PEDOT:PSS [37]. The high boiling point (BP) organic solvents included dimethyl sulfoxide (DMSO; BP = 189 ^{o}C), ethylene glycol (BP = 197 ^{o}C), *N*-methylpyrrolidone (BP = 202 ^{o}C), glycerol (BP = 290 ^{o}C) and sorbital (BP = 296 ^{o}C) [38-41]. The previous literatures also mentioned about the strong effect of solvent doping on the surface morphology of PEDOT:PSS thin films. The film surface roughness was dramatically increased as a result of phase separation between the PEDOT matrix and excess PSS, leading to an aggregation of the conductive PEDOT grains and the formation of PSS-enriched layer on the top surface of thin films [42, 43]. The surface roughness increased as a function of doping ratio of solvent to PEDOT:PSS, thus the electrical conductivity dropped significantly because it traps the charge carriers [44, 45]. Furthermore, removal of these solvents requires high temperature which is often in the range of the decomposition temperatures of PEDOT (150 ^{o}C) and PSS (250 ^{o}C), reducing the electrical properties and light transmittance of the prepared films [46, 47]. Hence, the types and concentrations of additional solvents are the crucial variables that can control physical properties and electrical conductivity of the PEDOT:PSS films. To reduce the effect of solvent doping, a polar-solvent vapor

annealing was proposed. The treated film showed good surface in which the solvent vapor only interacts with the surface of the PEDOT:PSS films [48]. The phase-separated morphology was induced resulting in better connection of conductive grains while the surface roughness of the top layer of films was substantially reduced from 1.31 nm to 0.32 nm. Dropping the solvent on the prepared conductive films was also studied. It was found that the dropping process can control the surface roughness with improved electrical conductivity similar to vapor annealing results [49]. However, the dipping process of conductive films in the solvent seemed to be more effective than the solvent vapor annealing and dropping method since it not only enhanced the interconnection of the conductive PEDOT grains, but also removed the insulating PSS phase on the top surface of films.

Besides the solvent treatment, the electrical conductivity of PEDOT:PSS was improved by incorporation of the electrically conductive fillers, e.g., gold nanoparticles [50] and carbon nanotubes [12, 51]. The incorporation of PEDOT:PSS with these fillers not only improved the electrical conductivity of PEDOT:PSS, but also increased the thermal stability and mechanical properties, especially decrease in cracking upon bending the flexible electronics. Among these fillers, graphene is the most interesting material that has been used in many electronic industries owing to its superior electrical property. Furthermore, graphene can be prepared from low cost graphite via chemical method with high yield and is easy to scale-up from laboratory process into

industrial process. The synthesis, modification and its dispersibility in polymer matrix are described in the next section.

2.4 Graphene

2.4.1 Synthesis of graphene

Graphene, two-dimensional single layer sheet of carbon atoms arranged in hexagonal lattice, was discovered in 2004. It is the thinnest conductive material, which has potential for the future development in electronics and sensors [52-54]. The characteristics of graphene and how to eliminate the defects have been consistently investigated since the discovery. Additionally, the synthetic methods of graphene have been reported for achieving various purposes including ecological awareness, scalable process and simplicity, as well as for focusing on controlling process parameters efficiently in order to obtain single graphene sheet. The synthetic methods, advantages and procedures can be categorized into six main methods, as summarized in Table 2.2. The suitable method to obtain high quality graphene for this research is preparation of graphene from natural graphite via chemical oxidation followed by chemical reduction with hydrazine under mild condition. The materials and instruments used in this chemical method are available in a common laboratory. Large quantity of graphene can be produced on laboratory scale and it can also be scaled up for the industrial production. The details of chemical oxidation and chemical reduction will be described in next content.

Table 2.2 Synthetic methods of graphene

Synthetic method	Advantage	Procedure
Chemical oxidation [55]	▪ Possible to control the number of layers	The route to produce graphene from natural graphite by oxidation processes, followed by various steps that will be transformed into the thin graphene sheets.
Mechanical exfoliation and cleavage [53]	▪ Reliable and easy ▪ No special equipment needed	This method uses mechanical or chemical energy to break weak van der Waals force between the layers and to separate out individual graphene sheets.
Chemical reduction [56-59]	▪ Easy to scale up to industrial level production ▪ Low cost synthesis	The oxygen-containing functional groups on graphene oxide surface will be removed by using reducing agents such as hydrazine.
Thermal reduction [60-62]	▪ Thin films containing high quality graphene nanosheets	Graphene oxide is heated to 1000-1050 °C in an inert atmosphere and hold in the furnace for 30 s to form graphene.
Thermal chemical vapor deposition techniques (CVD) [63]	▪ Eco-friendly ▪ Low cost precursor ▪ Controllable thickness sheets	Hydrocarbon precursor is pyrolyzed in chamber of the CVD furnace at above 700°C in Ar gas and cooled down to room temperature. The synthesized graphene is grown on the substrate surface.
Un-zipping CNTs [64, 65]	▪ Possible route to modify process of graphene synthesis	The CNTs as the precursor of this method will be un-zipped longitudinally receiving graphene nanoribbons, partially opened CNTs and graphene flakes.

Step 1: Chemical oxidation of graphite
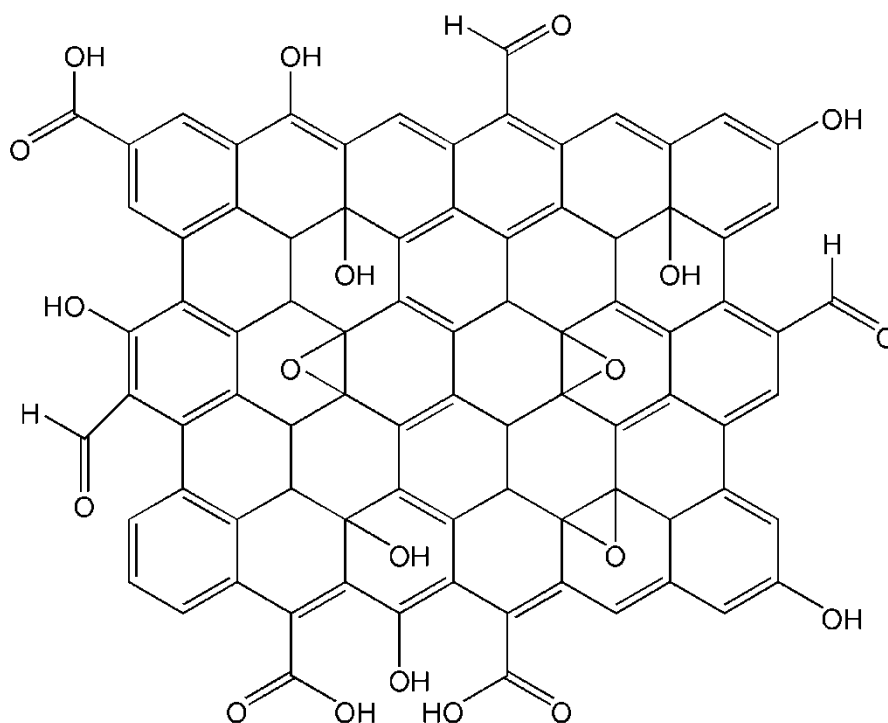
Figure 2.6 Schematic illustration of oxygen-containing groups of GO [66]

Graphene oxide (GO) is prepared by oxidation of natural graphite with strong oxidizing agents, such as sulfuric acid, nitric acid, and potassium permanganate, resulting in oxygen-containing functional groups on both basal planes and at the edges of GO sheets. Oxygen-functionalities existing in GO after chemical oxidation are epoxide (-O-), hydroxyl (-OH), carbonyl (-C=O), and carboxyl (-COOH). Epoxide and hydroxyl groups are the major components distributed on the basal planes, while carbonyl and carboxyl groups are the minor components located at the edges of GO sheets [56]. The schematic illustration of oxygen-containing groups in GO is shown in Figure 2.6.

During the oxidation process, the graphite flakes are broken down to small GO (around 10 µm in diameter). The initial size of graphite flakes does not significantly affect the final size of GO as shown in Figure 2.7. The hydroxyl and epoxide functional groups increase the interspacing between graphene layers. The layer spacing of GO is increased 2 times compared with graphite (0.34 nm), considerably reducing attractive interaction and enhancing dispersion of GO in water.
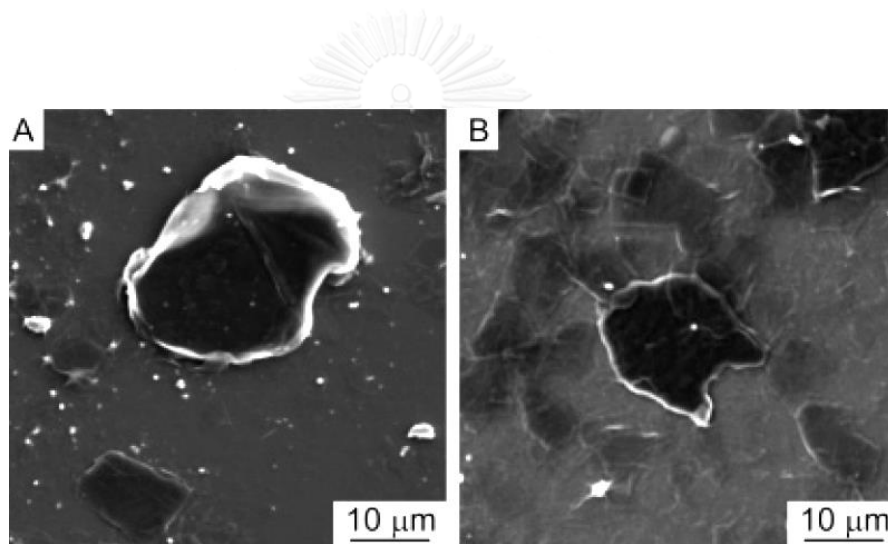
Figure 2.7 SEM images of GO synthesized from; (A) 400 µm diameter graphite

(B) 45 µm diameter graphite [67]

Step 2: Chemical reduction of graphene oxide
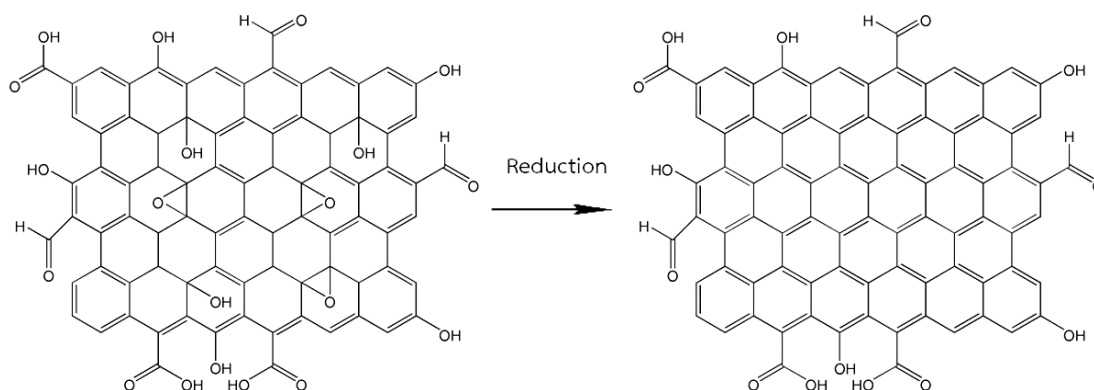
Figure 2.8 Chemical reduction of GO to graphene [66]

The electrical conductivity of GO is low due to oxygen-containing functional groups which can be removed by chemical reduction [59]. The advantages of the chemical reduction are low cost and able to scale up for a large quantity production. It is a well-known method for de-oxygenation of GO by reducing agents such as hydrazine [56], hydroquinone [55], or $NaBH_4$ [68]. Among them, hydrazine is the highest efficiency reducing agents, so it is used in this work to reduce oxygen-functional groups, in particular epoxide and hydroxyl groups. The illustration of the chemical reduction of GO to graphene with hydrazine is shown in Figure 2.8.

The chemical reduction of GO with hydrazine was proposed by Stankovich and coworkers that the hydrazine subjected to de-epoxidation of GO [58]. In addition, the mechanisms of graphene reduction via several routes as shown in Figure 2.9 was proposed Gao et al. [69].
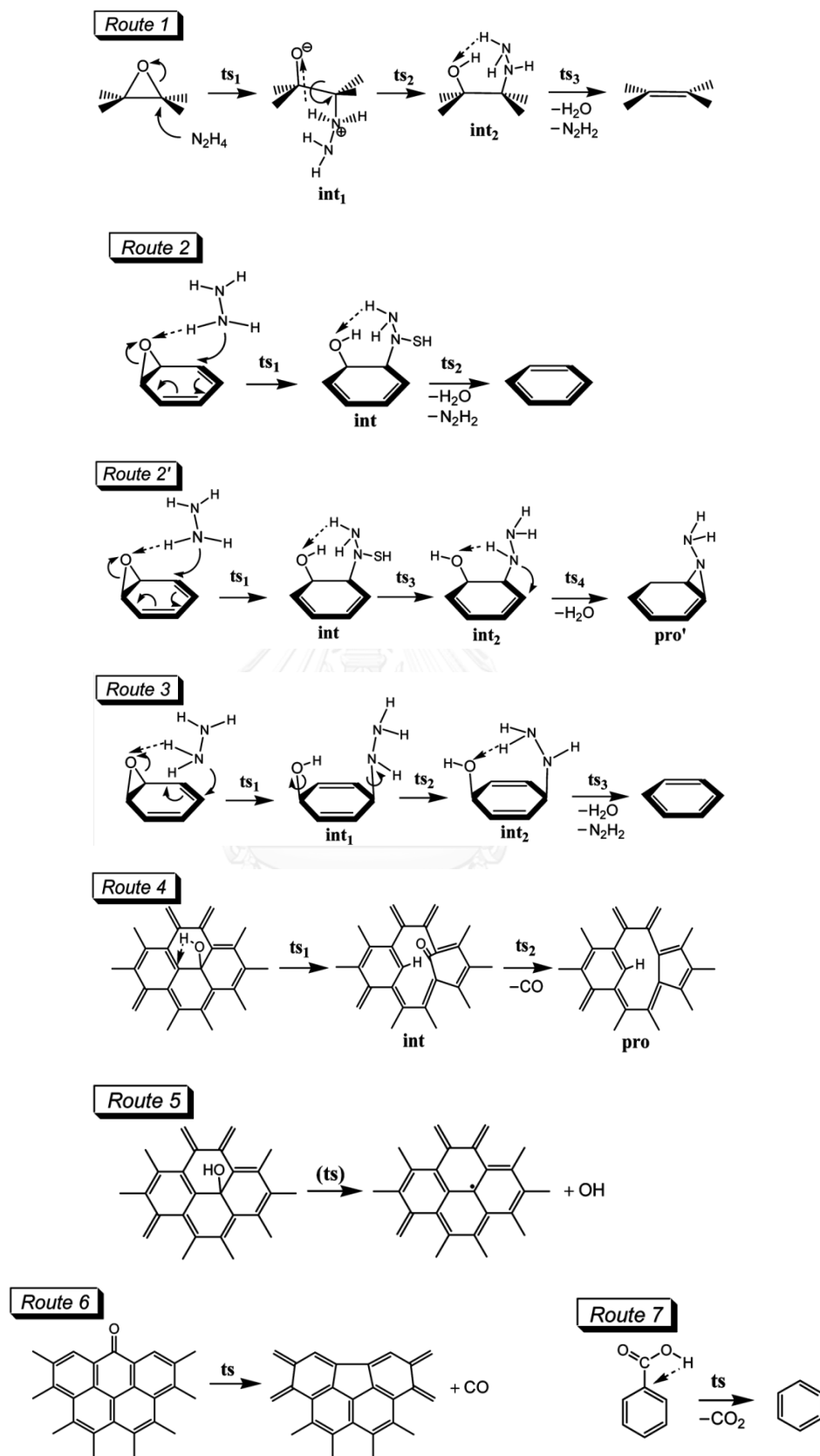
Figure 2.9 Possible GO reduction mechanisms [69]

Route 1 to 3 and 2' show the de-epoxidation mechanisms by hydrazine. Although, mechanism of removing other oxygen-functionalities (hydroxyl, carbonyl and carboxyl groups) of GO by chemical reduction with hydrazine was still unclear, they claimed that these functional groups can be eliminated by thermal reaction as demonstrated in route 4 to 7.

2.4.2 Modification of graphene

Hydrophobicity of graphene was a crucial obstacle to re-disperse graphene in water or organic solvents at highly filled concentration. The graphene sheets showed agglomeration due to cross-linking between sheets [70]. Therefore, the surface modifications of graphene with small molecules, polymer chains, surfactants, as well as charges during the chemical reduction were preferred. Alternatively, surface modification of GO could also be used prior the chemical reduction for increasing dispersibility in solvents. The surface modification was explained in two cases: covalent modification and non-covalent modification.

Method 1: Non-covalent modification of graphene

The dispersion of graphene in solvents was also improved by non-covalent modification. Generally, the stabilizers, surfactants and others have contributed to enhance the dispersion of graphene in the solvents. For example, a highly water-soluble graphene was achieved by incorporation of graphene dispersion with a

stabilizer poly(sodium 4-styrenesulfonate) (PSSNa) [71]. Moreover, Lee and coworkers also reported similar results that the dispersibility of graphene in water was enhanced when PSS and Nafion were used as surfactant [72]. Interestingly, the Nafion-coated graphene had higher electrical conductivity than that of PSS-coated graphene because Nafion surfactant was a conductive material but PSS was an insulating material. Besides the surfactants, an anionic conjugated polyelectrolyte was a modifying agent; for example, graphene surface was modified with poly(2,5-bis(3-sulfonatopropoxy)-1,4-ethynylphenylene-alt-1,4-ethynylphenylene) (PPE-SO$_3^-$) to achieve high electrical conductivity and stability graphene in water for 8 months [73]. The PPE-SO$_3^-$ molecules were absorbed onto both sides of graphene sheet and the functional groups of PPE-SO$_3^-$ prevented the agglomeration in aqueous solution because of the intermolecular electrostatic repulsion. In case of the graphene modification with polymer, poly(3-hexylthiophene) (P3HT)/graphene nanocomposite was obtained by *in situ* reduction of GO in presence of P3HT. The resultant material exhibited good dispersion in chloroform without precipitation for longer than 20 days and it can also be dispersed in organic solvents as well [74].

Method 2: Covalent modification of graphene

Preparation of covalently modified surface of GO and graphene has been reported for a decade. The surface modifying agents can decrease the hydrophilicity or increase hydrophobicity of GO sheets by forming a linkage on GO surface. Si and Samulski modified the hydrophilicity of graphene via sulfonation of GO with the aryl diazonium salt of sulfanilic acid following by reduction with hydrazine [68]. The graphene showed high dispersibility and stability in water; nevertheless, the electrical conductivity was reduced. In 2009, organophillic graphene was synthesized by modification of GO with allylamine and octadecylamine following by reduction with hydroquinone [55, 75]. Graphene-octadecylamine was obtained by functionalizing GO with octadecylamine first following by chemical reduction. In addition, it was also obtained by covalent bonding of the carboxyl groups of as-prepared graphene with amine group of octadecylamine [76]. For improving the hydrophobicity of GO and graphene, the long alkyl chains substances with amine groups distributed along the chains such as butylamine and Polyallylamine (PAA) were also used as modifying agent [75, 77]. The amine groups crosslinked with epoxy groups and carboxyl groups of graphene, while the long alkyl chains improved the dispersibility, forming homogeneous suspension of GO or graphene sheets [78] Phenylisocyanate containing a non-polar benzene ring is one of the high efficient modifying agents for enhancement of hydrophobicity of graphene. According to the literature reviews, the mechanical

properties such as the strength and stiffness of polymer composites incorporated with the modified graphene were improved significantly in comparison with those incorporated with the unmodified one.

2.4.3 Graphene composite in electronics

Because of the outstanding properties of graphene including high Young's modulus (1060 GPa), high thermal conductivity (4840-5300 $Wm^{-1}K^{-1}$) and excellent electrical properties[79], graphene has been used to substitute for metallic fillers in electronic fields. Recently, GO and graphene particles were filled into the conductive polymer in order to enhance its electrical conductivity and electrochemical sensitivity. For example, GO dispersed in PEDOT:PSS aqueous solution was used as non-metallic solders for connecting the electrical parts of organic optoelectronic devices [80]. Moreover, the stable suspension of functionalized graphene in the presence of PEDOT:PSS prepared by non-covalent functionalization exhibited high conductivity with a controllable light transmittance. It has a potential for a large-scale transparent and conducting thin film. [24]. In Thailand, PEDOT:PSS/graphene composite had been studied. PEDOT:PSS/graphene was deposited on a screen printed carbon paste electrode by inkjet printing technique to enhance the electrochemical sensitivity of electrode devices. [81]. In addition, the stable PEDOT-graphene dispersion was prepared via *in situ* polymerization of EDOT in a solution of sulfonated graphene. The sulfonate functional groups, which are hydrophilicity, assisted the dispersion of

graphene in PEDOT. The prepared PEDOT-graphene film showed high electrical conductivity of 0.2 S/cm and the great light transmittance higher than 80% in wavelength of 400 – 1800 nm (for 10 nm thin film) [82]. From the data, the competitive production of PEDOT:PSS-graphene is very interesting which was proposed on many publications. Therefore, we expects that the PEDOT:PSS-graphene will be the high performance material for the functional devices applications such as printed electrode and gas detector.

2.5 Click reaction for conductive polymer

In 2002, click reaction was firstly proposed independently by Sharpless and Meldal as a selection criteria for highly efficient coupling agent [83, 84]. The advantages of click reaction are modularity, high selectivity, fast reaction time, mild reaction condition and high yields production [85]. Furthermore, click reaction was feasible to perform in water or organic solvents at room temperature [86]. Click reaction is prepared via 1,3-dipolar cycloaddition reactions of azide and alkyne groups in the presence of copper catalyst, forming triazole linkage [87]. In addition, the triazole is a good electronic coupling for electrodes applications. The thiazole dose not obstruct the electron that transfer from the electrode to the connected part [88]. The cycloaddition generating 1,4-disubstituted 1,2,3-triazoles is depicted in Figure 2.10.
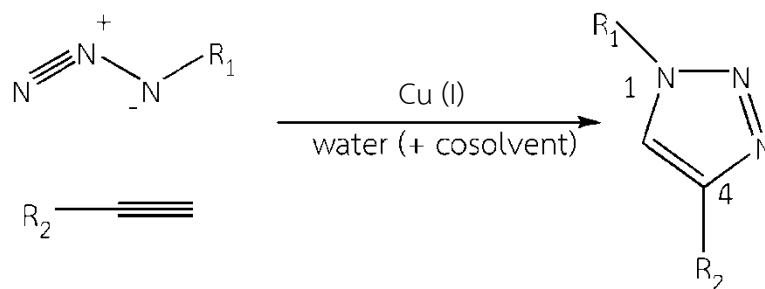
Figure 2.10 Copper-catalyzed azide-alkyne cycloaddition [89]

Because of these advantages, click reaction has become an interesting method that has been used in numerous ways, e.g., functionalization of linear polymer chains with desired functional groups and production of dendrimers [90, 91]. The click reaction can occur on the surface of solid particles as carbon nanotube [92-94]. In the biological systems, the mild click reaction conditions are often required [95]. It is also a well-known post-polymerization modification of some polymers such as PEDOT [96, 97]. During polymerization, PEDOT becomes insoluble which is very difficult for further process. Thus, click reaction is particularly useful to obtain the PEDOT with different functionalities and the reactive sites on the polymer chains [98].

CHAPTER III

CHEMICALS AND CHARACTERIZATION

3.1 Chemicals

For preparation of graphene-alkyne, graphite powder (99.99%, particle size ≤ 45 μm), hydrazine hydrate (5.51 wt%), 4-ethynylaniline (97%) and N,N'-dicyclohexylcarbodiimide (DCC, 99.0%) were purchased from Sigma-Aldrich. Sulfuric acid (H_2SO_4, 96.3%), sodium nitrate ($NaNO_3$, 99.69%), potassium permanganate powder ($KMnO_4$, 100%) and hydrogen peroxide (H_2O_2, 30%) were purchased from Ajax Finechem. Hydrochloric acid (HCl, 5 vol%) was purchased from Merck.

In case of synthesis of PEDOT-N_3:PSS, 3,4-dimethoxythiophene (97%), 3-bromo-1,2-propanediol (97%), p-toluenesulfonic acid (98%), sodium azide (NaN_3, 99.5%), iron (III) p-toluene sulfonate hexahydrate, sodium peroxodisulfates ($Na_2S_2O_8$, 98%) and polystyrene sulfonate (PSS, 18 wt% in H_2O), copper sulfate ($CuSO_4$, 99%), sodium ascorbate (98%) and dimethyl sulfoxide (DMSO) were bought from Sigma-Aldrich. All organic solvents were analytical grade and used as received without further purification. Poly(3,4-ethylenedioxythiophene):poly(styrene sulfonate) in an aqueous solution (Clevios PH 1000) was purchased from Heraeus GmbH. The solid content of PEDOT:PSS was 1.1 wt% and the weight ratio of PEDOT-to-PSS was 1:2.5.

3.2 Characterization

3.2.1 Fourier transform infrared (FTIR) spectroscopy

The functional groups of synthesized products were characterized by Fourier transform infrared spectrometer (Perkin Elmer instruments, Model: GX FT-IR Spectrum, USA). The crystalline potassium bromide (KBr) was ground and dried in vacuum oven at 100 ^{o}C to remove moisture before blending with sample. After that, it was compressed at 10 MPa for 60 seconds forming a thin disk, which was loaded into a sample holder and placed in a chamber, respectively. FTIR was operated in a spectral range of 4000-600 cm^{-1} with a number of scan of 128 and a resolution of 4 cm^{-1}.

3.2.2 Fourier transform Raman spectroscopy

The defects on the surfaces of GO, graphene and graphene-alkyne were analyzed by Fourier transform Raman spectrometer (Perkin Elmer, Spectrum GX). Moreover, The molecular structure at the surface of pristine PEDOT:PSS and dipped PEDOT:PSS films was also analyzed. A diode pumped Nd:YAG laser with a power of 50 mW was used for an excitation wavelength. Raman spectra were collected using a high-sensitivity InGaAs detector operated at room temperature.

3.2.3 Nuclear magnetic resonance (NMR) spectroscopy

Proton nuclear magnetic resonance (^{1}H NMR) was conducted on a BRUKER magnet system 400 MHz. The synthesized EDOT-Br and EDOT-N$_3$ were dissolved in

deuterated chloroform (CDCl$_3$, δ_H = 7.24 ppm) at room temperature using tetramethylsilane (TMS, δ_H = 0.0 ppm) as a reference.

3.2.4 X-ray photoelectron spectroscopy (XPS)

The surface chemistry was characterized on X-ray photoelectron spectroscope (XPS) (Shimadzu, ESCA-3400) equipped with non-monochromatic Mg-Kα radiation (1253.6 eV) as an excitation source at pressure $\leq$ 1$\times$10^{-5} Pa. The background in XPS data was subtracted using Shirley method [99] and the XPS curve-fitting was performed according to a Gaussian function at high resolution. The spectra in the C1s and N1s regions were deconvoluted by OriginPro 8.1 software to quantify the function groups.

3.2.5 Scanning electron microscopy (SEM)

The surface morphologies were observed by scanning electron microscope (SEM) (JEOL, JSM-6400) at an accelerating voltage of 10 and 15 kV and magnification of 500-5000. Re-dispersed graphene in de-ionized water as well as clicked and unclicked PEDOT:PSS-graphene aqueous solution were deposited onto glass and silicon substrates (Virginia Semiconductor Inc.) and air-dried at room temperature until completely dried composite films were accomplished. Composite films were then coated with gold layer using E1010 Hitachi ion sputtering device before SEM characterization. SEM was also coupled with energy dispersive X-ray analysis (EDX) at

an accelerating voltage of 15 kV. The EDX data was gathered to evaluate the elemental composition on the surface of the specimens.

3.2.6 Atomic force microscopy (AFM)

The surface topography and morphology of films were examined by atomic force microscope (AFM) (Veeco, USA) controlled by a Nanoscope IV in tapping mode. AFM is a surface analytical technique to give the high resolution images. The tapping-mode was used to scan the sample's surface. The sample was put onto the stack attached with carbon tape and then inserted and tipped into the microscope at adjusted maximum energy before sample scanning.

3.2.7 Ultraviolet-visible (UV-Vis) spectroscopy

The optical appearance of prepared films was measured by ultraviolet spectroscopy (Cary 5000 UV-Vis-NIR Spectrophotometer). The PEDOT:PSS was spin coated on the cleaned glass substrate at 1000 rpm for 40 seconds and dried on the hotplate at 150 $^{\circ}$C for a while, then the dried sample was loaded into the machine. The transmittance of each sample was measured over the wavelength range of 300 nm to 800 nm.

3.2.8 Thermogravimetric analysis (TGA)

Thermogravimetric analysis (TGA) was carried out on a Perkin Elmer (Pyris Diamond TG/DTA Simultaneous Thermal Analyser) to measure the thermal stability of PEDOT:PSS-graphene composite, i.e., degradation temperature and char yield. About 5-10 mg of sample was loaded in a ceramic pan and heated to 1000 $^{\circ}$C at a heating rate of 10 $^{\circ}$C/min under nitrogen purge at gas flow rate of 50 ml/min.

3.2.9 Electrical conductivity measurement

The electrical conductivity measurement of composites was done by four-point probe technique using a Keithley Instruments 6221 DC and AC current source and a Keithley 2182A nanovoltmeter. The clicked PEDOT:PSS-graphene solution was coated onto a glass slide and dried at room temperature forming a thin film. For the first part of this thesis, the four wires probe was used. The electrical conductivity (σ) can be calculated according to the Ohm's law, as $\sigma = L/(RWT)$, where L is the distance between wires (1.10 cm), W is the width of specimen (1.68 cm), T is the average thickness of specimen and R is the sheet resistance obtained from a slope of I-V curve.

For the second part of this thesis, the four probes arranged in line with same spacing was used instead of the four wires probes. This probe can measure the small sample as prepared spin coated films on glass substrate (2.5 cm x 2.5 cm). The electrical conductivity (σ) can be calculated as $\sigma = 1/(R_sT)$, where R_s is the sheet

resistance obtained using the equation $R_s = (\pi/\ln2)(V/I)$ and T is an average thickness of the thin films measured by surface profiler (Veeco Dektak 6M Stylus Profilometer).

CHAPTER IV

SYNTHESIS OF CLICKED PEDOT:PSS-GRAPHENE COMPOSITES

This chapter discusses about the electrical improvement of PEDOT:PSS by incorporation of graphene particles. Because of the poor dispersion of graphene in PEDOT:PSS, a large amount of graphene agglomerated causing the defects on the film surface. Thus, the interfacial interaction between PEDOT:PSS and graphene should be improved by click reaction .
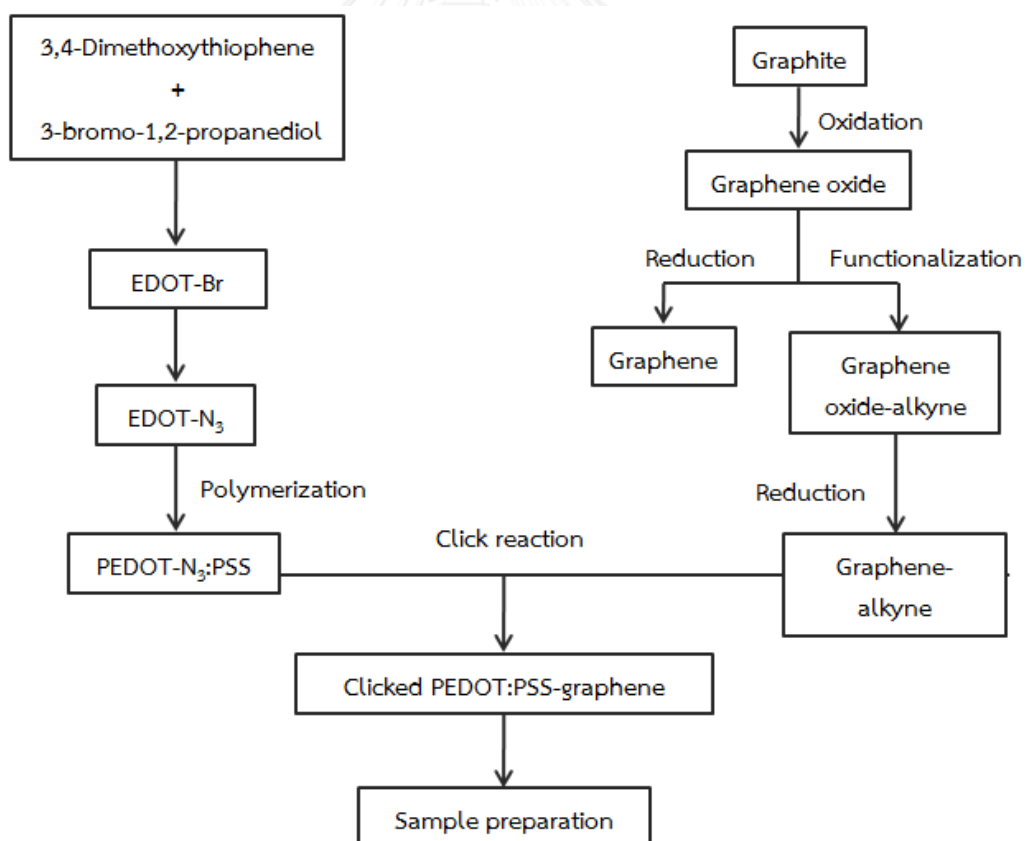
Figure 4.1 Preparation of clicked PEDOT-N$_3$:PSS-graphene

4.1 Experiment

The clicked PEDOT:PSS-graphene composite was prepared as shown in Figure 4.1. PEDOT-N$_3$:PSS was prepared by polymerization of EDOT-N$_3$ in presence of PSS while graphene and graphene-alkyne were synthesized by chemical method. Finally, both materials were coupled via click reaction. The preparation details were displayed further.

4.1.1 Synthesis of 3,4-(1-bromomethylethylene)dioxythiophene (EDOT-Br)
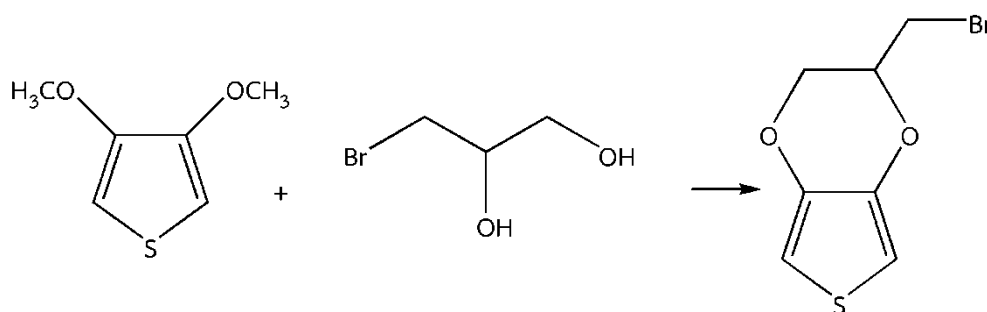
Figure 4.2 Synthesis of EDOT-Br

Synthesis of EDOT-Br was carried out according to a research done by Daugaard and coworkers [100]. 3,4-Dimethoxythiophene (0.41 g), 3-bromo-1,2-propanediol (1.11 g), and *p*-toluene sulfonic acid (80 mg) were mixed in a 100 ml one-necked round bottom flask. 30 ml of toluene was then added and stirred at 100 °C for 48 hours. After cooling down to room temperature, solvent was removed by rotary evaporation and the resultant solid was dissolved in CH$_2$Cl$_2$ and extracted with aqueous Na$_2$CO$_3$ and

de-ionized water several times. The organic phase was gathered, dried with anhydrous

$NaSO_4$, filtered, and concentrated in a rotary evaporator. The collected product was

purified by column chromatography (silica gel) using hexane/ethyl acetate (8/2, v/v) as

eluent. ^1H NMR (CDCl$_3$, 400 MHz, δ_H, ppm): 3.50-3.63 (m, 2H, CH$_2$-Br); 4.05-4.35 (m, 3H,

O-CH$_2$-CH-O); 6.38-6.40 (d, 2H, S-CH).

4.1.2 Synthesis of 3,4-(1-azidomethylethylene)dioxythiophene (EDOT-N$_3$)
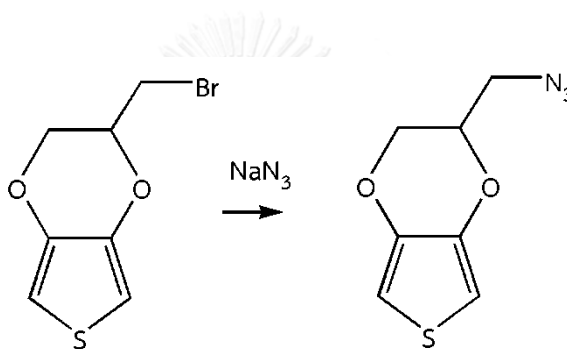
Figure 4.3 Synthesis of EDOT-N$_3$

EDOT-Br (0.22 g), NaN$_3$ (0.08 g) and DMF (10 ml) were vigorously stirred in a

conical flask at room temperature for 24 hours. Then, de-ionized water (15 ml) was

added and the solution was extracted with diethyl ether (5✕15 ml). The combined

organic phase was further extracted with de-ionized water several times and dried with

anhydrous $NaSO_4$. Afterwards, the collected product was concentrated using rotary

evaporator to remove remaining water. ^1H NMR (CDCl$_3$, 400 MHz, δ_H, ppm): 3.49-3.61

(m, 2H, CH$_2$-N$_3$); 4.05-4.33 (m, 3H, O-CH$_2$-CH-O); 6.38-6.40 (d, 2H, S-CH).

4.1.3 Polymerization of EDOT-N$_3$ and PSS
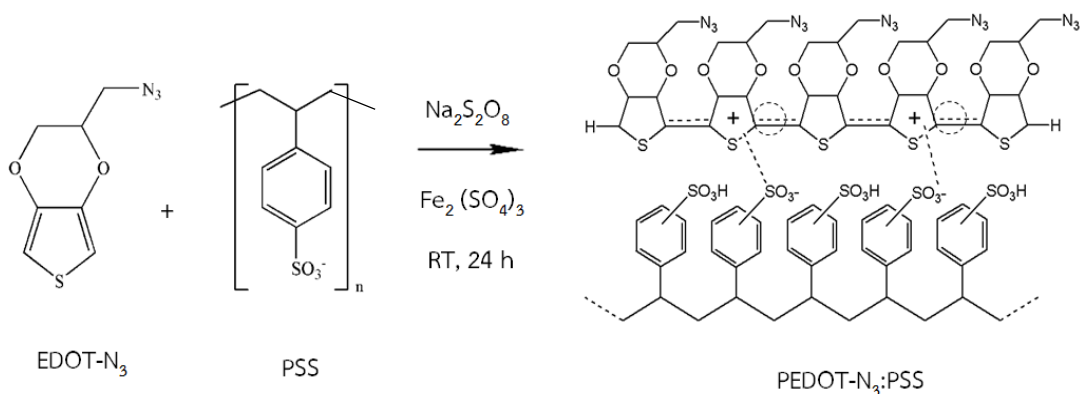
Figure 4.4 Polymerization of PEDOT-N$_3$:PSS

EDOT-N$_3$ (20 mg), 18 wt% PSS aqueous solution (278 mg) and Na$_2$S$_2$O$_8$ (33.4 mg) were dissolved in de-ionized water (5 ml) in a 10 ml amber glass bottle and stirred for 1 hour to get homogeneous solution. The click reaction was initiated when iron (III) *p*-toluene sulfonate (41.8 mg) as catalyst was added and the reaction mixture was stirred at room temperature for 24 hours, yielding a dark blue homogeneous solution. The crude product was purified with cation exchange resin (Amberlite IR-120) in hydrogen form and anion exchange resin (Amberlite IRA-400) in chloride form.

4.1.4 Synthesis of graphene oxide

Graphene oxide (GO) was prepared from high-purity natural graphite powder according to a modified Hummers method [101]. Graphite powder (2 g), H$_2$SO$_4$ (50 ml), and NaNO$_3$ (1 g) were stirred in a 100 ml one-necked round bottom flask immersed in

an ice bath at temperature below 20 ^{o}C for 15 minutes. KMnO$_4$ (6 g) was slowly

dropped and stirred in an ice bath for 2 hours and at room temperature for another 2

hours. After that, de-ionized water (100 ml) was then added into the mixture. At this

step, the temperature of the mixture was dramatically increased and after cooling

down to approximately 60 ^{o}C, H$_2$O$_2$ was gently added until a color became yellow

brown indicating the complete reaction. Next, 500 ml of aqueous HCl (1/20, v/v) were

added into the oxidized suspension. The brown suspension was centrifuged and

washed with de-ionized water repeatedly until pH was neutral. Re-suspended GO slurry

in de-ionized water was dried by freeze-drying process obtaining a fine dark brown

powder.

4.1.5 Chemical reduction of GO with hydrazine

GO (100 mg) was re-dispersed in de-ionized water (100 ml) by ultrasonication

for 45 minutes, yielding a homogeneous brown suspension. The aqueous GO

suspension and hydrazine (hydrazine/GO, 7/10, w/w) were poured into a 250 ml one-

necked round bottom flask equipped with reflux condenser and magnetic stirrer.

Chemical reduction was carried out at 95 ^{o}C for 10 hours. The graphene suspension

was washed with de-ionized water, filtered through PTFE membrane (47 mm in

diameter, 0.45 μm pore size; Membrane solutions) to remove excess hydrazine, and

then centrifuged to collect graphene particles. Re-suspended graphene slurry in de-

ionized water was freeze-dried for 3 days. The graphene powder was collected and kept in desiccator.

4.1.6 Synthesis of terminal alkyne-modified graphene sheets

Graphene-alkyne sheets were prepared by functionalizing GO via amidation reaction followed by chemical reduction. GO (30 mg) was re-dispersed in DMF (130 ml) in a 250 ml one-necked round bottom flask by ultrasonication for 45 minutes before a solution of 4-ethynylaniline (87 mg) in DMF (20 ml) and DCC (4.1 g) were added. The amidation was run at 90 $^{\circ}$C under N_2 flow for 2 hours followed by filtered through PTFE membrane and washed with ethanol. The crude product was then re-suspended in 30 ml of de-ionized water by ultrasonication for 20 minutes. Next, hydrazine was added and stirred at 95 $^{\circ}$C for 10 hours. After the chemical reduction was complete, the suspension was centrifuged and washed with de-ionized water until pH was neutral. Re-suspended graphene slurry in de-ionized water was freeze-dried for 3 days. The dried powder was collected and kept in the desiccator.

4.1.7 Click chemistry of graphene-alyne with PEDOT-N$_3$:PSS
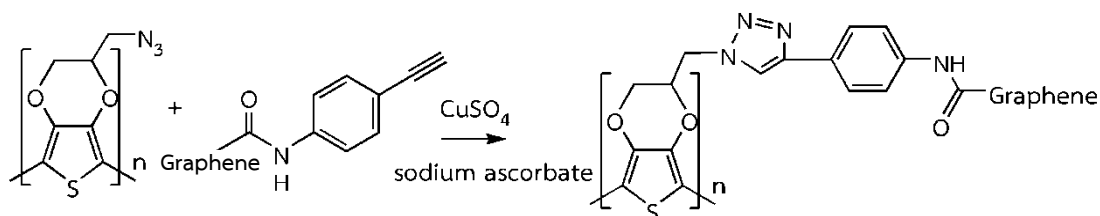
Figure 4.5 Click reaction between PEDOT-N$_3$ and alkyne-modified graphene

The determined amount of terminal alkyne-modified graphene was re-dispersed in PEDOT-N$_3$:PSS (5 ml) in a 20 ml amber glass bottle by ultrasonication for 45 minutes. Then, a premixed aqueous solution of CuSO$_4$ (0.1 M, 6.55 μmol) and sodium ascorbate (0.1 M, 19.6 μmol) was added into the suspension. The clicked PEDOT:PSS-graphene product was obtained after stirring at room temperature for 48 hours. The final product was contained in an amber bottom and stored in the refrigerator at the temperature lower than 20°c.

4.1.8 Preparation of composite films

To avoid confusion for readers, we would like to explain terms of "unclicked composites" representing composites prepared from PEDOT-N$_3$:PSS and un-functionalized graphene, and "clicked composites" given from PEDOT-N$_3$:PSS and alkyne-functionalized graphene. The clicked PEDOT:PSS-graphene aqueous solution was ultrasonicated for 45 minutes and coated on silicon substrates and pre-cleaned

glass slides for SEM and electrical conductivity measurements, respectively. Then, the composites were obtained after water removal by drying in air at room temperature for 18 hours.

4.2 Results and discussion

To investigate the chemical structures of clicked PEDOT:PSS-graphene composite, Fourier transform infrared spectroscopy (FTIR), Raman spectroscopy and X-ray photoelectron spectroscopy (XPS) were carried out. Thermal stability and electrical conductivity of composite films with different graphene loadings were also measured by thermogravimetric analysis (TGA) and four-point probe, respectively. The surface morphology of clicked composite film was monitored in comparison with unclicked composite film by scanning electron microscopy (SEM). The chemical structure of clicked PEDOT:PSS-graphene synthesized via click reaction of PEDOT-N_3:PSS and graphene-alkyne as shown in Figure 4.6.
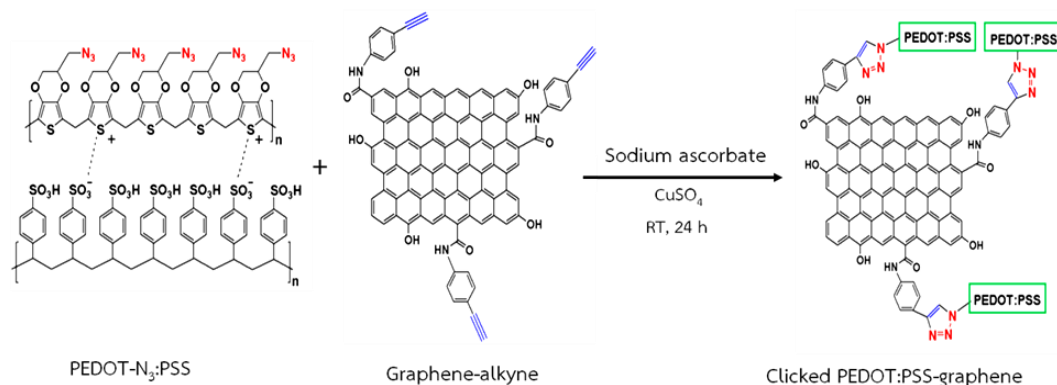
Figure 4.6 Click reaction between PEDOT-N_3:PSS and graphene alkyne

4.2.1 FTIR analysis

Graphene was prepared from graphite via a modified Hummers method. Then, alkyne-modified graphene and azide-modified PEDOT:PSS were synthesized. Further, these two functionalized materials were clicked using copper sulfate catalyst as illustrated in Figure 4.6. The chemical structures and surface chemistry were mainly analyzed by FTIR and XPS spectroscopy, respectively. The synthesized graphene from natural graphite flake was characterized by FTIR as shown in Figure 4.7a. It should be mentioned that broad bands of hydroxyl groups and adsorbed water molecules (ν_{O-H}) can be detected at 3435 cm^{-1} for all spectra. In addition, weak signals at 2926 cm^{-1} and 2855 cm^{-1} were corresponded to aliphatic CH$_2$ and CH$_3$ stretching (ν_{C-H}), respectively. After treating graphite with strong acid, carbon double bonds of graphite were oxidized into several attached oxygen-containing groups on GO skeleton as follows: a strong carbonyl stretching ($\nu_{C=O}$) of carboxylic and ketone at 1716 cm^{-1}, O-H bending (δ_{C-OH}) in carboxylic and carbonyl at 1398 cm^{-1}, C-O stretching (ν_{C-O}) of carbonyl at 1042 cm^{-1}, and epoxy ring at 1217 cm^{-1}. Moreover, a peak at 1612 cm^{-1} was also displayed, which is associated with the superimposed bands of carbonyl ($\nu_{C=O}$) and C=C stretching ($\nu_{C=C}$) of un-oxidized graphite. The spectrum of graphene exhibited a decrease in intensity of peaks at 1398 cm^{-1}, 1217 cm^{-1} and 1042 cm^{-1}, implying that the oxygen functionality (i.e., epoxide groups and hydroxyl groups) of GO were chemically reduced with hydrazine hydrate.
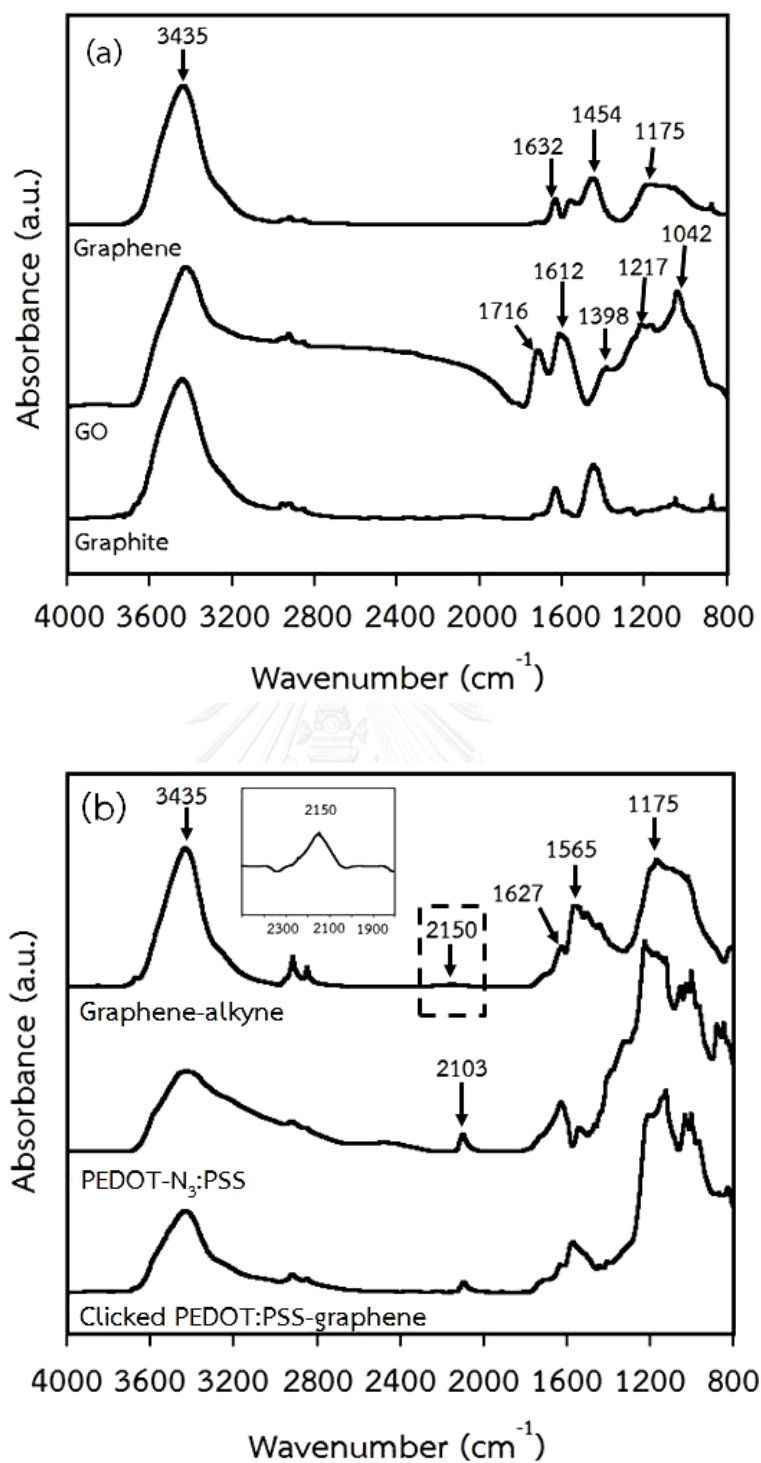
Figure 4.7 FTIR spectra of (a): graphite, GO, and graphene. (b): graphene-alkyne,

PEDOT-N$_3$:PSS, and clicked PEDOT:PSS-graphene composite. An inset is a magnified

FTIR peak of graphene-alkyne at about 2150 cm^{-1}

Furthermore, the absence of peaks at 1716 cm^{-1} and 1612 cm^{-1} and the presence of a new C=C skeleton vibration at 1632 cm^{-1} indicated that graphene was successfully synthesized from GO. The functionalization of graphene and PEDOT:PSS was also proved by FTIR spectroscopy (Figure 4.7b). Alkyne-modified graphene spectrum illustrated an amide carbonyl peak at 1627 cm^{-1} and amide N-H in-plane stretching at 1565 cm^{-1} [102], which confirmed the successful amidation reaction between carboxylic groups at the edges of graphene sheets and amine groups of 4-ethynylaniline. The existence of reactive terminal alkyne absorption band ($\boldsymbol{v}_{C\equiv C}$) at 2150 cm^{-1} was also observed; however, its intensity was very weak due to its high symmetry resulting in difficulty to detect by FTIR measurement [103], as displayed in an inset. FTIR spectrum of PEDOT-N$_3$:PSS demonstrated an azide stretching ($\boldsymbol{v}_{N=N^+=N^-}$) at 2103 cm^{-1}. Nevertheless, an intensity of azide band was decreased significantly after click reaction owing to the reaction with alkynes of graphene. The conversion of click reaction was estimated to be approximately 77% which was calculated from the relative areas of azide bands of pristine PEDOT-N$_3$:PSS and clicked PEDOT:PSS-graphene composite. The unreacted azide residue from click reaction was expected to remain there due to the steric hindrance of graphene sheets.

4.2.2 Raman analysis
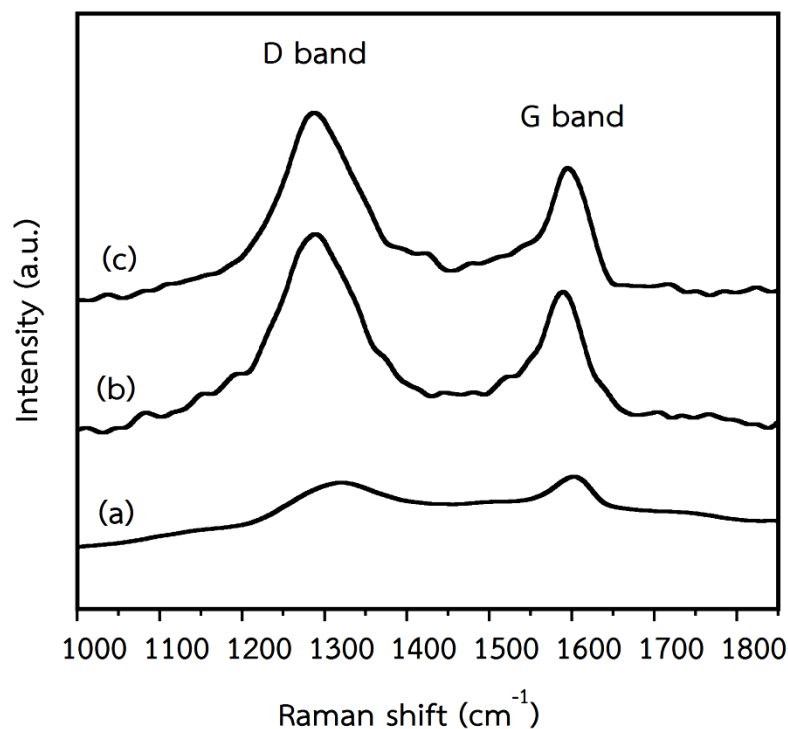
Figure 4.8 Raman spectra of (a) GO; (b) graphene; (c) graphene-alkyne

The changes in chemical structures of synthesized GO, graphene, and graphene-alkyne were detected using Raman spectroscopy. There are two important peaks: D band indicating defective and disordered carbon structures, and G band referring in-plane sp^2-hybridized carbon atoms (C=C). Moreover, integrated intensity ratio of D band to G band (I_D/I_G) is acquired to quantitatively characterize the defect of graphitic materials [104]. As displayed in Figure 4.8a, GO displayed a strong G band at ~1603 cm^{-1} and a broad D band at ~1321 cm^{-1} (I_D/I_G = 0.97). After chemical reduction, Raman spectrum of graphene (Figure 4.8b) exhibits the shifts of G band and D band to ~1589 and ~1289 cm^{-1} with I_D/I_G ratio of 1.32, which is

considerably higher than that of GO. This result indicates that chemical reduction decreased the size of in-plane sp^2 domains and an increase in degree of disorder and edge planes of synthesized graphene. In comparison to the Raman spectrum of synthesized graphene, the Raman spectrum of graphene-alkyne (Figure 4.8c) displayed a slight shift of G-band to ~1595 cm^{-1} owing to better exfoliation of functionalized graphene sheets, and a constant I_D/I_G ratio of 1.33 indicated that the defect-induced structure does not change after amidation reaction.

4.2.3 XPS analysis

The surface chemistry of synthesized GO, graphene, graphene-alkyne and PEDOT:PSS was also studied by XPS. In Figure 4.9, XPS spectrum of graphene revealed smaller intensity at O1s regions than that of GO because the oxygen functionalities of GO were mostly removed through reaction with hydrazine hydrate, as already discussed in FTIR results. Furthermore, N1s of graphene-alkyne (Figure 4.9c) at binding energy of ~400 eV was clearly observed, which confirm that amide linkages occurred from the amidation between carboxylic groups of graphene and the amine groups of 4-ethylnylaniline.

The deconvoluted C1s spectra of unmodified graphene, as displayed in the Figure 4.10a, present 6 different characteristics of carbon bonds. A large peak at 285.0 eV corresponded to sp^2 and sp^3 C-C carbon of non-oxygenated ring.
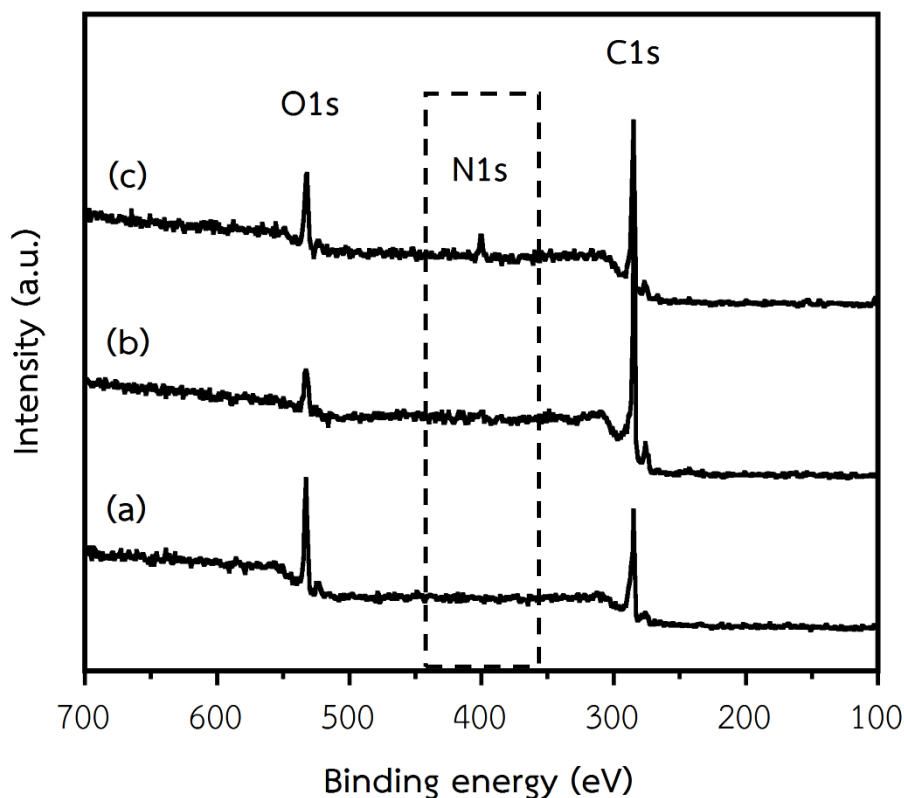
Figure 4.9 XPS spectra of (a) GO; (b) graphene; (c) graphene-alkyne

Moreover, C-O of hydroxyl (285.7 eV) and epoxy groups (286.6 eV), C=O of carboxyl (287.9 eV), O=C-OH (289.8 eV), and delocalized π-π^* electron of aromatic network (291.9 eV) were also proved [105, 106]. In the case of graphene-alkyne (Figure 4.10b), there are two new peaks at 283.9 and 288.8 eV, assigned to alkyne moiety (C≡C) and O=C-N bond, respectively. The other components were listed as follows: sp^2 and sp^3 carbon (285.0 eV), C-OH (285.7 eV), C-O (286.6 eV), C=O (287.8 eV), O=C-OH (290.0 eV), and π-π^* (291.7 eV). Hence, these XPS data evidenced the attachment of alkyne on graphene sheets. Additionally, a high-resolution N1s core-level spectrum of PEDOT-N$_3$:PSS (Figure 4.11a) comprised at least two distinct nitrogen atoms at 402.6

eV and 404 eV which are attributed to C-N and a negatively charged nitrogen atom of terminal azide (N=N$^+$=N$^-$), respectively. In addition, a shoulder peak which should be attributed to a positively charged nitrogen atom (N=N$^+$=N$^-$) was difficult to be seen in this research. After click reaction, a single C-N peak of thiazole linkage was newly generated at 402.5 eV, whereas N1s spectra of alkyne and azide were totally disappeared (Figure 4.11b). These XPS results were different from FTIR results, which showed a residue of azide group. We anticipated that click reaction between graphene-alkyne and PEDOT-N$_3$:PSS may not give 100% conversion and some of the azide groups were unreacted since azide stretching is very active and can be potentially detected by FTIR measurement [103].
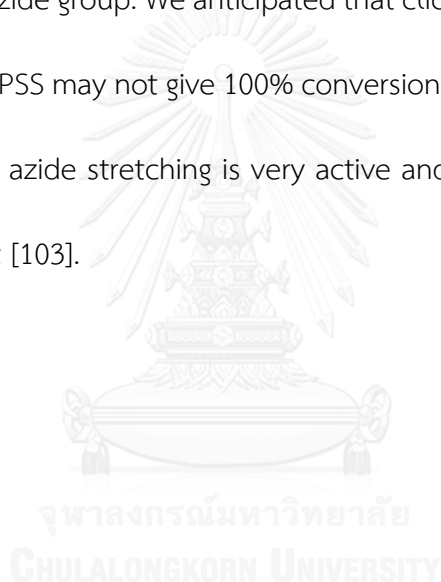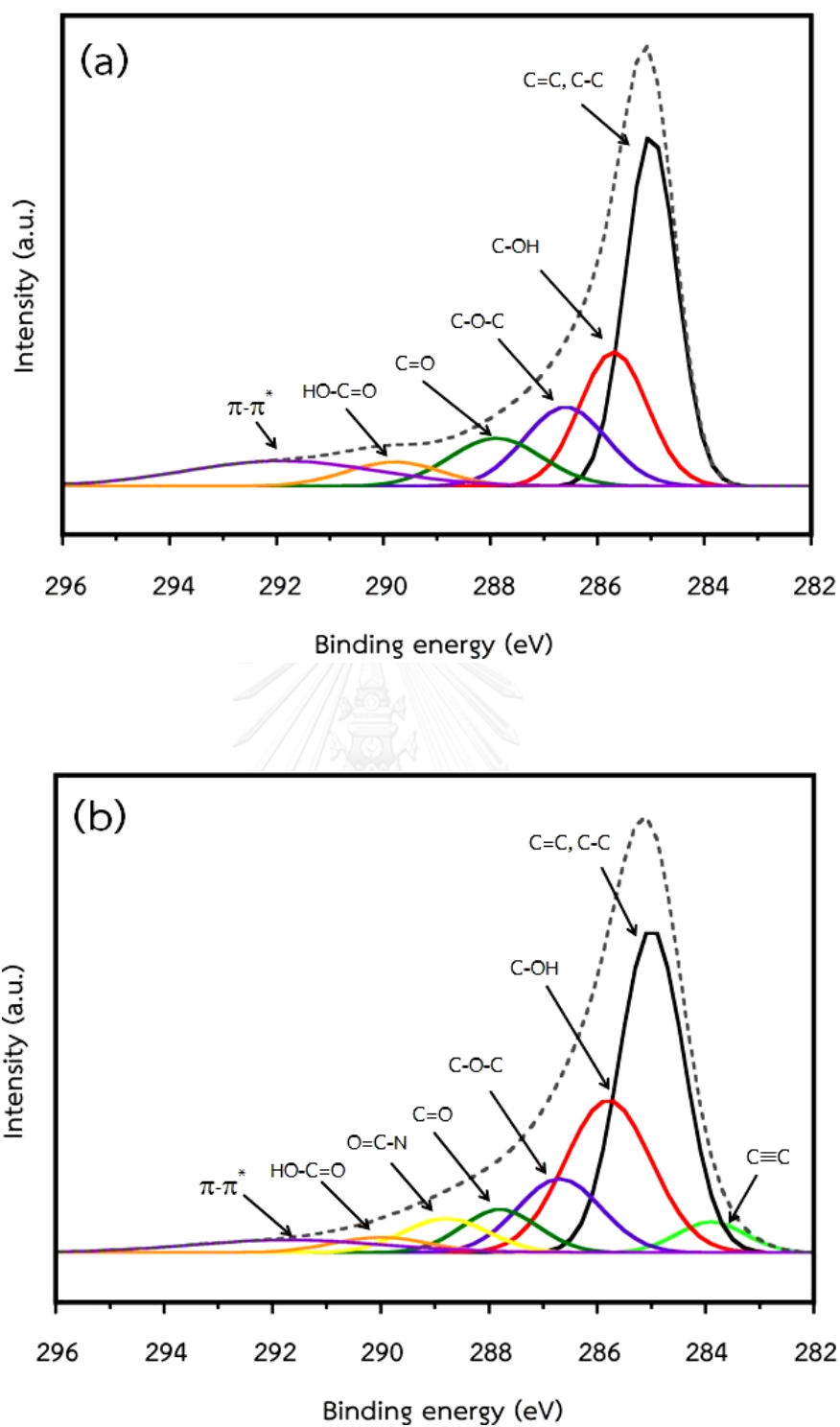
Figure 4.10 Deconvolution of XPS spectra: (a) C 1s region of graphene and

(b) C 1s region of graphene-alkyne
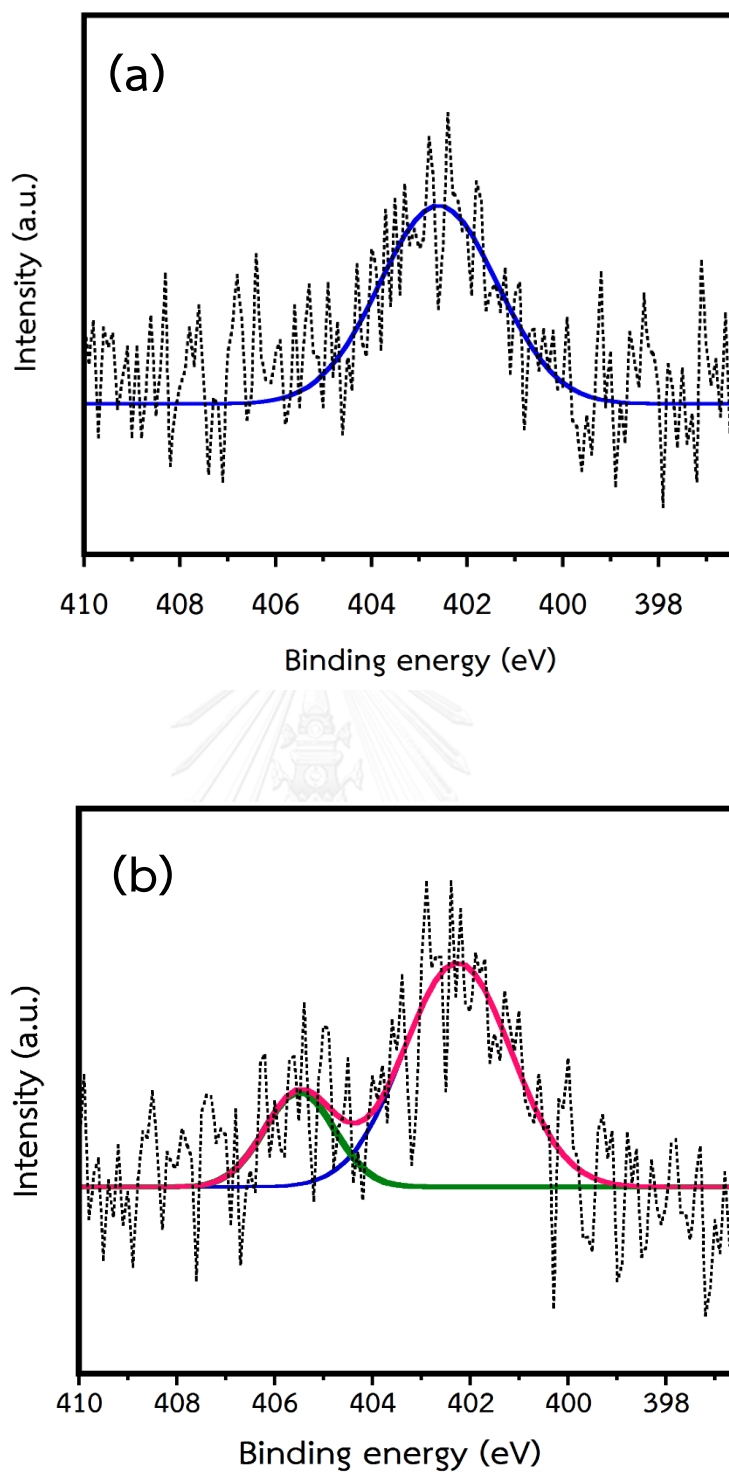
Figure 4.11 Deconvolution of XPS spectra: (a) N 1s region of PEDOT-N$_3$:PSS and

(b) N 1s region of clicked PEDOT:PSS-graphene composites

4.2.4 Dispersibility of GO and GO-alkyne

Graphene and graphene-alkyne were similarly difficult to disperse in water because graphene and alkyne group possess hydrophobic properties. From this reason, we expected that comparing the dispersibility difference between GO and GO-alkyne (which was reduced with hydrazine in the following step) instead can preliminarily identify the presence of non-polar alkynes on GO sheets. GO and GO-alkyne were ultrasonicated in mixed water/hexane solvents (1/1, v/v) for 45 minutes and monitored after leaving for 1 day. As illustrated in Figure 4.12, GO was stabilized in aqueous phase (lower layer) due to the polar hydroxyl and carbonyl group. On the other hand, GO-alkyne was moved and precipitated in organic phase (upper layer), which directly caused by the effect of grafted non-polar alkynes.

Figure 4.12 Dispersion of GO (left) and GO-alkyne (right) in water/hexane (0.5 mg/ml)

4.2.5 Surface morphology of composites

The surface morphologies of PEDOT:PSS film, graphene, and composite films were carried out by SEM observation. PEDOT:PSS film depicted very smooth surface (Figure 4.13a). Besides, graphene particle has an individual sheet-like characteristic (Figure 4.13b). At graphene loading of 1 wt%, unclicked PEDOT:PSS-graphene composite film (Figure 4.14a) showed higher surface roughness and more defects (dashed circles) than clicked PEDOT:PSS-graphene composite film (Figure 4.14b), indicating the poor dispersion and agglomeration of graphene. The reaction between graphene-alkyne and PEDOT-N_3:PSS via click chemistry created covalent thiazole linkages which enhance interfacial interaction and compatibility between graphene sheets and PEDOT:PSS matrix; therefore, clicked PEDOT:PSS-graphene composite film showed well dispersed graphene in polymer matrix.
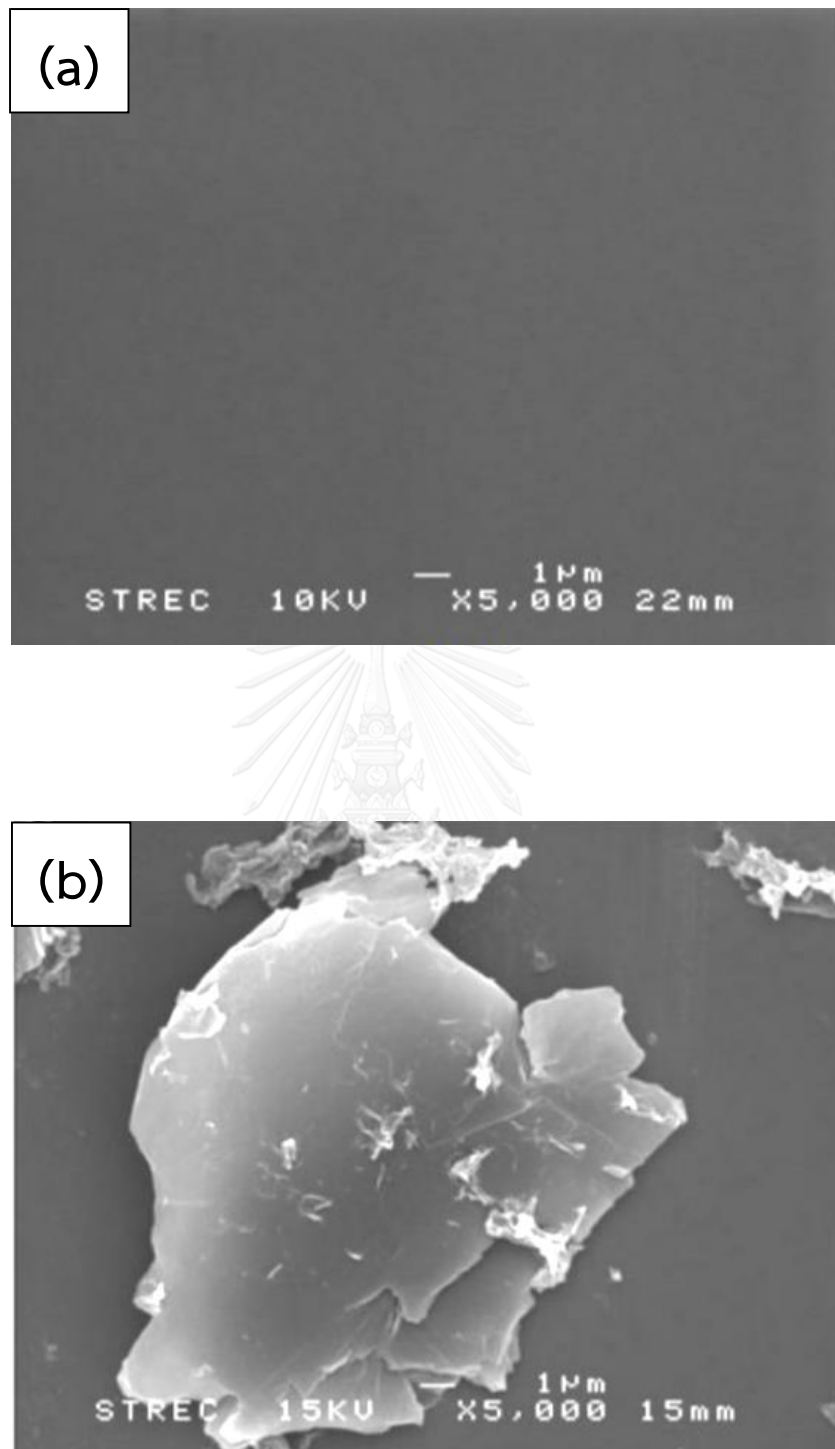
Figure 4.13 SEM images of the surface of (a) PEDOT:PSS and (b) graphene
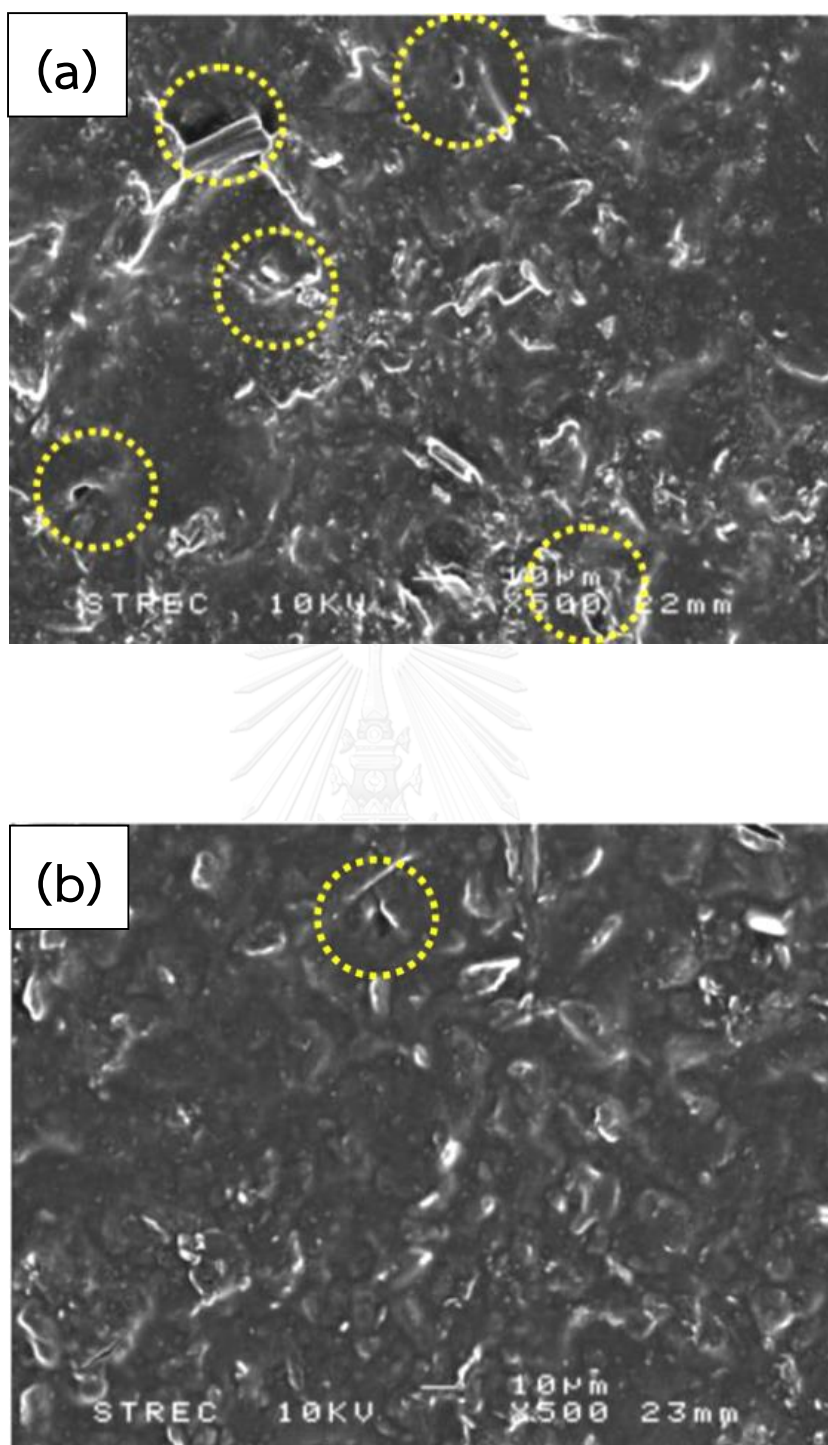
Figure 4.14 SEM images of the surface of (a) unclicked PEDOT:PSS-graphene

composite at 1 wt% graphene loading and (b) clicked PEDOT:PSS-graphene

composite at 1 wt% graphene loading

4.2.6 Thermal stability of composites
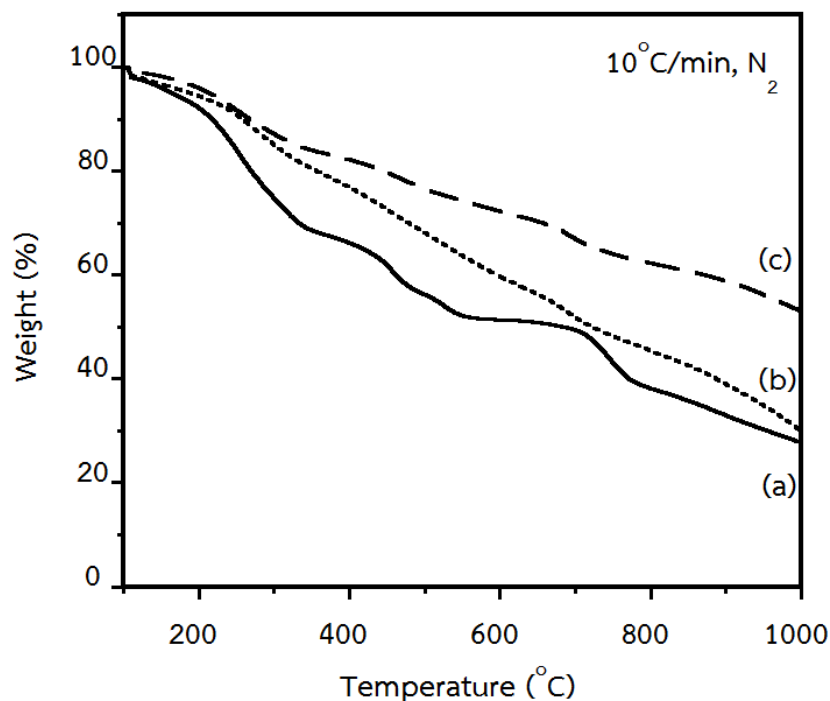
Figure 4.15 TGA curves of (a) PEDOT-N$_3$:PSS; (b) clicked PEDOT:PSS-graphene

composite; (c) unclicked PEDOT:PSS-graphene composite at 5 wt% graphene loading

Degradation temperature for 10 % weight loss (T_d) and char yield at 1000 $^{\circ}$C

(CY) acquired by TGA analysis under a nitrogen flow are selected as references to

collate thermal stabilities of PEDOT-N$_3$:PSS and composites, as illustrated in Figure

4.15a-c. Even though all samples were vacuum dried before testing in order to

eliminate moisture, they demonstrated slight weight loss around 100-110 $^{\circ}$C, which is

assigned to the evaporation of adsorbed water residue. It can be seen that PEDOT-

N$_3$:PSS (T_d = 217 $^{\circ}$C, CY = 27.7 %) was less thermally stable than clicked PEDOT:PSS-

graphene composites (T_d = 258 $^{\circ}$C, CY = 29.9 %) and unclicked PEDOT:PSS-graphene

composites (T_d = 267 $^{\circ}$C, CY = 53.0 %) at 5 wt% graphene loading because of high inherent thermal stability of graphene (T_d = 679 $^{\circ}$C, CY = 76.1 %). The destruction of amorphous carbon atom of graphene was referred in the previous work presenting between 200°C to 600°C. PSS decomposes in a temperature range of 100-370 $^{\circ}$C, while PEDOT backbone decomposes at temperature higher than 400 $^{\circ}$C [107]. Then, the weight loss in the temperature range higher than 400°C of composites was expected to be the degradation of graphene and PEDOT. Besides, TGA results present the same trend for composites at other loadings. Interestingly, the clicked PEDOT:PSS-graphene composites revealed lower thermal stability than the unclicked ones as a result of a loss of amide linkages, formed during functionalizing graphene with alkyne via amidation reaction, as well as cleavages of remaining oxygen-functionalities on graphene surface.

4.2.7 Electrical conductivity of composites

Figure 4.16 shows the electrical conductivities of composites at 1, 3 and 5 wt% graphene contents measured by four-point probe. The electrical conductivity of neat PEDOT:PSS film was 4.98$\times$10^{-2} S/cm and it gradually increased as graphene content increased. It is worth noting that the electrical conductivity of PEDOT:PSS strongly depends on film morphology [106]. The unclicked PEDOT:PSS-graphene composites exhibited lower electrical conductivities than those of clicked PEDOT:PSS-graphene composites resulting from the agglomeration of graphene in PEDOT:PSS matrix and

defects on the composites surface, as evidenced by SEM images (Figure 4.14a-b). These defects were the causes of discontinuous electron transmission pathway. On the contrary, clicked PEDOT:PSS-graphene composites demonstrated well dispersion mainly due to the fact that formed thiazole linkages improved interfacial interaction between graphene sheets and PEDOT:PSS matrix, increasing electrical conductivity of the films.
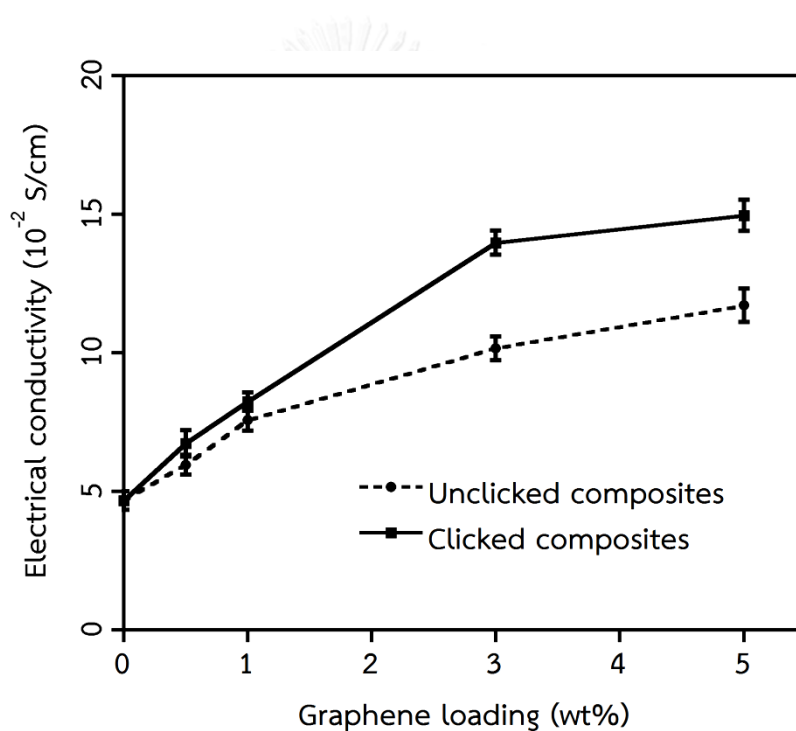
Figure 4.16 Electrical conductivities of unclicked and clicked PEDOT:PSS-graphene composites

CHAPTER V

DIPPING TREATMENT OF PEDOT:PSS FILMS IN AQUEOUS DMSO

SOLUTION

According to chapter IV, the electrical conductivity is slightly improved which is less than our expectation and the preparation is quite complicated. Then, the solvent treatment is applied for improving the electrical property of dried PEDOT:PSS films. This chapter shows the experiment and the results of a post treatment on the PEDOT:PSS films by dipping in aqueous DMSO solution. The PEDOT:PSS dispersion is fabricated on glass substrates by spin coating technique and subsequently dipping into an aqueous DMSO solution. The low concentration range of DMSO in water between 0 - 5 vol% is studied in comparison with pure water and pure DMSO. The effect of the concentration of DMSO in aqueous solution on the surface morphology, surface chemistry and electrical conductivity of the PEDOT:PSS thin films in the dipping process is investigated.

5.1 Experiment

The commercial PEDOT:PSS material was filtered through a glass membrane with 0.45 μm pore size and spin coated (G3P-8 Spincoat, Cookson electronics equipment) at 1500 rpm for 40 seconds on the glass substrates, which were

sequentially cleaned before use in an ultrasonic bath with detergent, de-ionized water, acetone and isopropyl alcohol, respectively. Subsequently, drying was carried out on a hot plate at 150 °C for 20 minutes in an ambient air. The prepared thin films were eventually dipped for 20 seconds in water or DMSO or an aqueous DMSO solution at various concentrations, ranged between 0 vol% to 5 vol%, followed by drying on a hot plate at 150 °C for few minutes.

5.2 Results and discussion

5.2.1 Electrical conductivity enhancement of PEDOT:PSS thin films via dipping method

The electrical conductivity of pristine PEDOT:PSS and dipped PEDOT:PSS films is shown in Figure 5.1. The pristine PEDOT:PSS film has low electrical conductivity of ~0.3 S/cm. Dipping in pure water leads to a slight increase in electrical conductivity to 1.8 S/cm possibly because of the physical removal of excess insulting PSS layer from the surface of the thin films, which is consistent with the work done by DeLongchamp et al. [108]. Interestingly, the electrical conductivity of the PEDOT:PSS films dipped in aqueous DMSO solutions is steadily improved at low concentrations of DMSO and then approached the constant value of 380 S/cm at 2 vol% of DMSO in solution, which is similar to those dipped in pure DMSO in our study (as displayed in a dashed line).
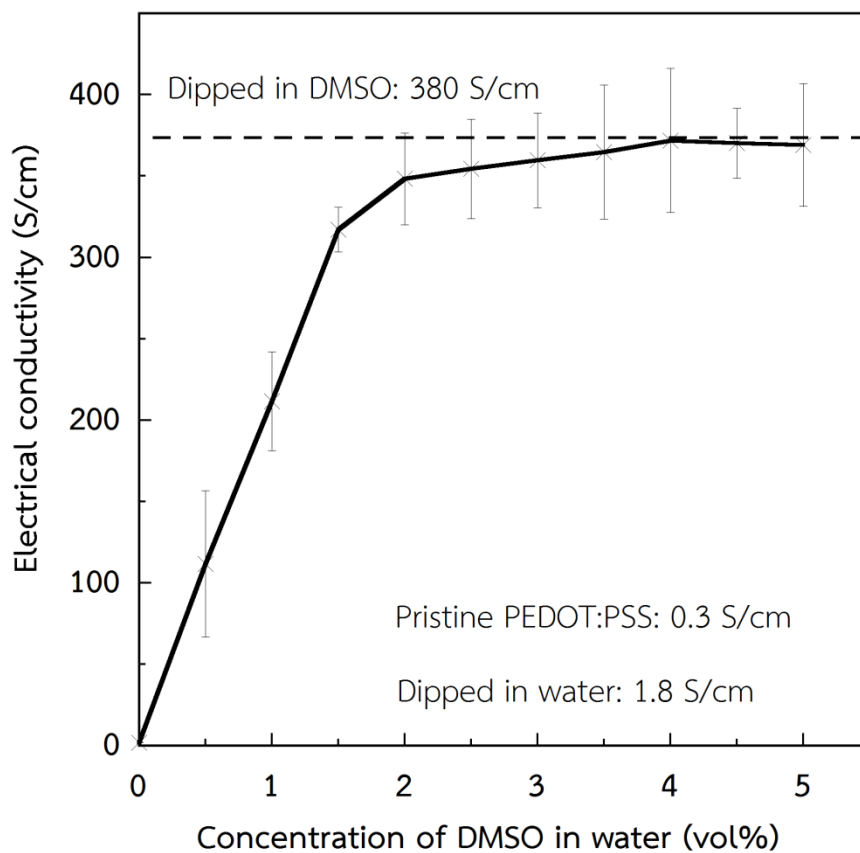
Figure 5.1 Electrical conductivity of PEDOT:PSS films dipped in various DMSO

concentrations. The dash line represents the electrical conductivity of the film

dipped in pure DMSO

These results imply that the use of a low concentration aqueous DMSO

solution with the dipping method shows the more practical process because this

technique is easier and requires shorter operating time than that of doping method

with DMSO, and only a small amount of high-boiling point DMSO is incorporated.

5.2.2 Raman spectroscopy

The molecular structure at the surface of pristine PEDOT:PSS and dipped PEDOT:PSS films are investigated by Raman spectroscopy as depicted in Figure 5.2 All samples display the band between 1300 and 1600 cm^{-1}, corresponding to the stretching vibration of carbon atoms on thiophene rings of PEDOT chains. The strong intensity at ~1427 cm^{-1} represents the C_α-C_β stretching vibration in favor of a quinoid structure, whereas the shoulder at ~1448 cm^{-1} is assigned to the stretching of C_α=C_β as to be favorable to a coil-like benzoid structure.
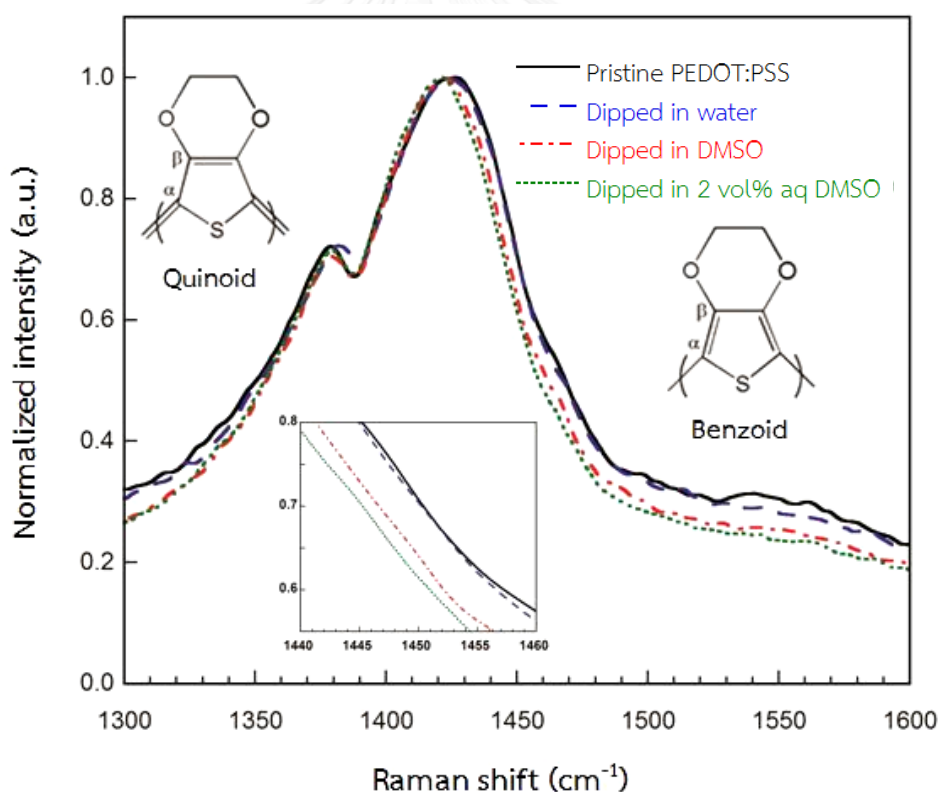
Figure 5.2 Raman spectra of pristine PEDOT:PSS film and dipped PEDOT:PSS films

In case of dipping in pure DMSO and aqueous DMSO solutions, the intensity of the benzoid structure is weakened and the band is red-shifted and becomes narrower, indicating that the PEDOT chains transform from a coil structure to a linear or expanded-coil structure [109]. It is expected that this conformational change is responsible for the enhanced electrical conductivity upon dipping in pure DMSO and aqueous DMSO solutions because the linear interchain interaction declines the energy barrier of the PEDOT chains, facilitating the charge delocalization along the π–conjugated PEDOT backbones [40]. On the other hand, the intensity of the films dipped in pure water demonstrates an insignificant change in comparison with that of pristine PEDOT:PSS films, suggesting that the benzoid-quinoid transformation rarely takes place. Therefore, a slight increase (~6 times) in the conductivity of films after treatment with pure water could be contributed to the washing effect of unassociated PSS rather than the conformational change.

5.2.3 XPS analysis

The washing effect of the unassociated PSS from PEDOT:PSS surface after dipping process is evaluated by comparing the XPS sulfur S2p core-level spectra, as demonstrated in Figure 5.3. The XPS spectra of all samples reveals the main peak between 167 and 171 eV, which is associated with the sulfur atoms of the complex PSS fragments containing poly(styrene sulfonic acid) (PSSH) and anionic polyelectrolyte poly(sodium styrene sulfonate) (PSSNa) [110].
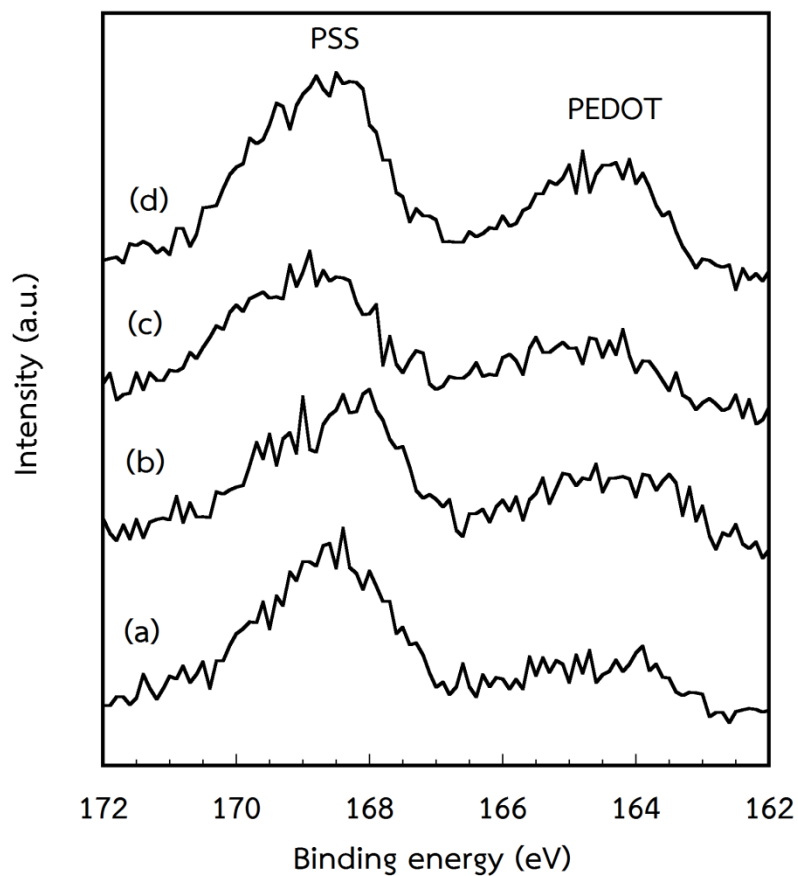
Figure 5.3 XPS S2p core-level spectra of (a) pristine PEDOT:PSS film and PEDOT:PSS

films dipped in (b) water, (c) DMSO and (d) 2 vol% of aqueous DMSO

The formation of PSSNa can possibly be explained by the presence of $Na_2S_2O_8$ as the

oxidizing agent upon the polymerization of PEDOT [111]. Further, the S2p contribution

peak between 163 and 167 eV is attributed to the spin-split components of the sulfur

atoms of the PEDOT chains. The area ratio of PSS to PEDOT is calculated to estimate

the content of remaining PSS after the surface treatment; in addition, it is found that

the area ratio for pristine PEDOT:PSS film is 3.17, meanwhile the ratios are 1.79, 1.94,

and 1.74 for the films dipped in water, DMSO, and 2 vol% of aqueous DMSO,

respectively. In other words, the existence of water in the used solvents is of great importance to remove the PSS by the dipping method. The XPS results also indicate that the surface composition is significantly changed after the dipping process. Namely, a great loss of insulating PSS fraction from the film surface can be described through the fact that the phase separation of unassociated PSS causes the enrichment of PSS on the film surface which is washed away by solvents upon dip-treatment, leading to a decreased film thickness and enhanced electrical conductivity. Moreover, it is worth mentioning that the removal of PSS is an advantage of the dipping technique because PSS acid exhibits hygroscopic property; the film surface containing of a PSS layer can absorb water which could reduce the stability of the film in moist condition over time.

5.2.4 Surface morphology and elemental composition

The surface morphology of PEDOT:PSS films coated on the glass substrates is observed by SEM. The surfaces of pristine PEDOT:PSS films (Figure 5.4a) and PEDOT:PSS films treated with pure water (Figure 5.4b) are relatively smooth; however, the crinkles on the film surface are clearly detected in case of pure water as indicated by inserted arrows which might be due to the peeling off of the film upon immersion.
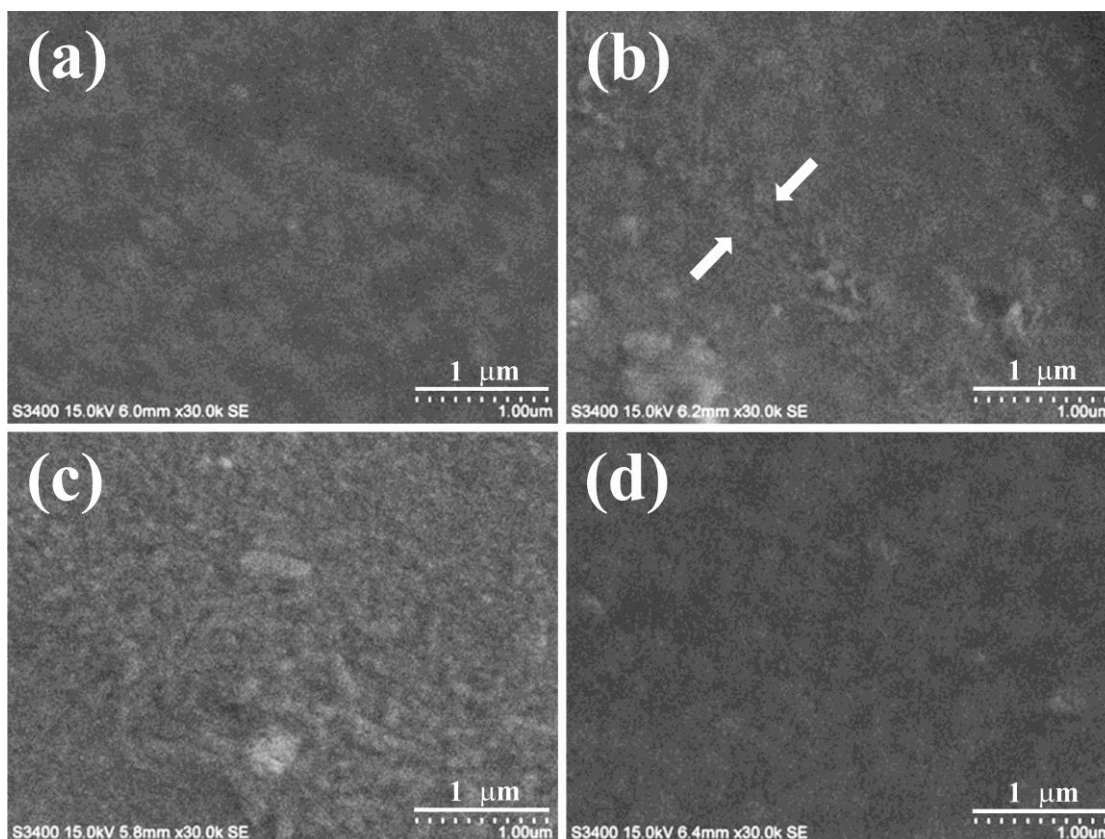
Figure 5.4 SEM images of (a) pristine PEDOT:PSS films and PEDOT:PSS film dipped in

(b) water, (c) DMSO, and (d) 2 vol% of aqueous DMSO solution

These defects damage the surface of the PEDOT:PSS films, resulting in lower

electrical conductivity, and thus the immersion time is of great importance to optimize

the films' properties. It is worth noting that dipping the films in pure water for a long

immersion time (~1 min) leads to a loss of almost PEDOT:PSS films from the glass

substrates. In addition, the insulating PSS layer on the film surface is also washed away

as confirmed by the XPS spectra; however, the significant change on the surface

morphology by this incident is not noticed by the SEM images. As displayed in Figure

5.4c, the films dipped in pure DMSO show the swelling of conductive PEDOT grains.

The good film forming surface is obtained after being dipped in 2 vol% of aqueous

DMSO solution (Figure 5.4d). The aqueous DMSO is a suitable solvent for the dipping

method because PEDOT:PSS film can be prepared without any defects.
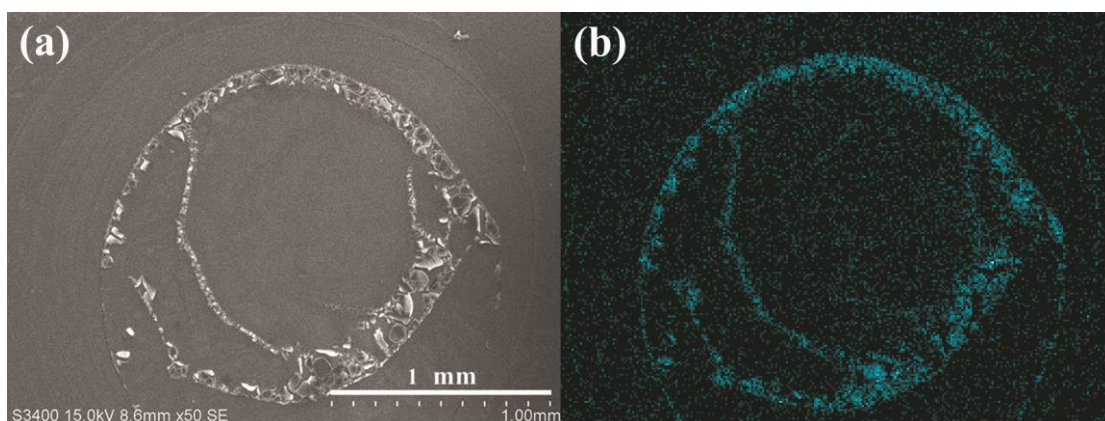
Figure 5.5 SEM images of (a) white patch on the surface of the film dipped in pure

DMSO and (b) EDX image of the sulfur dispersion

Although the films dipped in pure DMSO gives the highest conductivity, the

white patches as defects are obviously found on the whole film surface as illustrated

in Figure 5.5a. To describe this phenomenon, the elemental composition around the

white patches is measured by an energy dispersive X-ray (EDX) analysis. The EDX result

shown in Figure 5.5b reveals that the borders of the white patches specifically contain

the sulfur atoms of the aggregated PSS phase separated from the associated PEDOT

matrix with the uniform distribution of PSS in inner and outer regions of the white

patches [112]. This indicates the phase separation between the excess PSS and the

PEDOT matrix. Furthermore, these white patches can be easily removed by rinsing with

water, corresponding to the absent white patches for the PEDOT:PSS films dipped in pure water and 2 vol% of aqueous DMSO solution. Normally, the hydrophilic nature of DMSO molecules decreases the interchain interaction between conductive PEDOT-rich grains and the insulating PSS-rich shell and it is able to dissolve some unassociated PSS phase from the film surface [48]. Nonetheless, the washing efficiency using pure DMSO might be lower than using pure water, as shown in the calculation of the area ratio in the XPS results (reference to 5.2.3. XPS analysis), and thus the PSS was incompletely washed away by pure DMSO and the remaining PSS caused the formation of white patches.

5.2.5 Effect of solvents on surface topography of PEDOT:PSS thin films

The average thickness of PEDOT:PSS thin films is obtained by a surface profiler measured at five different positions per sample. Pristine PEDOT:PSS films have an average thickness of 1130 Å. After surface treatment, all dipped samples exhibit a decreased film thickness to approximately 940 Å (17 % reduction) because the unassociated PSS-enrich layer on the film surface was washed away upon the dipping process [108, 113].
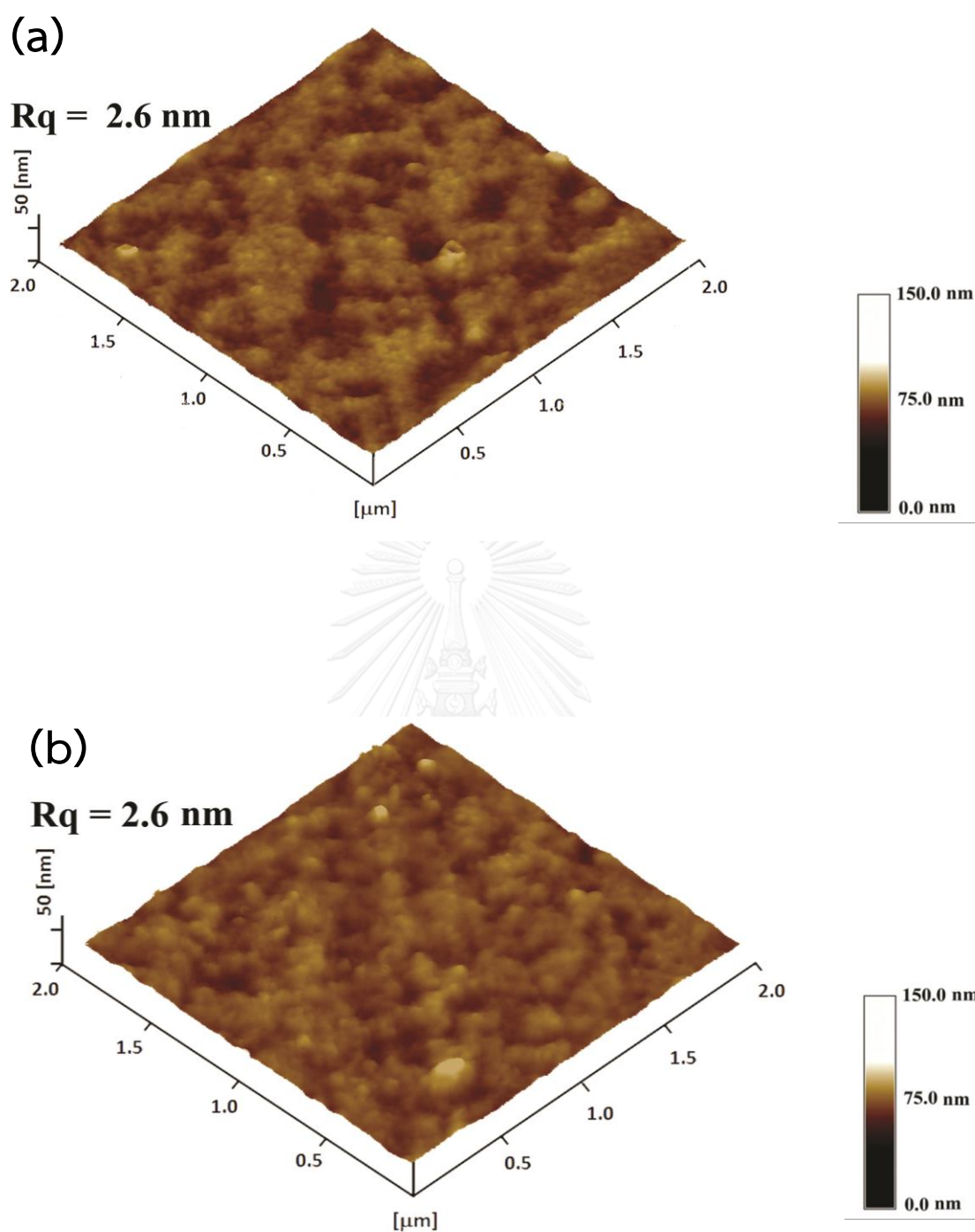
Figure 5.6 Tapping mode AFM topography of (a) pristine PEDOT:PSS films and

PEDOT:PSS films dipped in pure water
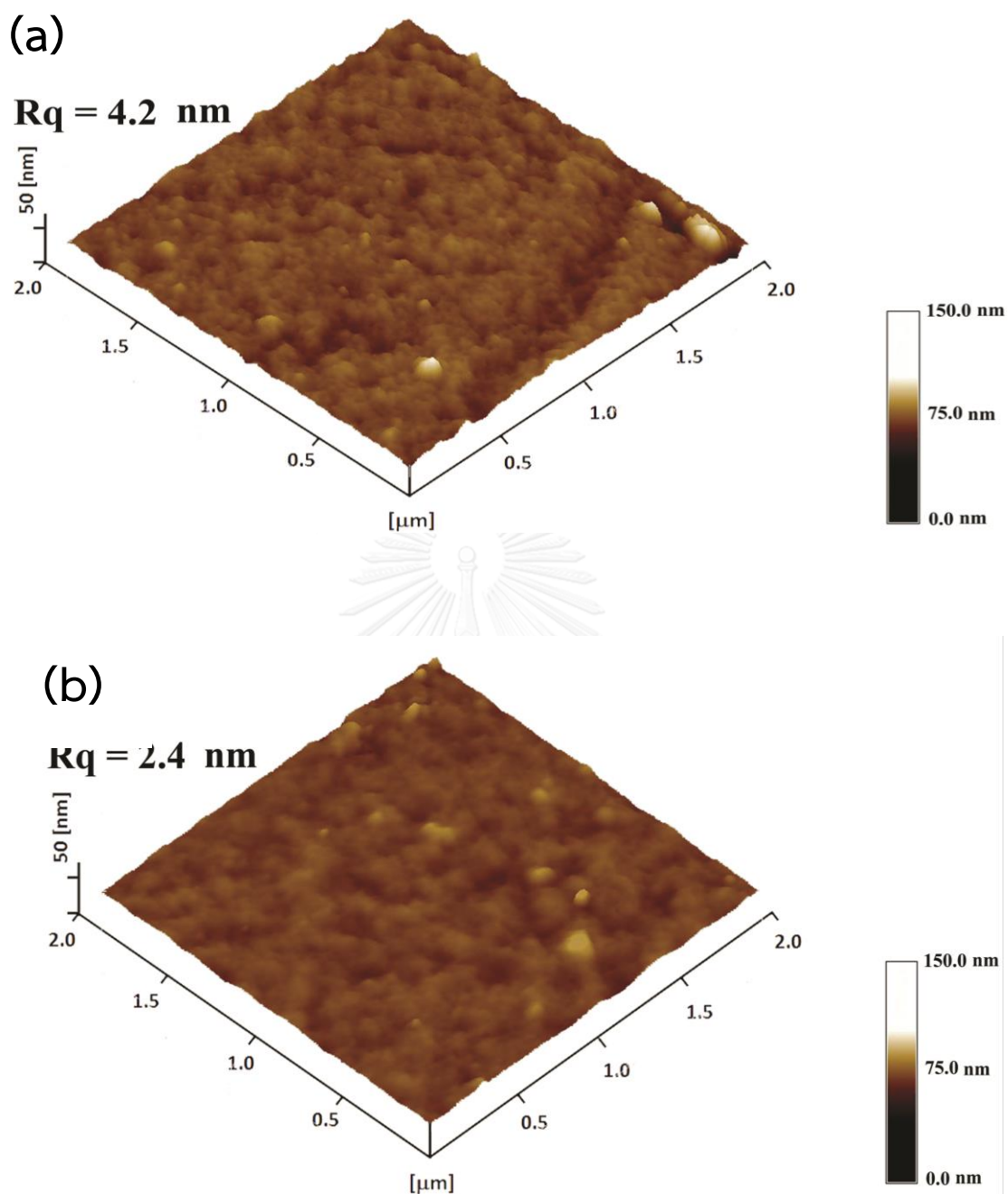
Figure 5.7 Tapping mode AFM topography of PEDOT:PSS films dipped in (c) pure

DMSO and (d) 2 vol% of aqueous DMSO solution

Additionally, the surface topography and the root mean square (RMS) roughness (R_q) are recorded by tapping mode atomic force microscopy (AFM) as illustrated in Figure 5.6 and 5.7. It is pointed out that the R_q values of PEDOT:PSS after dipping in water and 2 vol% of aqueous DMSO solution are in a same order of magnitude as that of pristine PEDOT:PSS films, ranging between 2.4 nm - 2.6 nm. It should be mentioned that the measured R_q values exclude the surface of the white patches. Conversely, the R_q value obviously increases to 4.2 nm for the PEDOT:PSS films dipped in DMSO since it induces the phase separation and the conformational change from the benzoid structure to the quinoid structure, as early discussed in the Raman results (5.2.2. Raman spectroscopy, Figure 5.2). Furthermore, the dipping method leads to a swelling of the PEDOT:PSS grains and the removed excess insulating PSS layer [114]. According to the previous literatures, the aggregation and the growth of conductive PEDOT grains usually detected in the conventional solvent doping are not observed in the dipping method in our study. The possible explanation could be that the doped solvents decline the interchain interaction of the excess PSS and the conductive grains as well as induce the aggregation of PEDOT:PSS grains during mixing before coating on the substrates [115]. In the dipping process, PEDOT:PSS is deposited on the substrates and subsequently dipped in the prepared solvents. It is informed that the phase separation and conformation of PEDOT chains occur when the films have already been formed but the conductive grains cannot be re-dispersed and diffused freely, yielding the unaltered conductive grain size [116].

5.2.6 UV-Vis spectroscopy
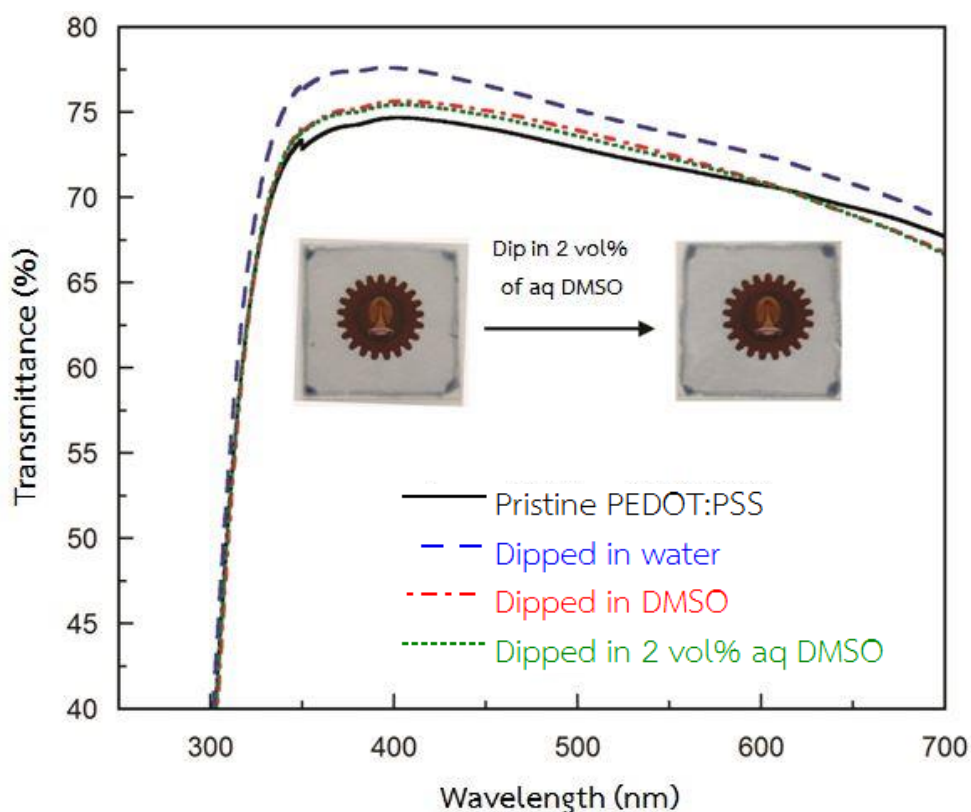
Figure 5.8 Transmittance as a function of wavelength of pristine PEDOT:PSS and

dipped PEDOT:PSS films

Figure 5.8 illustrates the UV-Vis spectra of pristine PEDOT:PSS and PEDOT:PSS

films dipped in various solvents. The maximum light transmittance at wavelength of

399 nm of pristine PEDOT:PSS is approximate 74.7 % and it increases to 77.6 %, 75.6

% and 75.4 % for the PEDOT:PSS films dipped in water, DMSO and 2 vol% of aqueous

DMSO, respectively. Further, the percent transmittance relatively depends on the

thickness of the films. Namely, the structure of PEDOT:PSS is a pancake-like particle

surrounded by a PSS shell and the unassociated PSS phase presents on the top layer.

Upon dipping, the unassociated PSS top layer was washed away, yielding the thinner films showing higher light transmittance.

CHAPTER VI

CONDUCTIVE FILMS PREPARATION BY LAYER BY LAYER DROP CASTING

Using different solvents for well dispersion of graphene and drop casting the lower and upper layers of the dried PEDOT:PSS films affect the surface morphology and the sheet resistance of the conductive films. The conductive films fabrication can be performed by layer by layer drop casting. The type of solvents and order of material deposition on the glass substrate were varied as follows:

G/P represents the graphene as the lower layer and PEDOT:PSS as the upper layer.

P/G represents the PEDOT:PSS as the lower layer and graphene as the upper layer.

6.1 Experiment

In this section, PEDOT:PSS (PH 1000) was bought from Heraeus, CleviousTM and graphene was bought from XG Science. Graphene was dispersed in neat PEDOT:PSS, aqueous sodium dodecyl sulfate (2 wt% SDS), acetone, and ethanol at 1 wt% by being once post treated with an ultrasonic probe for 10 minutes for achieving a homogeneous dispersion. Furthermore, before drop casting with a micropipette the dispersions were placed in an ultrasonic bath for 10 minutes. PEDOT:PSS containing graphene (PEDOT:PSS/G) was obtained by directly mixing 50 µl of PEDOT:PSS solution with graphene and then drop casting onto the glass substrate in an area of 1.5 cm x 1.5 cm. Two main casting sequences were conducted as follows:

P/G samples were obtained by preparing the dried PEDOT:PSS film as a lower layer first following by casting a graphene dispersed in solvent as a upper layer, as demonstrated in Figure 6.1.

G/P samples were achieved by casting the graphene dispersed in solvent as a lower layer on the glass substrate first and drop casting the PEDOT:PSS solution as a upper layer afterwards, as illustrated in Figure 6.2.

After finishing the layer by layer drop casting technique, the prepared samples were dried on a hotplate at 60 °C for 15 minutes. Overall, five drop casting were prepared and analyzed.
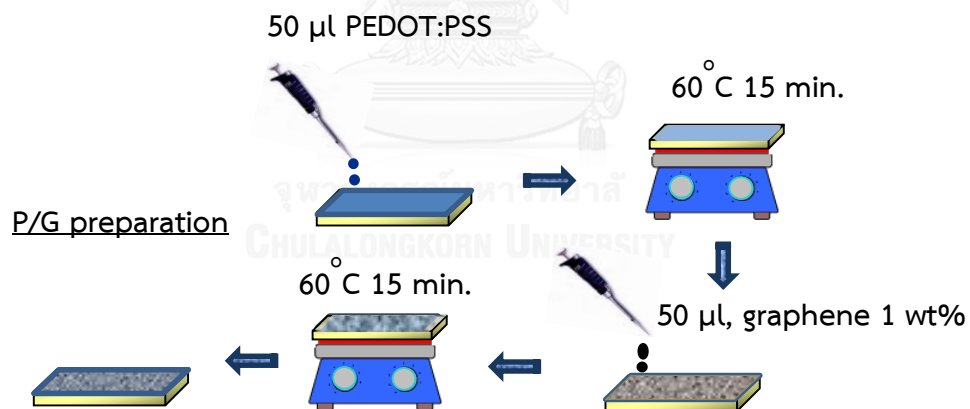
Figure 6.1 P/G preparation procedure
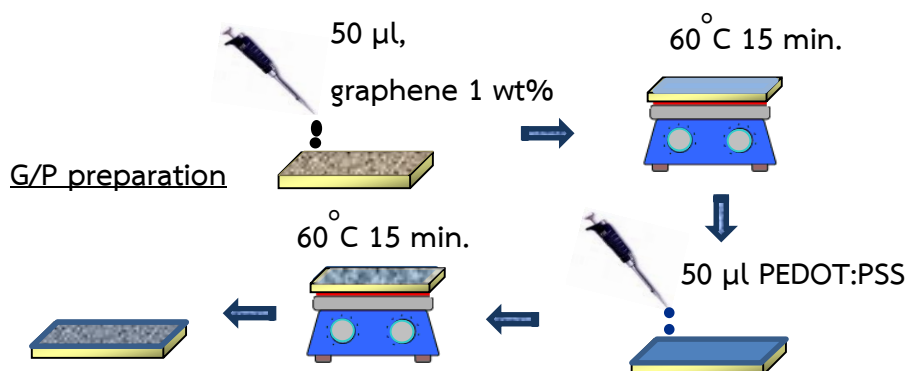
Figure 6.2 G/P preparation procedure
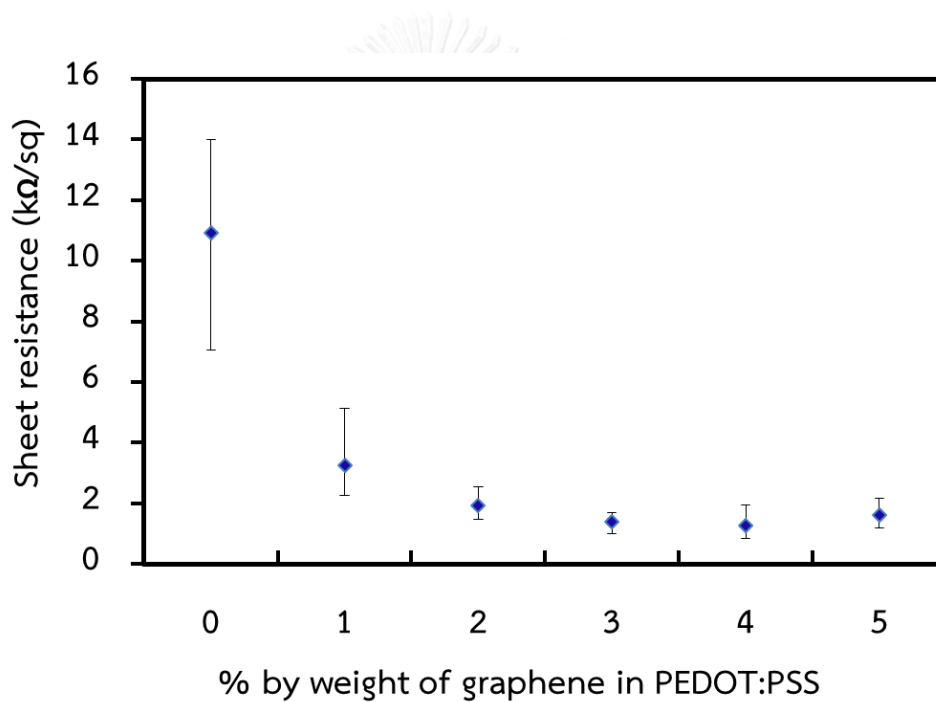
Figure 6.3 Sheet resistance of PEDOT:PSS mixed graphene

6.2 PEDOT:PSS mixed graphene films

The graphene loading in the PEDOT:PSS solution is varied from 0 wt% to 5 wt%. It is noticed that the sheet resistance drastically decreases as the graphene loading increases to 2 wt% and reaches the steady value (~1 kΩ/sq) at high graphene

loading of 3 wt%, as shown in Figure 6.3. However, the microscopic images show cracking as a defect on the surfaces of films containing 2 wt% of graphene loading, as depicted in Figure 6.4. From this reason, the maximum graphene loading prepared in this study is 1 wt%.
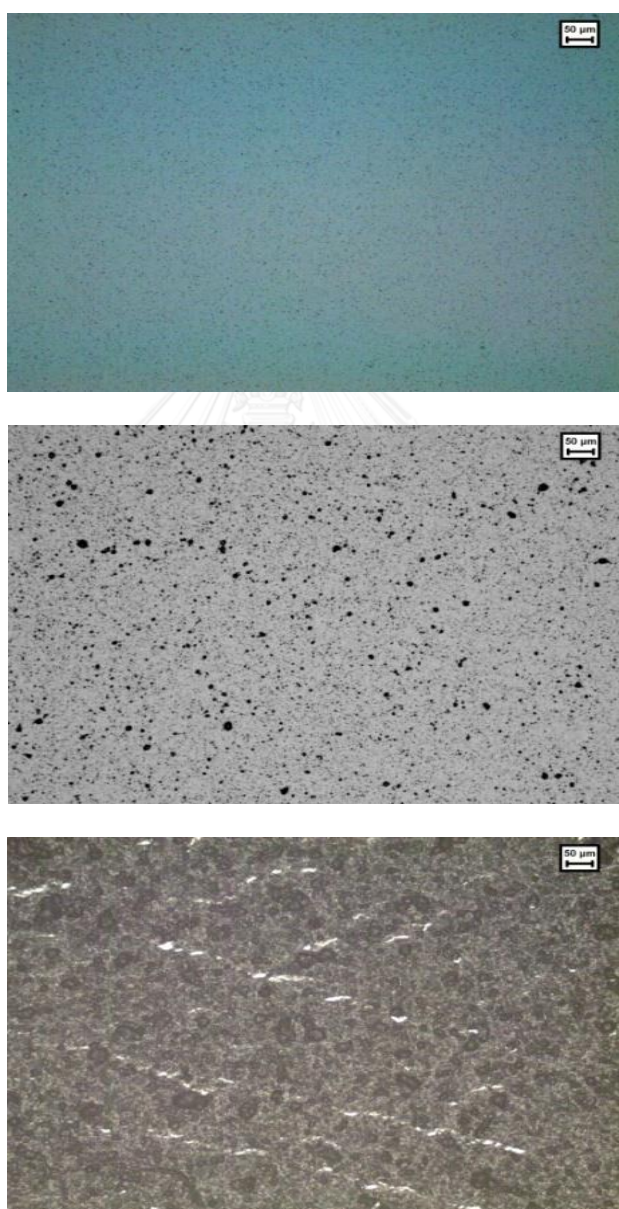
Figure 6.4 Microscopic images of (a) neat PEDOT:PSS; and PEDOT:PSS mixed graphene at (b) 1 wt% and (c) 2 wt%

6.3 Morphology of the conductive films

In Figure 6.5, the microscopic images of drop casted and dried PEDOT:PSS dispersions are displayed. PEDOT:PSS (Figure 6.5a) exhibits a homogeneous layer. The PEDOT:PSS/G layer in Figure 6.5c shows a relatively homogeneous distribution of graphene. The light parts are arising from defects. The films from individual drop casted methods generally show less homogeneous distribution of graphene. The P/G SDS (Figure 6.5d) as well as G/P SDS layers (Figure 6.5g) demonstrate distinguished darker and lighter areas depending on the graphene coverage. Spreading occurs over the entire area. The P/G acetone and G/P acetone dispersions show very large agglomerations and a non-uniform distribution (Figure 6.5e and 6.5h), whereas the agglomeration becomes even larger for P/G acetone (Figure 6.5e). Agglomeration occurs due to the very fast evaporation of acetone on the hotplate at 60 $^{\circ}$C after drop casting, resulting in reduced graphene spreading. Similar result is also detected for the films obtained from ethanol-dispersion. The P/G ethanol layer (Figure 6.5f) is comparable to the P/G SDS layer, and the G/P ethanol layer (Figure 6.5i) is comparable to the G/P acetone layer. However, the best results are shown for direct dispersion of graphene in PEDOT:PSS or a layer-by-layer methods of P/G ethanol.

a) PEDOT:PSS   b) Graphene SDS   c) PEDOT:PSS/G

d) P/G SDS   e) P/G acetone   f) P/G ethanol

g) G/P SDS   h) G/P acetone   i) G/P ethanol
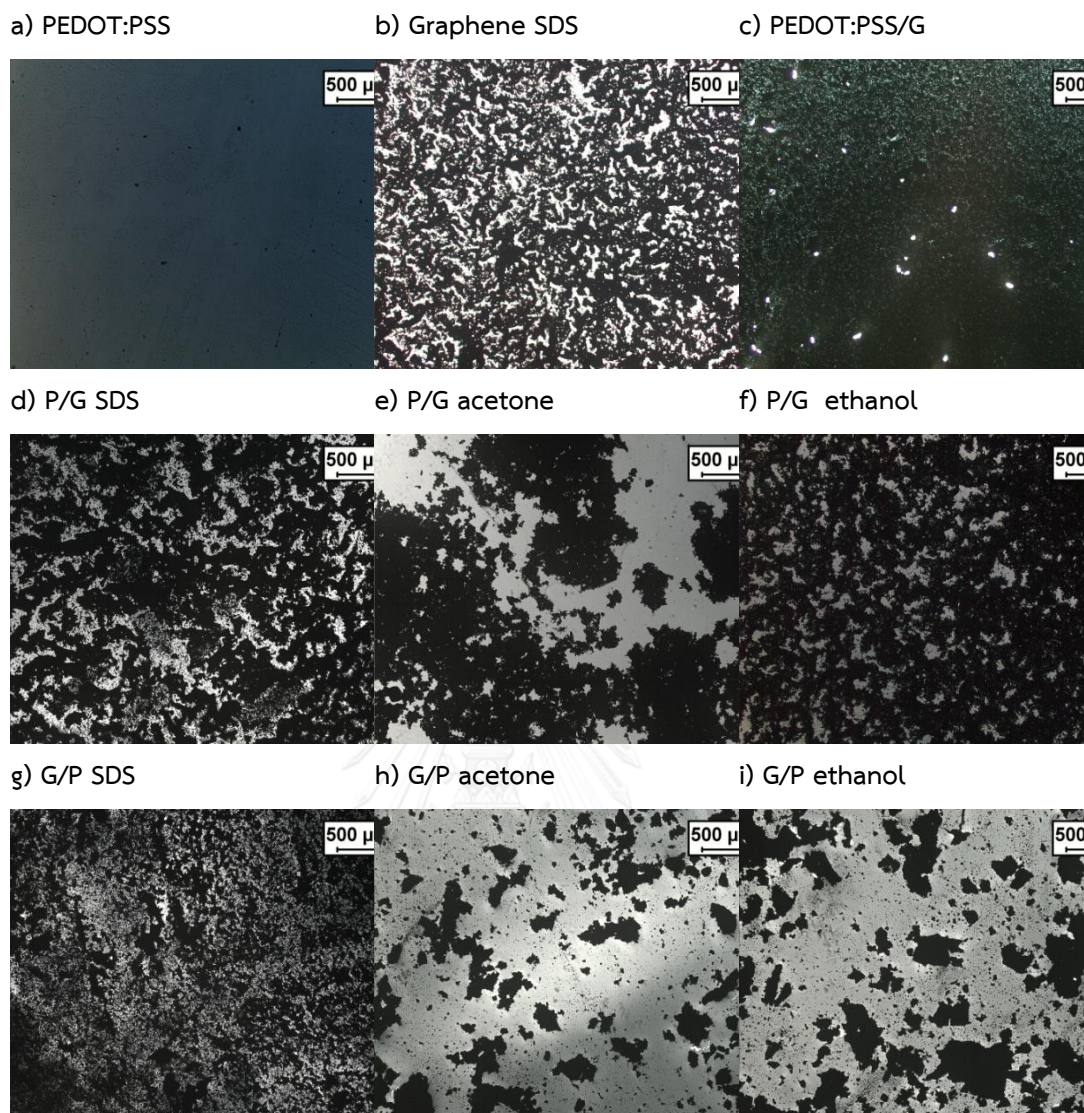
Figure 6.5 Microscopic images of PEDOT:PSS mixtures drop casted on glass substrates

6.4 Surface profiles

The surface profiles shown in Figure 6.6 are obtained from the surface profiler measurement. Each pattern is measured at five different positions. When comparing the profiles for the different positions inside one pattern, no crucial difference can be detected. Pure PEDOT:PSS (Figure 6.6a) shows a relatively smooth surface profile

without any noticeable hills. The average height is approx. 1.67 µm ± 0.39 µm with a surface roughness of 0.05 µm. Pure graphene (Figure 6.6b) displays distinct hills of graphene clusters with an average value up to 15 µm and one peak of 25 µm as well as valleys down to the level of the substrate. The PEDOT:PSS/G layer (Figure 6.6c) presents a combination of single PEDOT:PSS and graphene with the average layer thickness of 4.35 µm ± 1.21 µm, whose thickness is more than twice of that of neat PEDOT:PSS due to the graphene particles distributed inside the PEDOT:PSS layer as well as larger graphene agglomerations. The P/G SDS and G/P SDS layers show major average height thicker than that of PEDOT:PSS/G. Both films show high surface roughness and fluctuations due to less homogeneous graphene distribution. The systems with P/G acetone and G/P acetone show the highest fluctuations. The system with G/P ethanol layer also shows high surface roughness, but slightly smaller fluctuations. The system with P/G ethanol is comparable to that with graphene dispersed in SDS. The surface profiles reflect either uniform or non-uniform graphene distribution. Moreover, it seems that acetone is not a good choice for obtaining well graphene dispersion
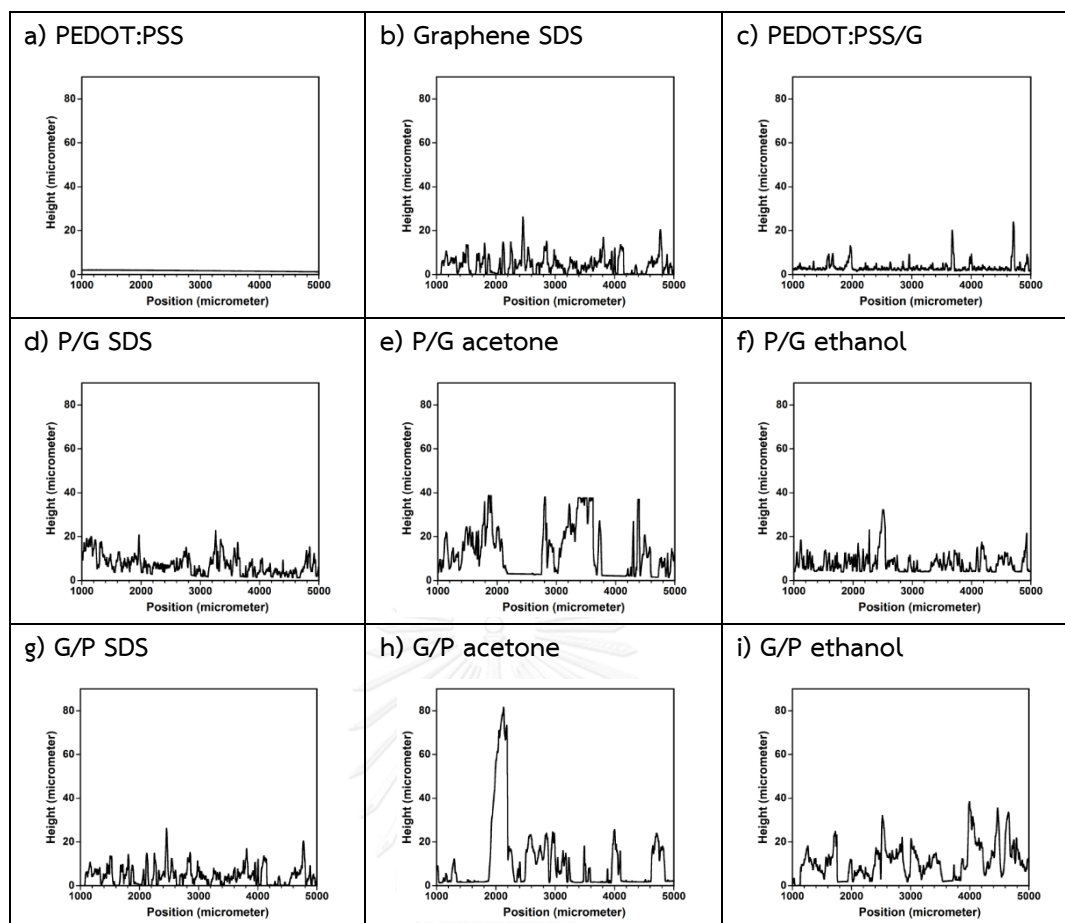
Figure 6.6 Surface profiles of PEDOT:PSS mixtures drop casted on glass substrates

6.5 Electrical resistance measurement

- P/G conductive films

The sheet resistance of PEDOT:PSS is significantly improved by directly mixing 1 wt%

of graphene in PEDOT:PSS as shown in Figure 6.7. Acetone and ethanol drop casted

on the surface of PEDOT:PSS layer show the similar effect like solvent treatment,

reducing the sheet resistance by a solvation of PEDOT:PSS during the drop casting and

drying [112]. The phase separation of PSS chain, which is the insulator, from PEDOT

grains leads to the fact that the PEDOT grains are moved closer with the adjacent ones forming the long path way for electron transfer.
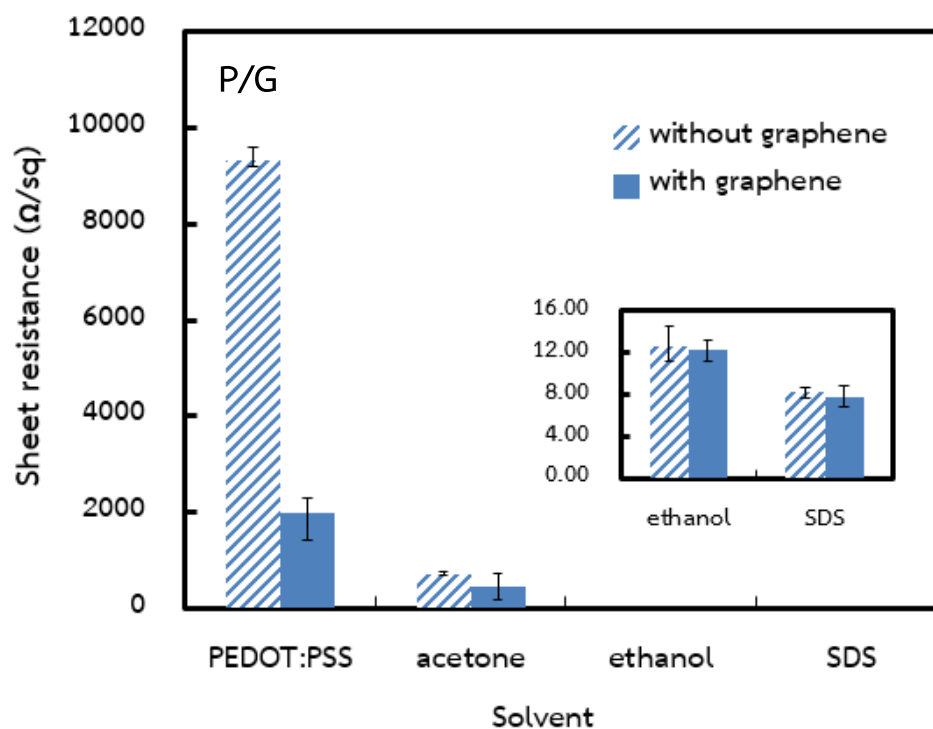
Figure 6.7 Sheet resistance of PEDOT:PSS films coated with graphene

Moreover, the effect of solvent treatment also changes the conformation of PEDOT from coil structure to linear structure. In comparison between acetone and ethanol, the ethanol can reduce the sheet resistance better than acetone because the hydroxyl group of ethanol has the effective properties to induce phase separation of PSS chains. Additionally, the casted films using SDS with/without graphene show lower sheet resistance than others. It is possible that SDS, which is an anionic surfactant, gives the same results to those casted with the high boiling point compound but

different mechanism. The anions of SDS can replace PSS as counter anions to PEDOT, leading to phase separation [117]. The PEDOT distortion structure also disappears, resulting in a reduction of the sheet resistance. For P/G conductive films, the sheet resistance of films with graphene on top is lower than those without graphene because graphene can reduce the sheet resistance. However, the solvent treatment seems to be a dominant effect compared with the addition of conductive graphene in P/G samples.

- <u>G/P conductive films</u>
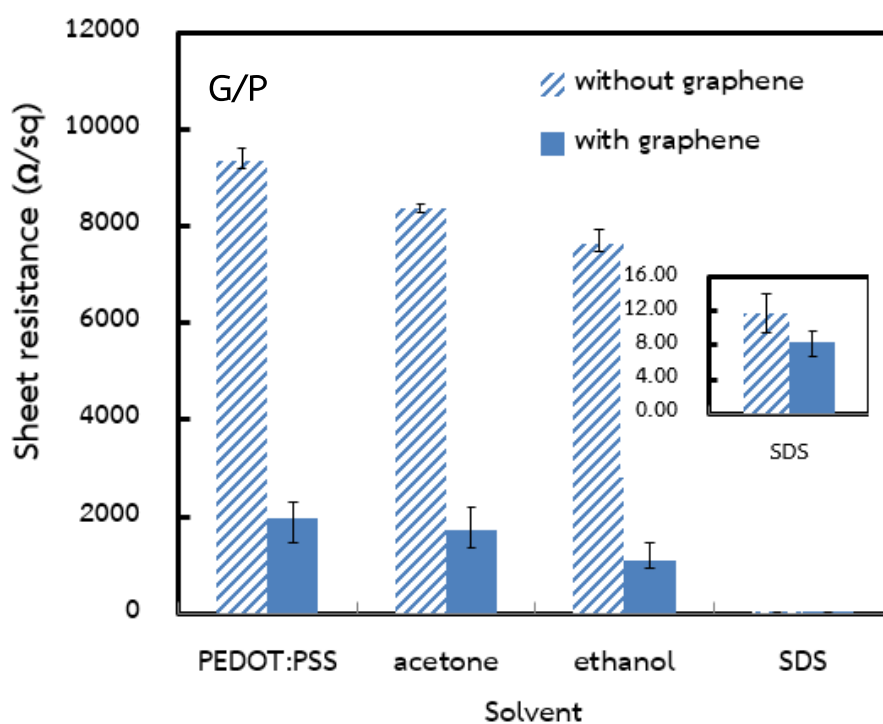
Figure 6.8 Sheet resistance of graphene coated with PEDOT:PSS films

In case of the solvents without graphene deposited on glass substrates as shown in Figure 6.8, acetone and ethanol have the effect on substrate cleansing but

not on the material properties. Namely, acetone and ethanol can improve the surface energy of glass substrates, leading to better deposition of PEDOT:PSS film and, in turn, an improvement of electrical resistance. In addition, SDS deposited on substrate cannot be completely removed upon drying due to its high boiling point. The films containing SDS lower layer has very low sheet resistance because SDS is able to diffuse into the upper layer of PEDOT:PSS layer during the second drop casting, resulting in a conformational change. With an incorporation of graphene, the sheet resistance significantly decreases due to the combination effect of improvement of surface energy of substrate and high conductive graphene. The sheet resistance of PEDOT:PSS containing the lower layer of graphene dispersed in various solvents exhibits the same trend as those containing the lower layer without graphene. The sheet resistance results can conclude that the major effect in G/P samples is the addition of graphene and the minor effect is the surface energy of cleaned substrates.

CHAPTER VII

CONCLUSIONS AND RECOMMENDATIONS

7.1 Conclusions

The improvement of electrical conductivity of PEDOT:PSS in this study was enhanced by (1) incorporation of functionalized graphene, and (2) dipping in aqueous DMSO solution, and (3) addition of graphene combining with layer-by-layer drop casting. The conclusions are detailed as follows.

For the first part; incorporation of graphene into PEDOT:PSS, the alkyne-functionalized graphene and azide-functionalized PEDOT:PSS were successfully synthesized as confirmed by FTIR, Raman and XPS techniques. The conversion of click chemistry was found to be 77%. A transfer of GO-alkyne from aqueous phase to hexane phase resulted from difference in affinity between polar GO sheets and non-polar alkynes. TGA results revealed that an incorporation of graphene can significantly increase the thermal stabilities of composites; however, clicked PEDOT:PSS-graphene composites showed less thermal stability than unclicked PEDOT:PSS-graphene composites owing to the thermal cleavages of amide bonds and oxygen-containing functional groups. From SEM observation, clicked PEDOT:PSS-graphene composites exhibited well dispersion of graphene and lower surface roughness because triazole linkages enhanced interfacial interaction between graphene sheets and PEDOT:PSS

matrix. Therefore, clicked PEDOT:PSS-graphene composites with less agglomeration and defects on the surface had higher electrical conductivity.

For the second part, the effect of a low concentration aqueous DMSO solution on the electrical conductivity, surface chemistry, and surface morphology of treated PEDOT:PSS films via dipping technique was investigated. The conductivity monotonically increased with increasing DMSO concentration and reached a constant value of 380 S/cm (more than 1000-times compared with that of pristine PEDOT:PSS) at 2 vol% of aqueous DMSO solution, which was close to that of films dipped in pure DMSO. The Raman spectra showed that the conductivity enhancement was attributed to the conformational change from a coil structure to a linear or expanded-coil structure, yielding the higher charge mobility on the PEDOT chains. Moreover, the XPS S2p core-level spectra indicated that the washing effect of the unassociated PSS-rich layer was more pronounced for treatment with solvents composed of water, while pure DMSO barely removed total PSS layer leading to the agglomeration of the PSS phase in the form of white patches. Furthermore, dipping the films in aqueous DMSO solution resulted in good film forming without any defects like crinkles in those dipped in water and white patches in those dipped in pure DMSO. It was pointed out by UV-Vis spectra that the transparency of dipped PEDOT:PSS films increased owing to the decreased film thickness as a result of the washing effect. Finally, it was worth noting that aqueous DMSO is the appropriate solvent for the dipping method in this

study because only a small amount of high boiling point DMSO was involved, which is beneficial for removal upon heating.

For the third part, the position of graphene layer and PEDOT:PSS layer in the film sample as well as the influence of type of solvent used for graphene dispersion are investigated. SDS seems to be the best solvent for achieving well graphene dispersion. It is reported that graphene can reduce the sheet resistance significantly because of its excellent electrical conductivity; however, the solvent also plays a key role in the phase separation of insulating PSS chains and PEDOT grains as well as the conformational change of PEDOT from coil structure into linear structure, leading to dramatically enhanced sheet resistance. Moreover, when the graphene layer is drop casted on top of PEDOT:PSS layer, the sheet resistance is lower than the films with PEDOT:PSS as a upper layer. This is because technically the sheet resistance measured only at the surface of the film, not in the bulk; therefore, films having graphene on top shows better sheet resistance owing to intrinsically high electrical conductivity of graphene and the conformational change by treatment of PEDOT:PSS from solvent used for dispersion of graphene.

7.2 Recommendations

1. The synthesis of graphene by chemical method should be improved because this method produces several layers of graphene, not the single layer.

2. The other catalysts should be compared to increase the conversion of click reaction.

3. Type of the functional groups treated on graphene sheets can be varied for different interactions.

4. The combination of the dipping treatment and other post-treatments should be studied.

5. The solvents for the dipping treatment such as ethylene glycol should be compared.
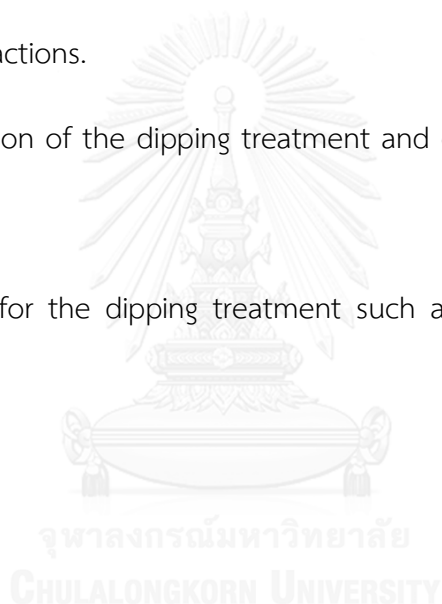
REFERENCES

[1]   Castagnola, V., Bayon, C., Descamps, E., and Bergaud, C. Morphology and conductivity of PEDOT layers produced by different electrochemical routes. **Synth. Met.** 189 (2014): 7-16.

[2]   Kuilla, T. et al. Recent advances in graphene based polymer composites. **Prog. Polym. Sci.** 35 (2010): 1350–1375.

[3]   Li, J., Liu, J.C., and Gao, C.J. On the mechanism of conductivity enhancement in PEDOT/PSS film doped with multi-walled carbon nanotubes. **J. Polym. Res.** 17 (2010): 713-718.

[4]   Deetuam, C., Samthong, C., Thongyai, S., Praserthdam, P., and Somwangthanaroj, A. Synthesis of well dispersed graphene in conjugated poly(3,4-ethylenedioxythiophene):polystyrene sulfonate via click chemistry. **Compos. Sci. Technol.** 93 (2014): 1-8.

[5]   Yoo, D., Kim, J., and Kim, J.H. Direct synthesis of highly conductive poly(3,4-ethylenedioxythiophene):poly(4-styrenesulfonate)(PEDOT:PSS)/graphene composites and their applications in energy harvesting systems. **Nano Res.** 7 (2014): 717-730.

[6]   Wallace, G.G., Spinks, G.M., Kane-Maguire, L.A.P., and Teasdale, P.R. Conductive electroactive polymers. **CRC Press**. New York, 2009.

[7]   Istamboulie, G. et al. Screen-printed poly(3,4-ethylenedioxythiophene) (PEDOT): A new electrochemical mediator for acetylcholinesterase-based biosensors. **Talanta** 82 (2010): 957-961.

[8]   Wen, Y. et al. A novel electrochemical biosensing platform based on poly(3,4-ethylenedioxythiophene):poly(styrenesulfonate) composites. **Synth Met** 162 (2012): 1308-1314.

[9]   Chen, L. et al. Synthesis and electrochemical capacitance of core-shell poly(3,4-ethylenedioxythiophene)/poly(sodium   4-styrenesulfonate)-modified multiwalled carbon nanotube nanocomposites. **Electrochim Acta** 54 (2009): 2335-2341.

[10]   Khan, M.A., Bhansali, U.S., and Alshareef, H.N. Fabrication and characterization of all-polymer, transparent ferroelectric capacitors on flexible substrates. **Org Electron** 12 (2011): 2225-2229.

[11]   Havare, A.K., Can, M., Demic, S., Kus, M., and Icli, S. The performance of OLEDs based on sorbitol doped PEDOT:PSS. **Synth Met** 161 (2012): 2734-2738.

[12]   Wang, G., Tao, X., and Wang, R. Fabrication and characterization of OLEDs using PEDOT:PSS and MWCNT nanocomposites. **Compos Sci Technol** 68 (2008): 2837-2841.

[13]   Jain, V., Yochum, H.M., Montazami, R., and Heflin, J.R. Millisecond switching in solid state electrochromic polymer devices fabricated from ionic self-assembled multilayers. **Appl Phys Lett** 92 (2008): 033304(1-3).

[14]   Pagés, H., Topart, P., and D., L. Wide band electrochromic displays based on thin conducting polymer films. **Electrochim Acta** 46 (2001): 2137-2143.

[15]   Chandrasekhar, P. Conducting polymers, fundamentals and applications. **Kluwer academic**. London, 1999.

[16]   Elachner, A., Kirchmeyer, S., Lovenich, W., Merker, U., and Reuter, K. PEDOT: Principles and applications of an intrinsically conductive polymer. **CRC Press**. New York, 2010.

[17]   Heeger, A.J. Semiconducting and metallic polymers: The fourth generation of polymeric materials **J. Phys. Chem.** 105 (2001): 8475-8491.

[18]   Hillman, A.R., Daisley, S.J., and Bruckenstein, S. Kinetics and mechanism of the electrochemical p-doping of PEDOT. **Electrochem. Commun.** 9 (2007): 1316-1322.

[19]   Rattan, S., Singhal, P., and Verma, A.L. Synthesis of PEDOT:PSS (poly(3,4-ethylenedioxythiophene)/poly(4-styrene sulfonate))/NGPs (nanographitic platelets) nanocomposites as chemiresistive sensors for detection of nitroaromatics. **Polym. Eng. Sci.** 53 (2013): 2045-2052.

[20]   Wu, T.Y. et al. Co-electrodeposition of platinum and rhodium in poly(3,4-ethylenedioxythiophene)-poly(styrene sulfonic acid) as electrocatalyst for methanol oxidation. **Int. J. Electrochem. Sci.** 7 (2012): 8076-8090.

[21]   Sakamoto, S., Okumura, M., Zhao, Z., and Furukawa, Y. Raman spectral changes of PEDOT-PSS in polymer light-emitting diodes upon operation. **Chem. Phys. Lett.** 412 (2005): 395-398.

[22]   Stavytska-Barba, M., and Kelley, A.M. Surface-enhanced Raman study of the interaction of PEDOT:PSS with plasmonically active nanoparticles. **J. Phys. Chem. C** 114 (2010): 6822-6830.

[23]   Michalska, A., and Maksymiuk, K. All-plastic, disposable, low detection limit ion-selective electrodes. **Anal. Chim. Acta** 523 (2004): 97–105.

[24]   Jo, K. et al. Stable aqueous dispersion of reduced graphene nanosheets via non-covalent functionalization with conducting polymers and application in transparent electrodes. **Langmuir** 27 (2011): 2014-2018.

[25]   Sonmez, G., Schottland, P., and Reynolds, J.R. PEDOT/PAMPS: An electricallly conductive polymer composite with electrochomic and cation exchange properties. **Synth. Met.** 155 (2005): 130-137.

[26]   Yamato, H., Ohwa, M., and Wernet, W. Stability of polypyrrole and poly(3,4-ethylenedioxythiophene) for biosensor application. **J. Electroanal. Chem.** 397 (1995): 167-170.

[27]   Yamato, H., Kai, K., Ohwa, M., Wernet, W., and Matsumura, M. Mechanical, electrochemical and optical properties of poly(3,4-ethylenedioxythiophene)/sulfonated poly(β-hydroxyethers) composite films. **Electrochim. Acta** 42 (1997): 2517-2523.

[28]   Nardes, A.M. <u>On the conductivity of PEDOT:PSS thin films.</u> Doctoral's Thesis, Department of the Polytechnic School, University of São Paulo, 2007.

[29]   Kim, W.H., Kushto, G.P., Kim, H., and Kafafi, Z.H. Effect of annealing on the electrical properties and morphology of a conducting polymer used as an anode in organic light-emitting devices. **J. Polym. Sci., Part B: Polym. Phys.** 41 (2003): 2522–2528.

[30]   Krebs, F.C. Fabrication and processing of polymer solar cell: A review on of printing and coating techniques. **Sol. Energy Mater. Sol. Cells** 93 (2009): 394-412.

[31]   Srichan, C. et al. Inkjet printing PEDOT:PSS using desktop inkjet printed. **IEEE** (2009): 1-4.

[32]   Natori, A.Y., Canestraro, C.D., Roman, L.S., and Ceschin, A.M. Modification of the sheet resistance of ink jet printed polymer conducting films by changing the plastic substrate. **Mater. Sci. Eng., B** 122 (2005): 231-235.

[33]   Choi, J.S., Cho, K.Y., and Yim, J.H. Micro-patterning of vapor-phase polymerized poly(3,4-ethylenedioxythiophene) (PEDOT) using ink-jet printing/soft lithography. **Eur. Polym. J.** 46 (2010): 389-396.

[34]   King, Z.A., Shaw, C.M., Spanninga, S.A., and Martin, D.C. Structural, chemical and electrochemical characterization of poly(3,4-ethylenedioxythiophene) (PEDOT) prepared with various counter-ions and heat treatments. **Polymer** 52 (2011): 1302-1308.

[35]   Farah, A.A. et al. Conductivity enhancement of poly(3,4-ethylenedioxythiophene)-poly(styrenesulfonate) films post-spincasting. **J. Appl. Phys.** 112 (2012): 113709(1-8).

[36]   Huang, J., Miller, P.F., Mello, J.C.d., Mello, A.J.d., and Bradley, D.D.C. Influence of thermal treatment on the conductivity and morphology of PEDOT/PSS films. **Synth. Met.** 139 (2003): 569–572.

[37]   Xia, Y., and Ouyang, J. Highly conductive PEDOT:PSS films prepared through a treatment with geminal diols or amphiphilic fluoro compounds. **Org. Electron.** 13 (2012): 1785-1792.

[38]   Mahatiyakul, K., Thongyai, S., Praserthdam, P., and Somwangthanaroj, A. Thermal stability and electrical conductivity of PEDOT:PSS enhanced with secondary dopants, The 17th Regional Symposium on Chemical Engineering (RSCE 2010), Bangkok, 2010.

[39]   Ouyang, J. ''Secondary doping'' methods to significantly enhance the conductivity of PEDOT:PSS for its application as transparent electrode of optoelectronic devices. **Displays** 34 (2013): 423-436.

[40]   Ouyang, J. et al. On the mechanism of conductivity enhancement in poly(3,4-ethylenedioxythiophene):poly(styrene sulfonate) film through solvent treatment. **Polymer** 45 (2004): 8443-8450.

[41]   Jönsson, S.K.M. et al. The effects of solvents on the morphology and sheet resistance in poly(3,4-ethylenedioxythiophene)–polystyrenesulfonic acid (PEDOT–PSS) films. **Synth. Met.** 139 (2003): 1-10.

[42]   Dimitriev, O.P., Grinko, D.A., Noskov, Y.V., Ogurtsov, N.A., and Pud, A.A. PEDOT:PSS films—Effect of organic solvent additives and annealing on the film conductivity. **Synth. Met.** 159 (2009): 2237–2239.

[43]   Ouyang, J. Solution-processed PEDOT:PSS films with conductivities as indium tin oxide through a treatment with mild and weak organic acids. **ACS Appl. Mater. Interfaces** 5 (2013): 13082-13088.

[44]   Huang, C.J. et al. Study of solvent-doped PEDOT: PSS layer on small molecule organic solar cells. **Synth. Met.** 164 (2013): 38-41.

[45]   Hu, Z., Zhang, J., and Zhu, Y. Effects of solvent-treated PEDOT:PSS on organic photovoltaic devices. **Renewable Energy** 62 (2014): 100-105.

[46]   Wang, G.F., Tao, X.M., Xin, J.H., and Fei, B. Modification of conductive polymer for polymeric anodes of flexible organic light-emitting diodes. **Nanoscale Res. Lett.** 4 (2009): 613-617.

[47]   Xiong, Z., and Liu, C. Optimization of inkjet printed PEDOT:PSS thin films through annealing processes. **Org. Electron.** 13 (2012): 1532-1540.

[48]   Yeo, J.S. et al. Significant vertical phase separation in solvent-vapor-annealed poly(3,4-ethylenedioxythiophene):poly(styrene sulfonate) composite films leading to better conductivity and work function for high-performance indium

tin oxide-free optoelectronics. **ACS Appl. Mater. Interfaces** 4 (2012): 2551-2560.

[49]   Alemu, D., Wei, H.Y., Hod, K.C., and Chu, C.W. Highly conductive PEDOT:PSS electrode by simple film treatment with methanol for ITO-free polymer solar cells. **Energy Environ. Sci.** 5 (2012): 9662-9671.

[50]   Fung, D.D.S. et al. Optical and electrical properties of efficiency enhanced polymer solar cells with Au nanoparticles in a PEDOT-PSS layer. **J Mater Chem** 21 (2011): 16349-16356.

[51]   Antiohos, D. et al. Compositional effects of PEDOT-PSS/single walled carbon nanotube films on supercapacitor device performance. **J Mater Chem** 21 (2011): 15987-15994.

[52]   Sodano, S., Mahmood, A., and Dujardin, E. Production, properties and potential of graphene. **Carbon** 48 (2010): 2117-2150.

[53]   Dhakate, S.R. et al. An approach to produce single and double layer graphene from re-exfoliation of expanded graphite. **Carbon** 49 (2011): 1946-1954.

[54]   Shao, Y. et al. Graphene based electrochemical sensors and biosensors: A review. **Electroanalysis** 22 (2010): 1027-1036.

[55]   Wang, G. et al. Facile synthesis and characterization of graphene nanosheets. **J. Phys. Chem. C** 112 (2008): 8192-8195.

[56]   Zhu, P., Shen, M., Xiao, S., and Zhang, D. Experimental study on the reducibility of graphene oxide by hydrazine hydrate. **Physica B** 406 (2011): 498-502.

[57]   Ju, H.M., Huh, S.H., Choi, S.H., and Lee, H.L. Structures of thermally and chemically reduced graphene. **Mater. Lett.** 64 (2010): 357-360.

[58]   Stankovich, S. et al. Synthesis of graphene-based nanosheets via chemical reduction of exfoliated graphite oxide. **Carbon** 45 (2007): 1558-1565.

[59]   Li, D., Muller, M.B., Gilje, S., Kaner, R.B., and Wallace, G.G. Processable aqueous dispersions of graphene nanosheets. **Nat. Nanotechnol.** 3 (2008): 101-105.

[60]   Hsiao, M.C. et al. Preparation of covalently functionalized graphene using residual oxygen-containing functional groups. **ACS Appl. Mater. Interfaces** 2 (2010): 3092-3099.

[61]   Chen, W., Yan, L., and Bangal, P.R. Preparation of graphene by the rapid and mild thermal reduction of graphene oxide induced by microwaves. **Carbon** 48 (2010): 1146-1152.

[62]   Akhavan, O. The effect of heat treatment on formation of graphene thin films from graphene oxide nanosheets. **Carbon** 48 (2010): 509-519.

[63]   Reina, A. et al. Large area, few-layer graphene films on arbitrary substrates by chemical vapor deposition. **J. Am. Chem. Soc.** 9 (2009): 30-35.

[64]   Shinde, D.B., Debgupta, J., Kushwaha, A., Aslam, M., and Pillai, V.K. Electrochemical unzipping of muti-walled carbon nanotubes for facile synthesis of high-quality graphene nanoribbons. **J. Am. Chem. Soc.** 133 (2011): 4168-4171.

[65]   Jiao, L., Zhang, L., Wang, X., Diankov, G., and Dai, H. Narrow graphene nanoribbons from carbon nanotubes. **Nature** 458 (2009): 877-880.

[66]   Li, C., and Shi, G. Synthesis and electrochemical applications of the composites of conducting polymers and chemically converted graphene. **Electrochim. Acta** 56 (2011): 10737-10743.

[67]   McAllister, M.J. et al. Single sheet functionalized graphene by oxidation and thermal expansion of graphite. **Chem. Mater.** 19 (2007): 4396-4404.

[68]   Si, Y., and Samulski, E.T. Synthesis of water soluble graphene. **Nano Lett.** 8 (2008): 1679-1682.

[69]   Gao, X., Jang, J., and Nagase, S. Hydrazine and thermal reduction of graphene oxide: reaction mechanism, product structures, and reaction design. **J. Phys. Chem. C** 114 (2010): 832-842.

[70]   Park, S., and Choi, I.S. Production of ultrahigh-molecular-weight polyethylene/pristine MWCNT composites by half-titanocene catalysts. **Adv. Mater.** 21 (2009): 902-905.

[71]   Stankovich, S. et al. Stable aqueous dispersions of graphitic nanoplatelets via the reduction of exfoliated graphite oxide in the presence of poly(sodium 4-styrenesulfonate). **J. Mater. Chem.** 16 (2006): 155-158.

[72]   Lee, S., Lim, S., Lim, E., and Lee, K.K. Synthesis of aqueous dispersion of graphene via reduction of graphite oxide in the solution of conductive polymer. **J. Phys. Chem. Solids** 71 (2010): 483-486.

[73]   Yang, H. et al. Stable, conductive supramolecular composite of graphene sheets with conjugated polyelectrolyte. **Langmuir** 26 (2010): 6708–6712.

[74]   Yang, Z., Shi, X., Yuan, J., Pu, H., and Liu, Y. Preparation of poly(3-hexylthiophene)/graphene nanocomposite via in situ reduction of modified graphite oxide sheets. **Appl. Surf. Sci.** 257 (2010): 138-142.

[75]   Wang, G., Shen, X., Wang, B., Yao, J., and Park, J.H. Synthesis and characterisation of hydrophilic and organophilic graphene nanosheets. **Carbon** 47 (2009): 1359-1364.

[76]   Cao, Y., Feng, J., and Wu, P. Alkyl-functionalized graphene nanosheets with improved lipophilicity. **Carbon** 48 (2010): 1670-1692.

[77]   Bon, S.B., Valentini, L., and Kenny, J.M. Preparation of extended alkylated graphene oxide conducting layers and effect study on the electrical properties of PEDOT:PSS polymer composites. **Chem. Phys. Lett.** 494 (2010): 264-268.

[78]   Park, S., Dikin, D.A., Nguyen, S.T., and Ruoff, R.S. Graphene oxide sheet chemically cross-linkaged by polyallylamine. **J. Phys. Chem. C** 113 (2009): 15801-15804.

[79]   Balandin, A.A. et al. Superior thermal conductivity of single-layer graphene. **Nano Lett.** 8 (2008): 902-907.

[80]   Tung, V.C., Kim, J., Cote, L.J., and Huang, J. Sticky interconnect for solution-processed tandem solar cells. **Journal of the American Chemical Society** 133 (2011): 9262-9265.

[81]   Sriprachuabwong, C. et al. Enhancing electrochemical sensitivity of screen printed carbon electrode by inkjet printed graphene-PEDOT/PSS Layers, <u>ECTI-CON</u>, 54-57, Khon Kaen in Thailand, 2011.

[82]   Xu, Y. et al. A hybrid material of graphene and poly(3,4-ethyldioxythiophene) with high conductivity, flexibility, and transparency. **Nano Res.** 2 (2009): 343-348.

[83]   Rostovtsev, V.V., Green, L.G., Fokin, V.V., and Sharpless, K.B. A Stepwise huisgen cycloaddition process: copper(I)-catalyzed regioselective "ligation" of azides and terminal alkynes. **Angew. Chem. Int. Edit.** 41 (2002): 2596 – 2599.

[84]   Tornoe, C.W., Christensen, C., and Meldal, M. Peptidotriazoles on Solid Phase: [1,2,3]-Triazoles by Regiospecific Copper(I)-Catalyzed 1,3-Dipolar Cycloadditions of Terminal Alkynes to Azides. **J. Org. Chem.** 67 (2002): 3057 – 3064.

[85]   Binder, W.H., and Sachsenhofer, R. 'Click' chemistry in polymer and materials science. **Macromolecules** 28 (2007): 15-54.

[86]   Kolb, H.C., Finn, M.G., and Sharpless, K.B. Application of click chemistry to the generation of new chemical libraries for drug discovery. **Angew. Chem. Int. Ed.** (2001): 2004-2021.

[87]   Devaraj, N.K., and Collman, J.P. Copper Catalyzed Azide-Alkyne Cycloadditions on Solid Surfaces: Applications and Future Directions. **QSAR Comb. Sci.** 26 (2007): 1253 – 1260.

[88]   Devaraj, N.K., Decreau, R.A., Ebina, W., Collman, J.P., and Chidsey, C.E.D. Rate of Interfacial Electron Transfer through the 1,2,3-Triazole Linkage. **J. Phys. Chem. B** 110 (2006): 15955 – 15962.

[89]   Colombo, M., and Bianchi, A. Click chemistry for the synthesis of RGD-containing integrin ligands. **Molecules** 15 (2010): 178-197.

[90]   Bu, H.B. et al. Efficient post-polymerization functionalization of conducting poly(3,4-ethylenedioxythiophene) (PEDOT) via 'click'-reaction. **Tetrahedron** 62 (2011): 1114-1125.

[91]   Yilmaz, G. et al. Polysulfone based amphiphilic graft copolymers by click chemistry as bioinert membranes. **Mater. Sci. Eng., C** 31 (2011): 1091-1097.

[92]   Li, H., and Adronov, A. Water-soluble SWCNTs from sulfonation of nanotube-bound polystyrene. **Carbon** 45 (2007): 984-990.

[93]   Li, H., Cheng, F., Duft, A.M., and Adronov, A. Functionalization of single-walled carbon nanotubes with well-defined polystyrene by "click" coupling. **J. Am. Chem. Soc.** (2005): 14518-14524.

[94]   Zhang, Y., He, H., Gao, C., and Wu, J. Covalent layer-by-layer functionalization of multiwalled carbon nanotubes by click chemistry. **Langmuir** 25 (2009): 5814-5824.

[95]   Han, J., and Gao, C. Functionalization of carbon nanotubes and other nanocarbons by azide chemistry. **Nano-micro letters** 2 (2010): 213-226.

[96]   Lind, J.U. et al. Solvent composition directing click-functionalization at the surface or in the bulk of azide-modified PEDOT. **Macromolecules** 44 (2011): 495-501.

[97]   Daugaard, A.E., Hansen, T.S., Larsen, N.B., and Hvilsted, S. Microwave assisted click chemistry on a conductive polymer film. **Synth. Met.** 161 (2011): 812-816.

[98]   Daugaard, A.E., and Hvilsted, S. Conductive polymer functionalization by click chemistry. **Macromolecules** 41 (2008): 4321-4327.

[99]   Shirley, D.A. High-resolution X-ray photoemission spectrum of the valence bands of gold. **Phys Rev B** 5 (1972): 4709-4714.

[100]   Daugaad, A.E., and Hvilsted, S. Conductive polymer functionalization by click chemistry. **Macromolecules** 41 (2008): 4321-4327.

[101]   Hummers, W., and Offeman, R. Preparation of graphitic oxide. **J. Am. Chem. Soc.** 80 (1958): 1339.

[102]   Kuila, T., Khanra, P., Mishra, A.K., Kim, N.H., and Lee, J.H. Functionalized-graphene/ethylene vinyl acetate co-polymer composites for improved mechanical and thermal properties. **Polym Test** 31 (2012): 282-289.

[103]   Castelaín, M. et al. Graphene functionalisation with a conjugated poly(fluorene) by click coupling: Striking electronics properties in solution. **Chem Eur J** 18 (2012): 4965-4973.

[104]   Pimenta, M.A. et al. Studying disorder in graphite-based systems by Raman spectroscopy. **Phys Chem Chem Phys** 9 (2007): 1276-1291.

[105] Teng, C.C. et al. Thermal conductivity and structure of non-covalent functionalized graphene/epoxy composites. **Carbon** 49 (2011): 5107-5116.

[106] Tien, H.W., Huang, Y.L., Yang, S.Y., Wang, J.Y., and Ma, C.C.M. The production of graphene nanosheets decorated with silver nanoparticles for use in transparent, conductive films. **Carbon** 49 (2011): 1550-1560.

[107] Wang, X., Schreuder-Gibson, H., Downey, M., Tripathy, S., and Samuelson, L. Conductive fibers from enzymatically synthesized polyaniline. **Synth Met** 107 (1999): 117-121.

[108] DeLongchamp, D.M. et al. Influence of a water rinse on the structure and properties of poly(3,4-ethylene dioxythiophene):poly(styrene sulfonate) films. **Langmuir** 21 (2005): 11480-11483.

[109] Keawprajak, A. et al. Effects of tetramethylene sulfone solvent additives on conductivity of PEDOT:PSS film and performance of polymer photovoltaic cells. **Org. Electron.** 14 (2013): 402-410.

[110] Hwang, J., Amy, F., and Kahn, A. Spectroscopic study on sputtered PEDOT PSS: Role of surface PSS layer. **Org. Electron.** 7 (2006): 387-396.

[111] Greczynski, G., Kugler, T., and Salaneck, W.R. Characterization of the PEDOT-PSS system by means of X-ray and ultraviolet photoelectron spectroscopy. **Thin Solid Films** 354 (1999): 129-135.

[112] Xia, Y., and Ouyang, J. PEDOT:PSS films with significantly enhanced conductivities induced by preferential solvation with cosolvents and their

application in polymer photovoltaic cells. **J. Mater. Chem.** 21 (2011): 4927-4936.

[113] Higgins, A.M. et al. Interfacial structure in semiconducting polymer devices. **J. Mater. Chem.** 13 (2003): 2814-2818.

[114] Yan, H., and Okuzaki, H. Effect of solvent on PEDOT/PSS nanometer-scaled thin films: XPS and STEM/AFM studies. **Synth. Met.** 159 (2009): 2225-2228.

[115] Cruz-Cruz, I., Reyes-Reyes, M., Aguilar-Frutis, M.A., Rodriguez, A.G., and López-Sandoval, R. Study of the effect of DMSO concentration on the thickness of the PSS insulating barrier in PEDOT:PSS thin films. **Synth. Met.** 160 (2010): 1501-1506.

[116] Gasiorowski, J., Menon, R., Hingerl, K., Dachev, M., and Sariciftci, N.S. Surface morphology, optical properties and conductivity changes of poly(3,4-ethylenedioxythiophene):poly(styrenesulfonate) by using additives. **Thin Solid Films** 536 (2013): 211-215.

[117] Romyen, N., Thongyai, S., Praserthdam, P., and Sotzing, G.A. Modification of novel conductive PEDOT:sulfonated polyimide nano-thin films by anionic surfactant and poly(vinyl alcohol) for electronic applications. **J. Electron. Mater.** 42 (2013): 3471-3480.

APPENDICES

APPENDIX A

CALCULATION OF ELECTRICAL CONDUCTIVITY

Table A.1 Electrical current and voltage of the prepared PEDOT:PSS-graphene

composite film

I (mA)	V (V)
0.00	0.0428
0.05	0.2639
0.10	0.4859
0.15	0.707
0.20	0.9147
0.25	1.1347
0.30	1.3594
0.35	1.5865
0.40	1.8067
0.45	2.0224
0.50	2.2499
0.55	2.4735
0.60	2.6966
0.65	2.8991
0.70	3.1172
0.75	3.3334
0.80	3.5425
0.85	3.7378
0.90	3.9504
0.95	4.1553
1.00	4.3653
1.05	4.5764
1.10	4.7624
1.15	4.9134

The electrical conductivity of composites is measured by four-point technique. The probe used in the first part is 4 wires probe with same spacing of 1.10 cm. The electric currents (I-values) in unit of mA from a Keithley Instruments 6221 DC and AC current source are varied. The electric voltages (V-values) are collected by a Keithley 2182A nanovoltmeter as shown in the Table A.1.

The V-values are plotted versus the I-values; the slope is calculated representing the electrical resistance (R) as shown in Figure A.1
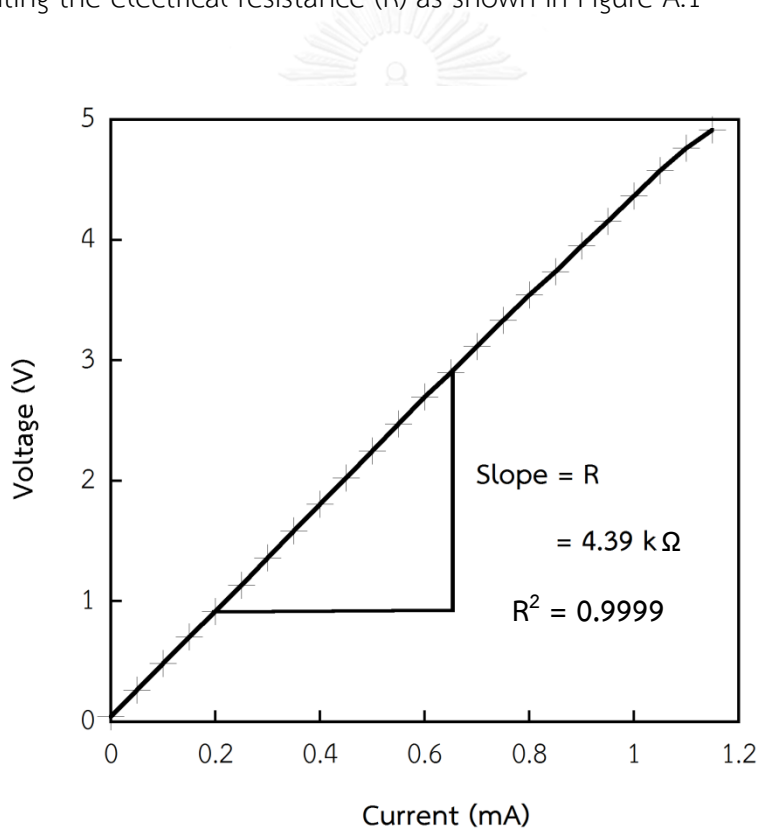

Figure A.1 The V-I slope of the prepared PEDOT:PSS-graphene composite film

The electrical conductivity (σ) can be calculated according to the Ohm's law, as showed below

$$\sigma = \frac{L}{RWT}$$

Where;

σ is the electrical conductivity (S/cm)

L   is the distance between wires (1.10 cm)

W   is the width of specimen (1.68 cm)

T   is the average thickness of films measured by surface profiler (Veeco

         Dektak 6M Stylus Profilometer) (2.5×10^{-3} cm)

R   is the sheet resistance obtained from a slope of I-V curve (4.39 kΩ)

$$\sigma = \frac{1.10\,\text{cm}}{(4.39\,\text{k}\Omega)\,(1.68\,\text{cm})(2.5\times10^{-3}\,\text{cm})}$$

$$= 0.0596\ \text{S/cm}$$

$$= 5.96 \times 10^{-2}\ \text{S/cm}$$

In the second part of this thesis, the samples are too small (2.5 cm x 2.5 cm) to measure by the 4 wires probe as used in the first part. The different probe is the four probes arranged in line with same spacing (2.5 mm).

Table A.2 Electrical current and voltage of the pristine PEDOT:PSS (PH1000) film

I (μA)	V (mV)
0	0.2
20	1.5
40	2.6
60	3.9
80	5.2
100	6.4
120	7.6
140	8.9
160	10.1
180	11.4
200	12.6
300	18.8
400	24.9
500	31.2
600	37.4
700	43.5
800	49.8

The V-values are plotted versus the I-values; the slope is calculated represented the electrical resistance (R) as shown in Figure A.2
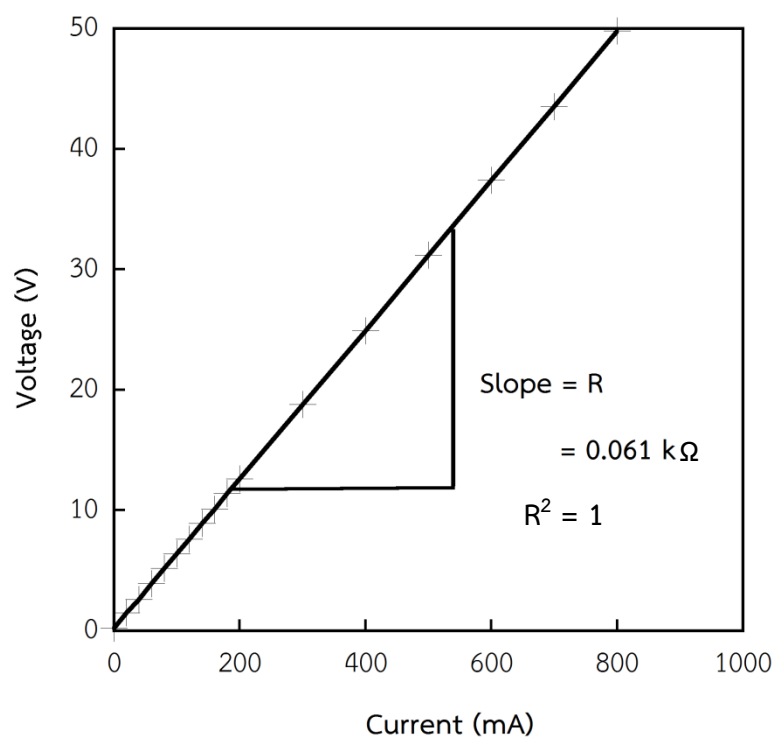

Figure A.2 V-I slope of the pristine PEDOT:PSS (PH1000) film

The electrical conductivity (σ) can be calculated as

$$\sigma = \frac{1}{RT}$$

where

$$R = \left(\frac{\pi}{\ln 2}\right)\left(\frac{V}{I}\right)$$

R   is the sheet resistance (S/cm)

T   is an average thickness of films measured by surface profiler (Veeco

Dektak 6M Stylus Profilometer) (9.34×10^{-6} cm)

V/I   is slope of V-I slope (0.061 kΩ)

$$R = (4.532)(0.061 \text{ k}\Omega)$$

$$R = 0.28 \text{ k}\Omega$$

And;

$$\sigma = \frac{1}{(0.28 \text{ k}\Omega)(9.34 \times 10^{-6} \text{ cm})}$$

$$\sigma = 381.48 \text{ S/cm}$$

APPENDIX B

INKJET PRINTABLE PEDOT:PSS AND GRAPHENE

B.1 Materials

PEDOT:PSS

- Orgacon™ IJ-1005 (Sigma Aldrich)

- Contains: 1-5% ethanol, 5-10% diethylene glycol

- Concentration: 0.8% in H_2O

Graphene

- xGnP® Graphene Nanoplatelets (xGnP-C-750)

- Thickness of 1-5 nanometer, diameter of 1-2 μm

- Typical surface area of 750 m²/g

- Bulk density 0.2-0.4 g/cc

B.2 Inkjet printable PEDOT:PSS

PEDOT:PSS was printed onto the clean glass substrate with various drop spacings (10, 15, 20 μm) and number of layer of printing (1-4 layers). It is found that the sheet resistance decreases as the drop spacing decreases because the amount of PEDOT:PSS deposited on the substrate increases. Namely, films prepared by drop spacing of 10 μm should have more PEDOT:PSS loading on the substrate than those

prepared by drop spacing of 15 μm and 20 μm, respectively. Unfortunately, the drop spacing of 10 μm and 15 μm show the non-uniform of excess PEDOT:PSS on the substrate, as indicated by the merged PEDOT:PSS around the edge of the substrate during inkjet printing, as shown in figure B.1. Thus, the drop spacing of 20 μm is suitable because the PEDOT:PSS can form the uniform film.
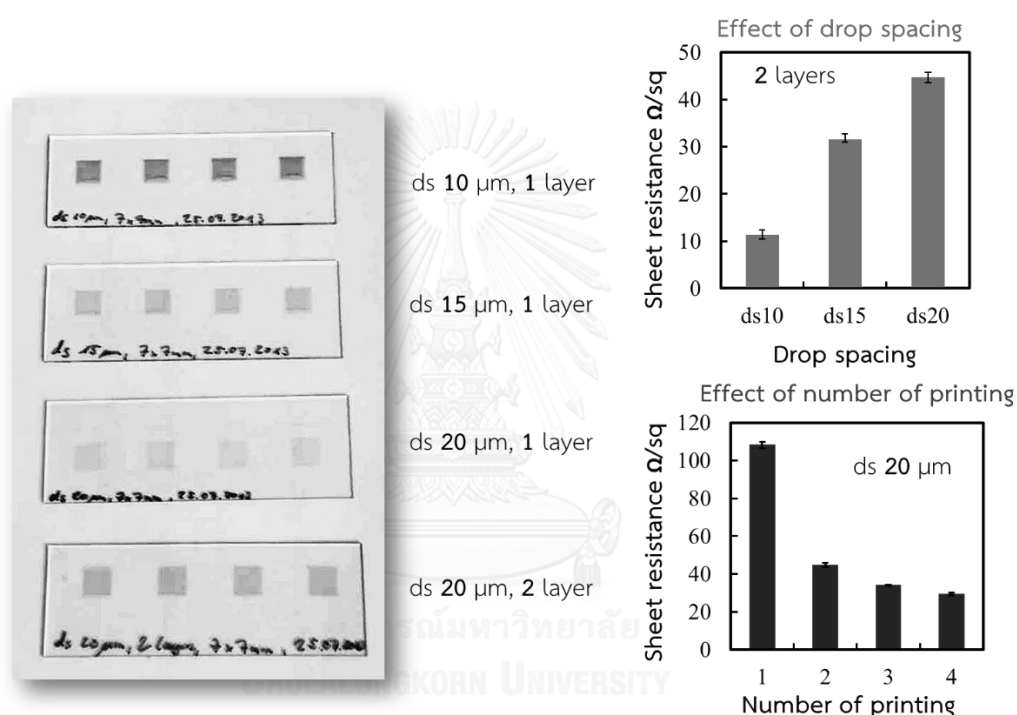
DMP 2831 operated without printing table heating and post treatment on hotplate 60 °C 15 minutes

Figure B.1 PEDOT:PSS printing varied the drop spacing and number of printing

B.3 Inkjet printable graphene

About 1 ml of 1 wt% graphene was diluted with 20 ml of DI water and sonicated for 30 minutes. It was filtrated through glass filter of 4.5 μm. The permeate dispersion was sonicated for further 30 minutes following by filtration with glass filter of 1 μm.

The permeate dispersion was sonicated again for 1 hour, yielding graphene ink 0.1 wt%.

The graphene dispersion and printable graphene are shown in figure B.2. 1 wt%

graphene dispersion is able to sediment in 1 week while the printable graphene can

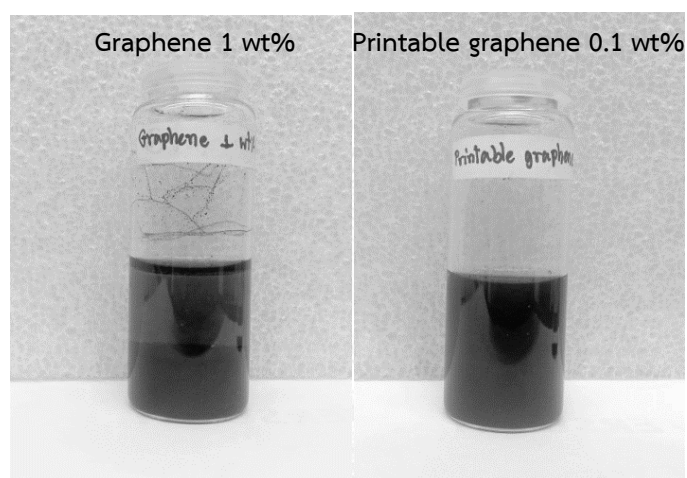stay its homogeneous dispersion without sedimentation for 1 month.

Figure B.2 Graphene dispersion at 1 wt% and printable graphene at 0.1 wt%

Printable graphene dispersion is printed on the glass, paper and polyethylene

naphthalate (PEN) substrates and PEDOT:PSS layer as displayed in figure B.3. The drop

spacing is 15 μm with 3 nozzles following by drying on the printing table at 50 $^{\circ}$C. The

number of layer of printing increases the darkness of graphene pattern, and at higher

number of layer of printing than 2 layers of graphene shows poor deposition on the

previous hydrophobic graphene layer causing the non-uniform patterns as depicted in

figure B.4. Furthermore, printable graphene can also be deposited on various substrate

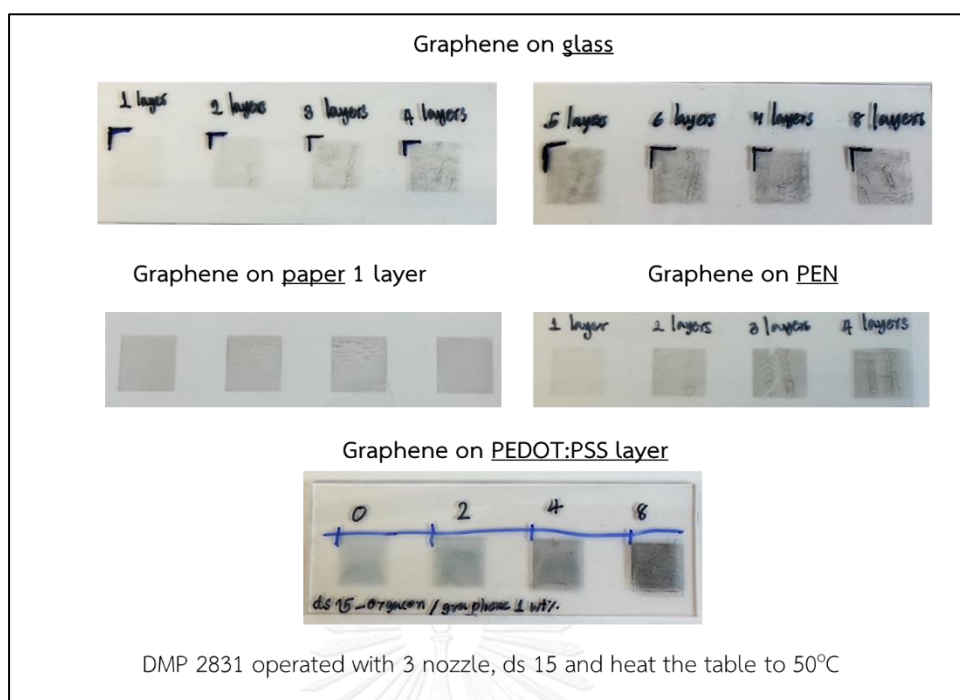like paper and PEN and PEDOT:PSS.

Figure B.3 Printable graphene dispersion deposited on glass, paper, PEN and
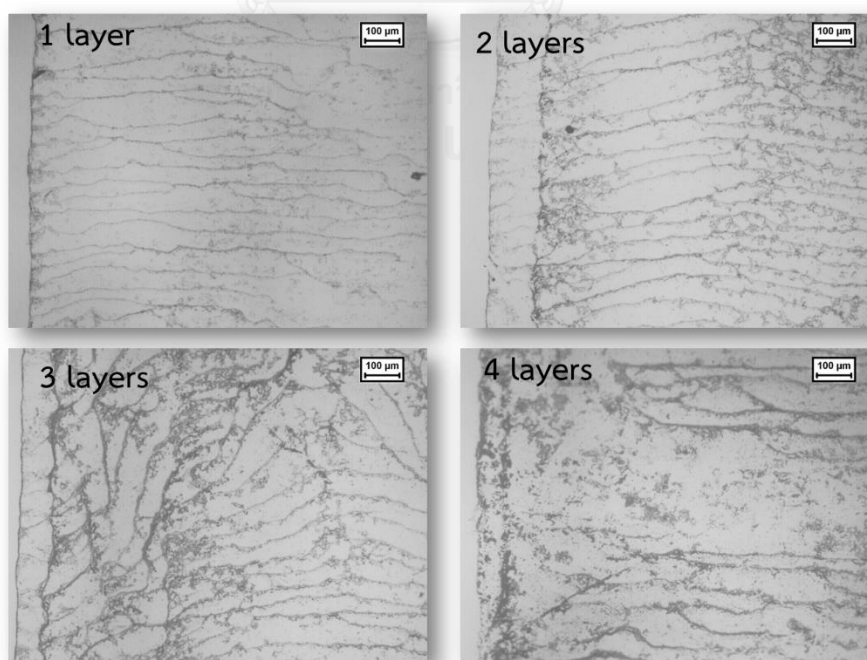
PEDOT:PSS

Figure B.4 Microscopic images of printable graphene deposited on glass (1-4 layers)

APPENDIX C

LIST OF PUBLICATIONS

1. Deetuam, C.; Wiese, D.; Samthong, C.; Praserthdam, P.; Somwangthanaroj, A.; Baumann, R. R. *Electrical conductivity enhancement of PEDOT:PSS thin film via the dipping method in low concentration aqueous DMSO* **J. Appl. Polym. Sci.** (Submitted).

2. Deetuam, C.; Samthong, C.; Thongyai, S.; Praserthdam, P.; Somwangthanaroj, A. *Synthesis of well dispersed graphene in conjugated poly(3,4-ethylenedioxy thiophene):polystyrene sulfonate via click chemistry* **Compos. Sci. Technol.** 93 (2014): 1-8. DOI: 10.1016/j.compscitech.2013.12.024.

3. Deetuam, C.; Wiese, D.; Samthong, C.; Somwangthanaroj, A.; Baumann, R. R. *Synthesis and effect of graphene in PEDOT:PSS on conductivity for biosensor application*. The 5th Printing and Future Days conference, September 10-12, 2013, Chemnitz, Germany (Poster Presentation).

4. Deetuam, C.; Somwangthanaroj, A. *Facile synthesis of highly conductive polymer composite PEDOT:PSS-graphene with covalent linkage*. Frontier of Polymer in Science, May 21-23, 2013, Sitges, Spain (Poster Presentation).

5. Deetuam, C.; Somwangthanaroj, A. *Modification of highly conductive polymer PEDOT:PSS with graphene*. Proceeding of Pure and Applied Chemistry International Conference (PACCON), January 23-25, 2013, Chon Buri, Thailand (Poster Presentation).

VITA

Miss Chutimar Deetuam was born on May 8, 1987 in YALA, Thailand. She completed high school from Somdejphapiyamaharajrommaneeyakate School, Kanchanaburi. In 2009, she received the Bachelor's Degree from Department of Chemical Engineering, Faculty of Engineering and Industrial Technology, Silpakorn University, Thailand. After graduation, she pursued her graduate study for a Doctoral Degree in Chemical Engineering, Department of Chemical Engineering, Faculty of Engineering, Chulalongkorn University in December, 2014.